DEUTSCHES ELEKTRONEN-SYNCHROTRON DESY

DESY 79/26
May 1979

RECENT EXPERIMENTS AT DESY

by

Günter Flügge

NOTKESTRASSE 85 · 2 HAMBURG 52

To be sure that your preprints are promptly included in the
HIGH ENERGY PHYSICS INDEX ,
send them to the following address (if possible by air mail) :

DESY
Bibliothek
Notkestrasse 85
2 Hamburg 52
Germany

RECENT EXPERIMENTS AT DESY

by

Günter Flügge
Deutsches Elektronen-Synchrotron DESY, Hamburg

Lectures presented at the
XVIII. Internationale Universitätswochen für Kernphysik
Schladming, Austria, 28 February - 10 March 1979

CONTENTS

Introduction

The main task of an experimental talk at a theoreticians school should probably be a tempering one. In this respect, e^+e^- physics may have been a bad choice. The field has so rapidly developped and discoveries are chasing each other that much of the optimism of theory has passed over to e^+e^- experimentalists.

A vast amount of experimental material arose from the simple reaction of e^+e^- annihilation. I, therefore, have to limit myself to recent results - most of them less than one year old. The paper will be organized as follows:

In the first lecture (chapter I and II) I will give a short introduction to e^+e^- machines and cross sections. In particular I will discuss the total cross section and - after a short summary on charm - concentrate on the third generation of quarks and leptons: the heavy lepton τ and the Y family. In my second lecture the various aspects of event topologies in the DORIS energy range will be discussed, including the Y decay. In the third lecture I will then describe the new storage ring PETRA and present first results on QED checks, total cross section, jet structure and two-photon processes.

I. GENERAL REMARKS ON e^+e^- REACTIONS

1. e^+e^- storage rings

The history of e^+e^- storage rings dates back to 1960 when B. Touschek in FRASCATI built the first machine of this kind[1]. The original motivation for e^+e^- storage rings was to study QED limits at large energies. Very soon, however, the prime interest turned to hadron production[2]. The annihilation of electrons and positrons into hadrons via the one-photon channel presents several advantages. Contrary to hadron collisions the system has well defined quantum numbers of the photon. In (symmetric) storage rings the full energy of both beams becomes available in the head-on collisions of the stored particles.

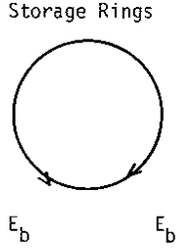

$E_{CM} = 2\ E_b$ (for zero crossing angle)
E_b = beam energy
E_{CM} = center of mass energy

The laboratory frame is identical with the center of mass system (for zero crossing angle and equal energies). This highly facilitates the data analysis although it requires large angular acceptance of the apparatus.

Table 1 gives a survey of e^+e^- machines which have been built[2,3]. I will mainly concentrate on two machines belonging to the third and fourth generation of these e^+e^- storage rings: DORIS[4] and PETRA[5] which have been built in Hamburg at DESY.

Table 1 History of electron storage rings

Name	Location	First Beam	Maximum Beam Energy (GeV)
AdA	Frascati	1961	0.25
Princeton-Stanford	Stanford	1962	0.55
ACO	Orsay	1966	0.55
VEPP-2	Novosibirsk	1966	0.55
ADONE	Frascati	1969	1.55
BYPASS	Cambridge (USA)	1970	3.5
VEPP-3	Novosibirsk	1970	3.5
SPEAR	Stanford	1972	3.9
DORIS	Hamburg	1974	5.0
VEPP-2M	Novosibirsk	1975	0.67
DCI	Orsay	1976	1.8
PETRA	Hamburg	1978	19
PEP	Stanford	(1979)	18
CESR	Cambridge (USA)	(1979)	8
VEPP-4	Novosibirsk	(1979)	8

Fig. 1 shows the storage ring DORIS which was originally built for beam energies ranging from 1.5 to 4.3 GeV. Electrons and positrons are produced and preaccelerated in the two LINACs I and II and then injected into the DESY synchrotron. Here they are accelerated to their final storage energy and then transferred into the DORIS storage rings. Electrons and positrons are stacked separately in two rings on top of each other and eventually brought to collision in two intersection regions.

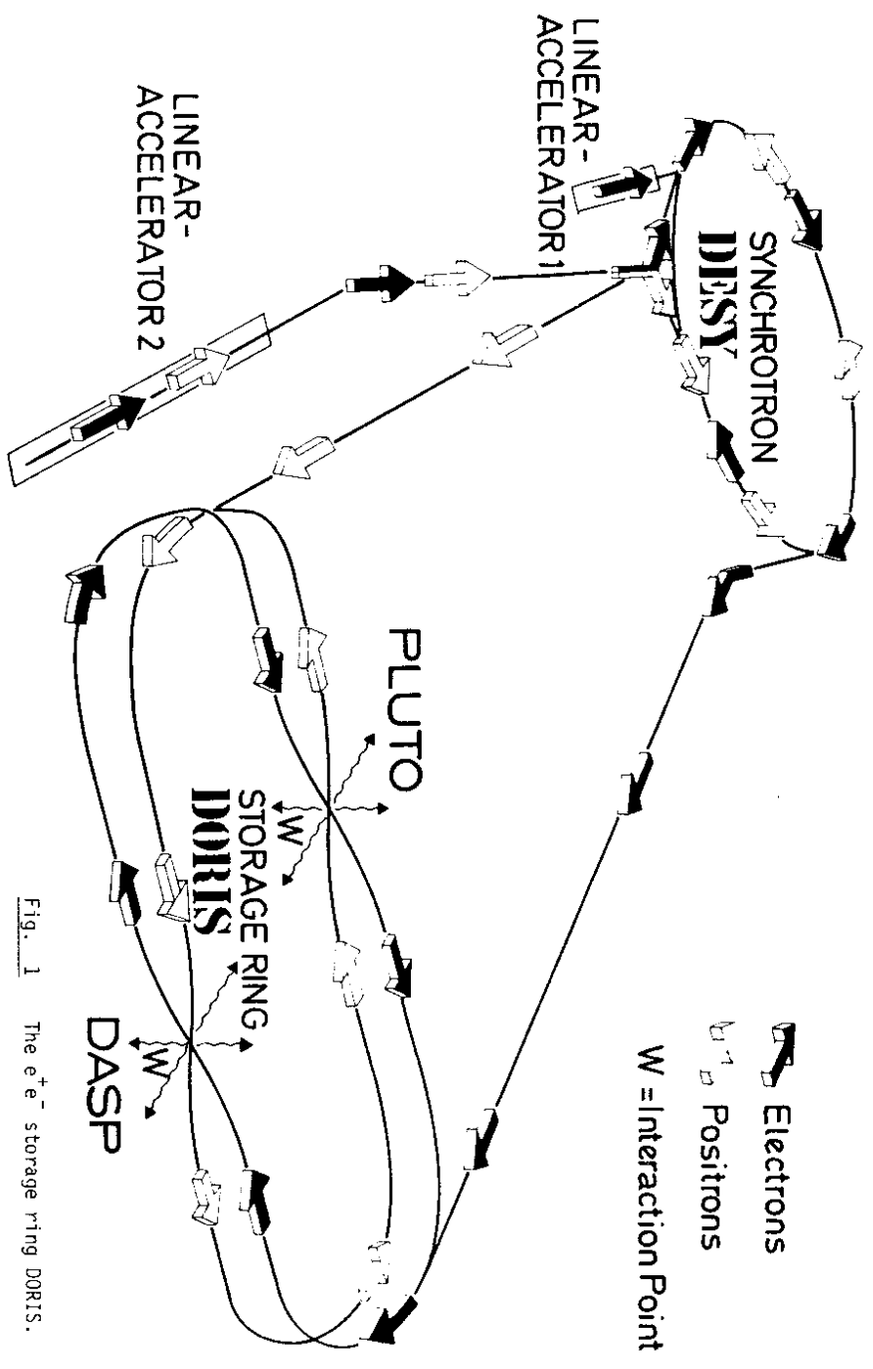

Fig. 1 The e^+e^- storage ring DORIS.

Next to the center of mass energy the rate of interaction is, of course, of largest importance in an e^+e^- storage ring. This interaction rate is given by the formula

$$N = \frac{n_+ n_-}{t F} B \cdot \sigma$$

where the proportionality constant between the cross section and the interaction rate is called the luminosity:

$$L = \frac{n_+ n_-}{t F} B .$$

With B number of bunches

$F = 4\pi \sigma_x \sigma_y$ interaction area

$I_\pm = n_\pm e/t$ total currents per beam

f revolution frequency

one finally obtains

$$L = \frac{1}{4 \pi e^2} \frac{I_+ I_-}{f B \sigma_x \sigma_y} .$$

This formula shows that the luminosity is proportional to the product of the two currents I_+ and I_-. To see the energy dependence of the luminosity we have to insert machine parameters. Without further derivation let me just quote the result of a rather lengthy calculation which can for instance be found in ref. 6:

$$L \sim \frac{(\Delta Q)^2}{\beta_y} B \varepsilon_x E_b^2$$

ΔQ is a measure of the frequency range which is available to the circulating beam without hitting a higher order resonance. It cannot easily be predicted. Experience shows, however, that ΔQ is usually $\leq .06$. The vertical amplitude function β_y is proportional to the vertical beam dimension σ_y. Therefore the beam has to be focussed vertically to get a high luminosity. The emittance ε_x finally measures the available phase volume in the machine. For fixed beam optics this quantity is proportional to E_b^2. Thus we finally get

$$L \sim E_b^4 .$$

At most e^+e^- machines this theoretical variation of luminosity is in practice limited to a power behaviour $L \sim E_b^2$. At a certain energy the synchrotron radiation losses in the machine take over and the luminosity drops rapidly roughly as E_b^{-8}. The energy dependence of L is sketched in fig. 2.

Typical parameters of the DORIS storage ring are

maximum energy:	3.6 GeV E_{CM}	(we will see later that this was upgraded to 10 GeV)
average luminosity:	$3 \cdot 10^{29}/cm^2$ s	
beam lifetime:	typically 5 to 10 hours for single beams	

Let me mention in this context a technical term which is of practical importance in e^+e^- physics, the 'integrated luminosity'

$$\int L \, dt .$$

The dimension commonly used for this quantity is

$$1 \text{ nb}^{-1} \equiv 10^{33} \text{ cm}^{-2} .$$

As an example let us take a luminosity of $3 \cdot 10^{29}$ integrated over one day.

$$\int L \, dt = 3 \cdot 10^{29} \cdot 24 \cdot 3600 \approx 26 \cdot 10^{33} \text{ cm}^{-2} = 26 \text{ nb}^{-1}$$

The usefulness of this quantity is apparent from the equation

$$\sigma(\text{nb}) \cdot \int L \, dt \, (\text{nb}^{-1}) = \text{number of events} .$$

2. Cross sections

In this section I want to give a short introduction to the main processes encountered in e^+e^- physics. The expected cross sections will be estimated to provide a feeling for the rates we are dealing with.

μ-pair production

The μ-pair production

$$e^+ e^- \rightarrow \mu^+ \mu^-$$

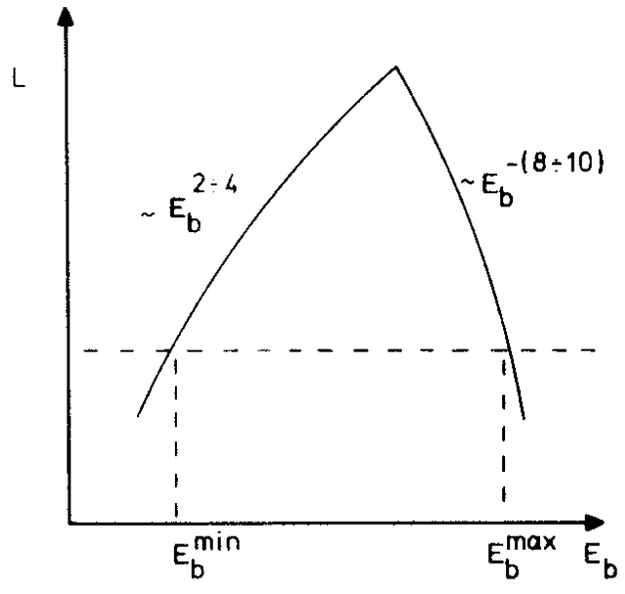

Fig. 2 Typical energy dependence of the luminosity in e^+e^- storage rings.

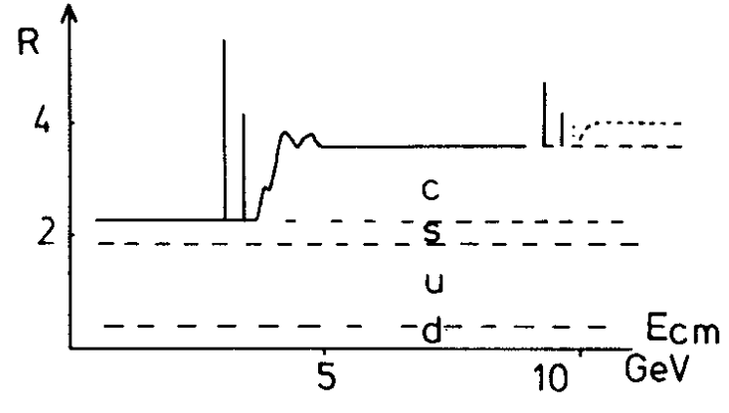

Fig. 3 Schematic behaviour of $R = \sigma_{had}/\sigma_{\mu\mu}$ as a function of energy.

is kind of a pilot reaction in e^+e^- physics since it is represented by the simple graph

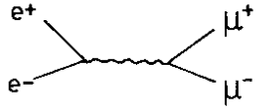

The total cross section for this reaction is given by the formula

$$\sigma_{\mu\mu} = \frac{4\pi\,\alpha^2}{3\,E_{cm}^2} \approx \frac{21.7\ \text{nb}}{E_b^2\ (\text{GeV}^2)} \quad (\text{spin } 1/2,\ \text{pointlike},\ E_{CM} >> m_\mu)$$

Cross sections in e^+e^- reactions will mostly be given in terms of $\sigma_{\mu\mu}$. Let us, therefore, calculate the $\mu\mu$ rates to get a feeling for the number of events one expects in e^+e^- physics. Assume an average luminosity of $3 \cdot 10^{29}$ at E_{cm} = 5 GeV varying like E_b^2. Then the energy dependence cancels out in the product $L \cdot \sigma_{\mu\mu}$ and the expected average rate will be

$$N_{\mu\mu} = L \cdot \sigma_{\mu\mu} \approx 10^{-3}\ s^{-1} \approx 90\ d^{-1}\ .$$

To demonstrate the usefulness of the 'integrated luminosity' let me quickly redo the calculation in nb^{-1}: Within a day one integrates 26 nb^{-1}. Multiplying this by $\sigma_{\mu\mu}$ = 3.5 nb we again get 90 events/day.

Bhabha scattering

Another important QED cross section is the Bhabha scattering

$$e^+ e^- \rightarrow e^+ e^-$$

which is represented by the two graphs

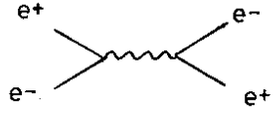

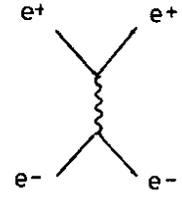

Bhabha scattering is used as a monitor reaction in e^+e^- collisions because it gives a large calculable cross section at small angles where the validity of QED is proven (low momentum transfer).

Hadron production

The most important cross section in e^+e^- physics is, however, hadron production via the one-photon channel.

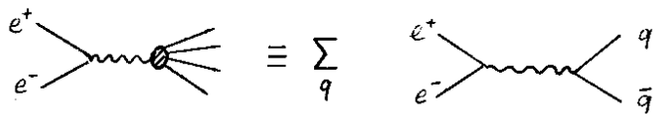

In the quark-parton model this process is simply described by the sum over all quark pair cross sections. It is therefore related to $\sigma_{\mu\mu}$ by the formula (assuming pointlike spin 1/2 massless coloured quarks)

$$R = \frac{\sigma_{had}}{\sigma_{\mu\mu}} = 3 \sum_q Q_q^2 \qquad q = \text{quark flavours}$$

Thus R is just the sum over all quark charges where the sum runs over all quark flavours and colours. The expected values for R are summarized in table 2. This table also contains the expectation for R if we include QCD corrections in first order[7]. The energy dependence of R is schematically demonstrated in fig. 3

Table 2 Theoretical predictions for $R = \sigma_{had}/\sigma_{\mu\mu}$

Quark q	Charge Qq	$R_{QPM} = 3\sum Q_q^2$	R_{QCD} +
u	2/3	} 2	
d	- 1/3		- 2.3 (E_{cm} = 3.6 GeV)
s	- 1/3		
c	2/3	} 3 1/3	- 3.9 (E_{cm} = 5.0 GeV)

+ Gluonic corrections in first order QCD:

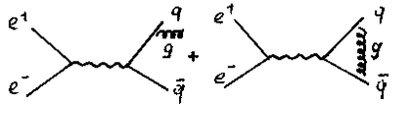

$$R_{QCD} = R_{QPM}\ (1 + \frac{\alpha_s}{\pi})$$

$$\alpha_s(E_{cm}) = \frac{12\pi}{(33 - 2N)\log \frac{E_{cm}^2}{\Lambda^2}};$$

Λ = 0.5 GeV

N = number of flavours

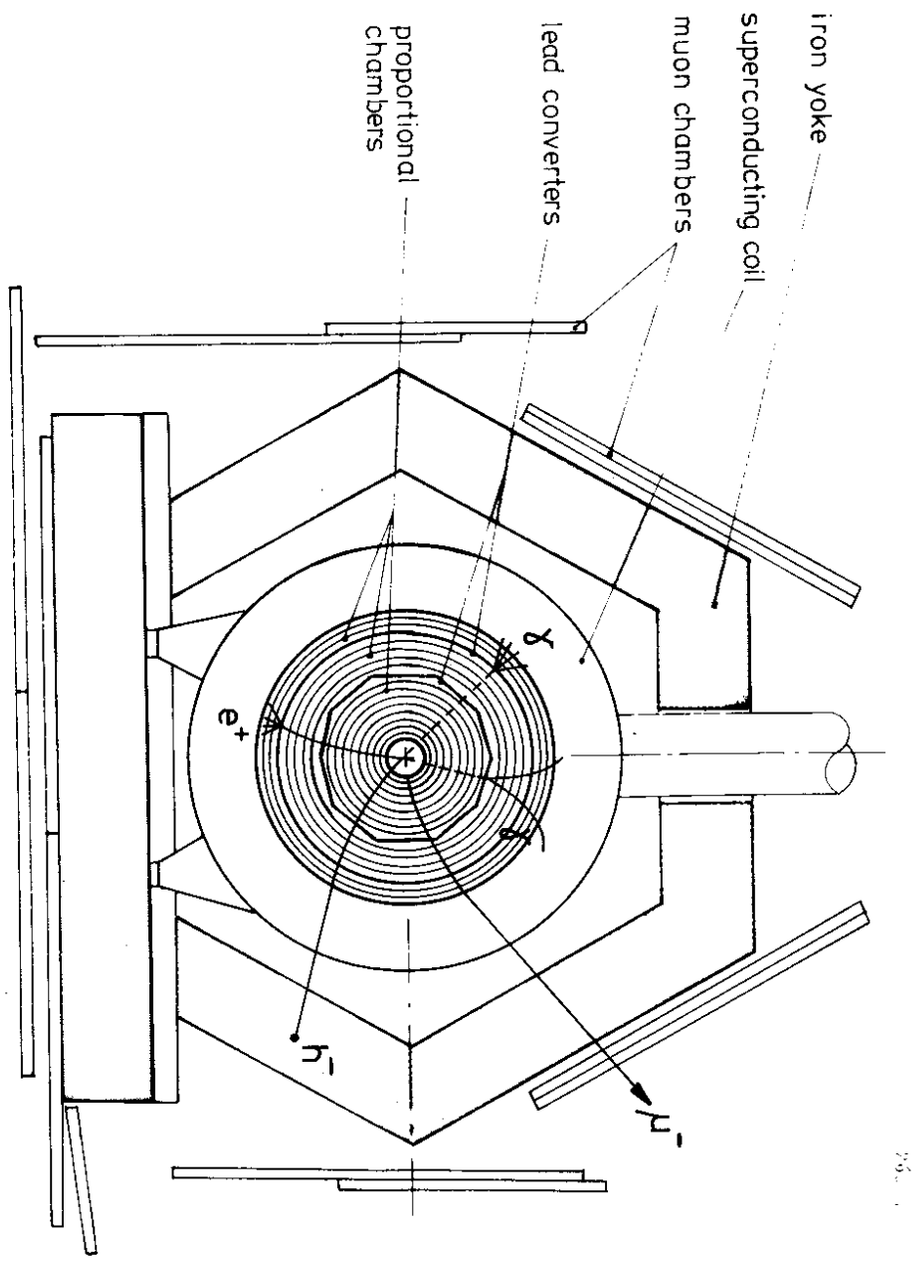

Fig. 4 PLUTO detector at DORIS (1976 version).

Near to a new flavour threshold bumps and peaks appear in the cross section. In addition also new leptons show up by their hadronic decay modes. Like in the case of $c\bar{c}$ and $\tau^+\tau^-$ production lepton and quark thresholds may (accidentally?) overlap. In the following I will first talk about the asymtotic behaviour of the total cross section and then come back to the threshold region.

3. Measurement of σ_{had} below 5 GeV

The total hadronic cross section in e^+e^- reactions is measured according to

$$\sigma_{had} = \frac{N}{\varepsilon \cdot \int L\,dt}$$

where N is the number of events seen in the detector. ε is the acceptance of the detector and $\int L\,dt$ is the integrated luminosity.

A typical detector for measuring total cross sections is the PLUTO spectrometer[8] shown in fig. 4. It consists of a superconducting coil which produces a magnetic field of 1.7 T. The magnetic field volume is filled with a set of cylindrical proportional chambers to detect the tracks of charged particles. In addition two lead cylinders are inserted to detect photons and electrons. A set of proportional tube chambers outside the iron flux return yoke is used to separate hadrons and muons. The acceptance of such a detector for hadronic events is slightly energy dependent. In the energy range around 5 GeV for instance the event acceptance of PLUTO is of the order of 80 %.

Hadronic events are accepted if they have at least two tracks originating from the interaction point. In addition non collinearity of the tracks is required to remove QED contributions. Note that such a signature includes at least part of the cross section for the production of new leptons.

The integrated luminosity is recorded simultaneously to the measurement of σ_{had} by counting small angle Bhabhas in the forward direction. Fig. 5 shows the results of the total cross section measurements of the PLUTO collaboration[9] in terms of $R = \sigma_{had}/\sigma_{\mu\mu}$. The systematic error of ±15 % is indicated in the figure. For comparison[10] also the results of three other experiments are shown: SLAC-LBL[11], DASP[12] and DELCO[13]. Below charm threshold around 3.5 GeV all data agree remarkably well. Also far above threshold in the asymptotic region around 5 GeV there is good agreement between all four experiments.

How well do these 'asymptotic' values above and below charm threshold reproduce the theoretical predictions? All measurements are higher than the simple quark-parton prediction. However, they agree well with the expectation of four quark flavours, heavy-lepton production and gluonic corrections. Since, however, both the gluonic corrections and the systematic errors are of the same level of 10 to 15 % we cannot draw any definite conclusions about QCD contributions in the total cross section.

In the resonance region near charm threshold there are considerable differences between all four experiments, in width, height and also position of the resonances. All data agree about the dip in the cross section around 4.2 GeV which shows that charm production drops down to a very low level between the resonances even above threshold.

4. Bumps and peaks below 5 GeV: charm

Since the discovery of the J/ψ resonance [14] in 1974 enormous progress has been achieved in the study of charmed particles and charmonium[15]. During the past year, however, the interest has rather moved to the higher energy region. Therfore I will only give a very short summary of the situation of charm and charmonium in this lecture[16].

Our experimental knowledge on charm is schematically summarized in fig. 6. The odd C-parity ^3S state J/ψ, its radial excitations ψ', and the ^3D state $\psi''(3.77)$ show up in the total e^+e^- cross section, the latter due to its mixing with the nearby ^3S state. The existence of the $\psi'(4.16)$ is somewhat controversial[10]. Quarkonium models would like it to be a ^3D state[17].

The ^3P states are established, although their quantum number assignment is not rigorously proven[15]. Evidence for a $\chi(2.82)$ state based on a 5 standard deviation signal has been reported from the DASP group. However, preliminary results from the crystal ball experiment do not show any comparable signal[18]. The existence of the states $\chi(3.45)$ and $\chi(3.59$ or $3.18)$ is not established[19]. The quantum numbers of all three states (if they exist) are unknown, except for their even C-parity.

The upper part of fig. 6 indicates, how the production of D,D^*, F and F^* mesons comes in with increasing energy: $D\bar{D}$ at the $\psi''(3.77)$, $D^*\bar{D}$ and $D^*\bar{D}^*$ at $\psi'(4.03)$[15,20], $F\bar{F}$ at $\psi'(4.15)$ and $F^*\bar{F}$ and/or $F^*\bar{F}^*$ at $\psi'(4.42)$[21]. The evidence

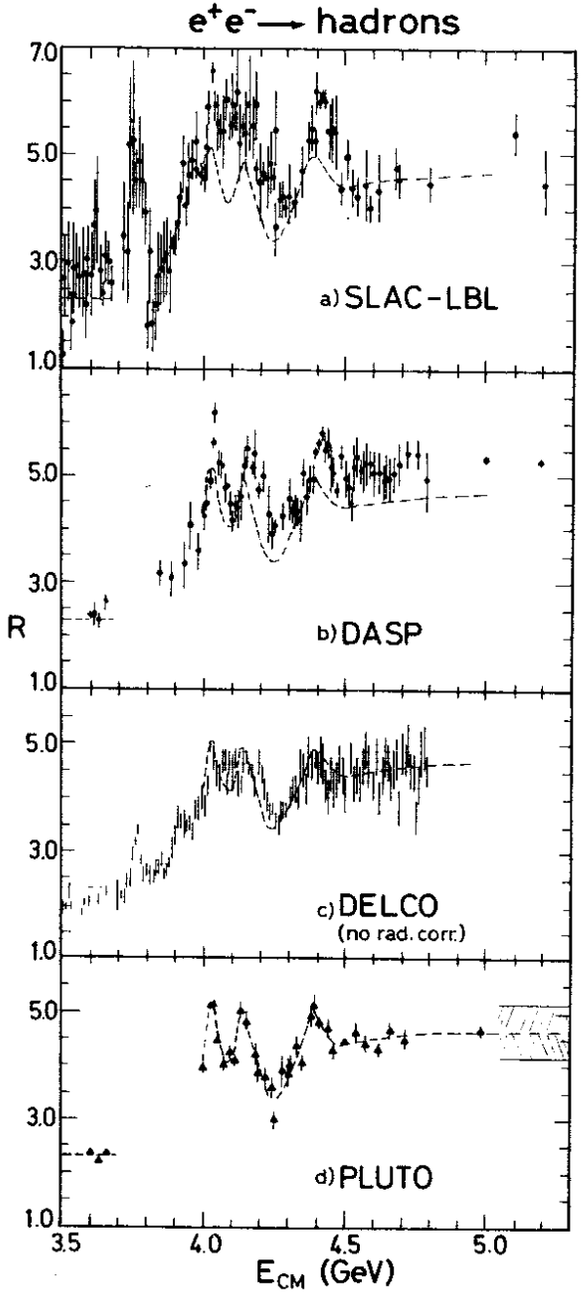

Fig. 5 Measurements of R as a function of energy.
a) SLAC-LBL group[11]
b) DASP group[12]
c) DELCO group[13] (no radiative corrections)
d) PLUTO group[9]
Adopted from G. Feldman[10].

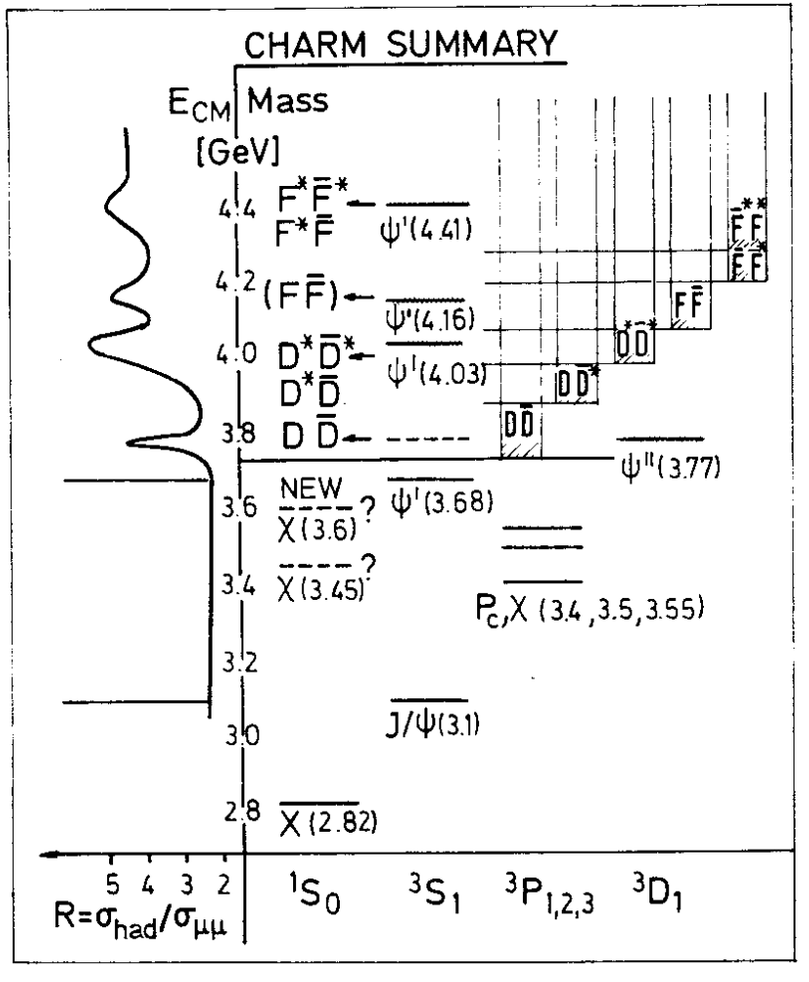

Fig. 6 Schematic summary of the experimental situation on CHARM.

for $F\bar{F}$ production at the $\psi'(4.16)$ is suggestive but not compelling, since it is only based on the inclusive η signal of the DASP group. No clear distinction between $F^*\bar{F}^*$ and $F^*\bar{F}$ production at the $\psi'(4.42)$ can be made.

In summary, although many aspects of the charmonium system and the charmed mesons D and F are well understood, the pseudoscalar components η_c and η_c' are still not established.

II. THIRD GENERATION OF QUARKS AND LEPTONS

Since the discovery of a new lepton τ in 1975[22] and of a new quark b in 1977[23] our interest has rather turned to the study of a third generation of quarks and leptons.

Generation	1	2	3
Quarks	u d	c s	t b
Leptons	ν_e e^-	ν_μ μ^-	ν_τ τ^-

The rest of this lecture I will, therefore, concentrate on the achievements which have been obtained in the study of heavy leptons and Ypsilon particles during the last year.

1. The heavy lepton τ

The new heavy lepton τ was first seen in the celebrated $e\mu$ events observed at SLAC in 1975. Fig. 7 shows an example of the $e\mu$ events seen at PLUTO in 1976 which confirmed[24] the existence of the heavy lepton τ. The figure clearly shows the apparent nonconservation of energy and momentum in this event. Both groups, SLAC-LBL and PLUTO, were able to demonstrate that only neutrinos could be responsible for the missing energy. In 1977 it could then be shown that also inclusive μ two prong events could only be explained by the production of a new type of heavy lepton in e^+e^- collision[24,25,26].

a) τ mass

Until 1977 the mass of the τ was rather unprecisely determined[27]. Mainly for this reason a certain scepticism remained that the τ might be confused with a charm particle. A major break through in this issue came with the discovery of the DASP group that τ production was already present at the ψ' resonance[28] (fig. 8a). From the inclusive electron production of fig. 8a a mass of M_τ = 1.807 ±.02 GeV could be determined by the DASP group. The DESY-Heidelberg group (fig. 8b) followed very quickly with an even better determination of the mass[29] $M_\tau = 1.790\ ^{+.007}_{-.010}$ GeV. Both values were finally topped by the excellent measurement of the DELCO group[30] at SPEAR which is shown in fig. 8c. This measurement

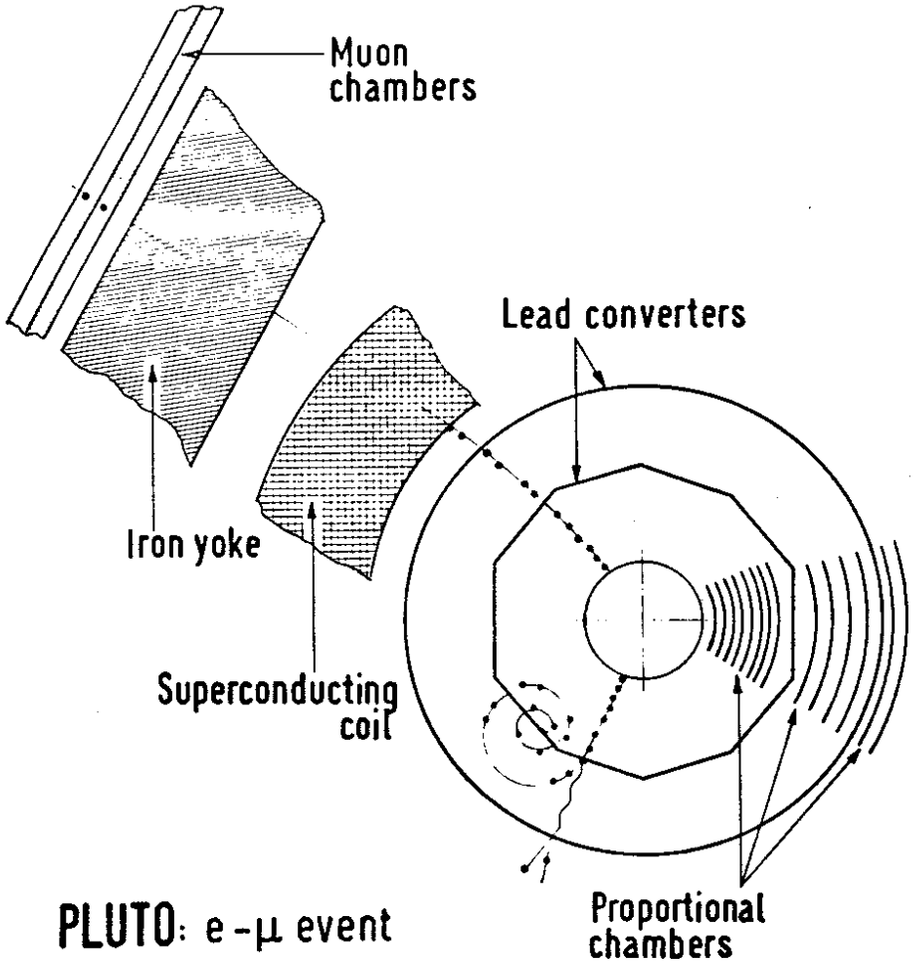

Fig. 7 $e\mu$ event measured at PLUTO.

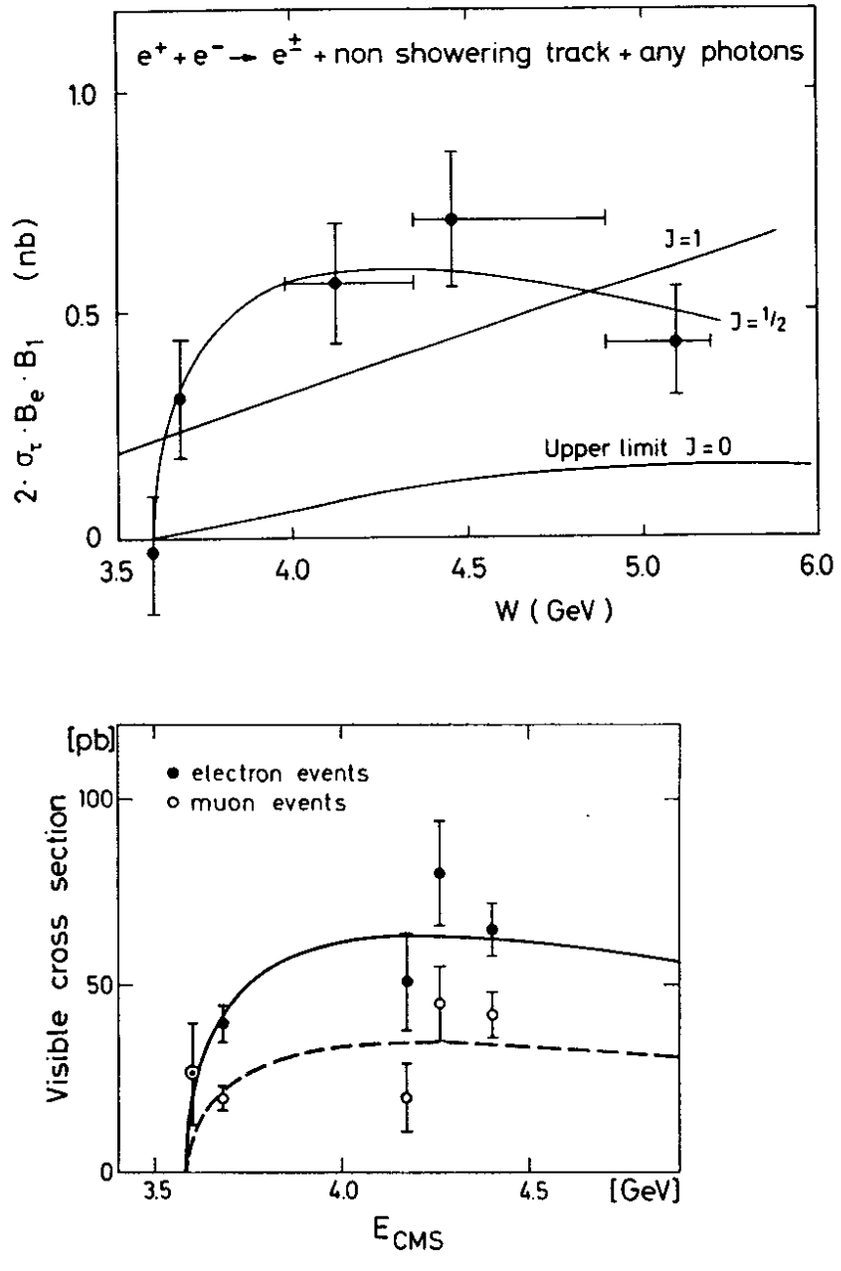

Fig. 8 Inclusive lepton production near the τ threshold

a) DASP results on $e^+e^- \to e^\pm$ + non showering track + any photons

b) DESY-Heidelberg data on $e^+e^- \to e^\pm(\mu^\pm)$ + non showering track + no photons

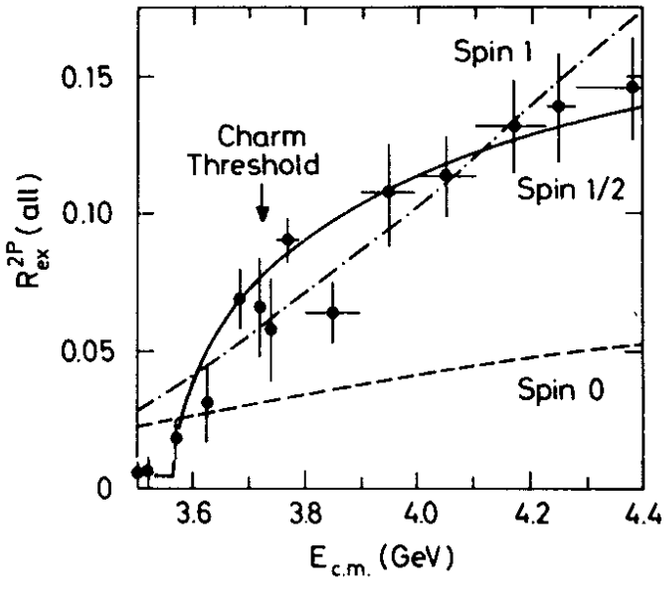

Fig. 8 Inclusive lepton production near the τ threshold

c) DELCO result on $e^+e^- \to e^\pm$ + non showering track

of the inclusive electron production in two-prong events sets a mass value of $1.782\ ^{+.003}_{-.004}$ GeV to be compared with the $D^\pm$ meson mass of $M_D = 1.868 \pm .001$ GeV.

The very precise determination of the τ mass definitely excludes charm as a source for these particles. In addition all three measurements of fig. 8 show very clearly that only a spin 1/2 hypothesis describes the energy dependence of the measured cross sections.

b) τ decays

According to the heavy sequential lepton hypothesis this new particle τ has a conventional weak coupling to its own massless neutrino. In this model we can readily predict its decay branching ratios (fig. 9). In 1977 the experimental situation was such that the leptonic decay branching ratios were in fair agreement with the theoretical predictions. The same was true for most of the semi-hadronic decays of the τ. The only exception was the π decay which was found to be too low (S. Yamada in ref. 19).

This situation was extremely puzzling since the "A_1" decay which is due to the axial component of the weak current had been found in good agreement with the prediction. Why should now the divergence of the axial current which causes the π decay be absent?

Let us first look into the $\tau \to$ "A_1" ν decay which is representing the 1^+ component of the axial current. The PLUTO group[31] searched for evidence for this decay in the process

$$e^+ e^- \to \tau\,\tau \;\begin{cases} \to \mu\,\nu\,\nu,\ e\,\nu\,\nu \\ \to \pi^+\,\pi^-\,\pi^\pm\,\nu \end{cases}$$

This reaction gives a very nice signature with one lepton and three pions travelling in opposite directions. The PLUTO group[31] could isolate this reaction and determined that the full cross section could be accounted for by the decay $\tau \to \rho^0\,\pi\,\nu$. The branching ratio for this decay mode was found to be

$$BR(\tau \to \rho\pi\nu) = (10.4 \pm 2.4)\ \% \qquad (I(\rho\pi) \stackrel{!}{=} 1)$$

The existence of a $\rho\pi$ final state with negative G-parity in itself proves that an axial piece is present in the hadronic weak current in τ decays. (Provided

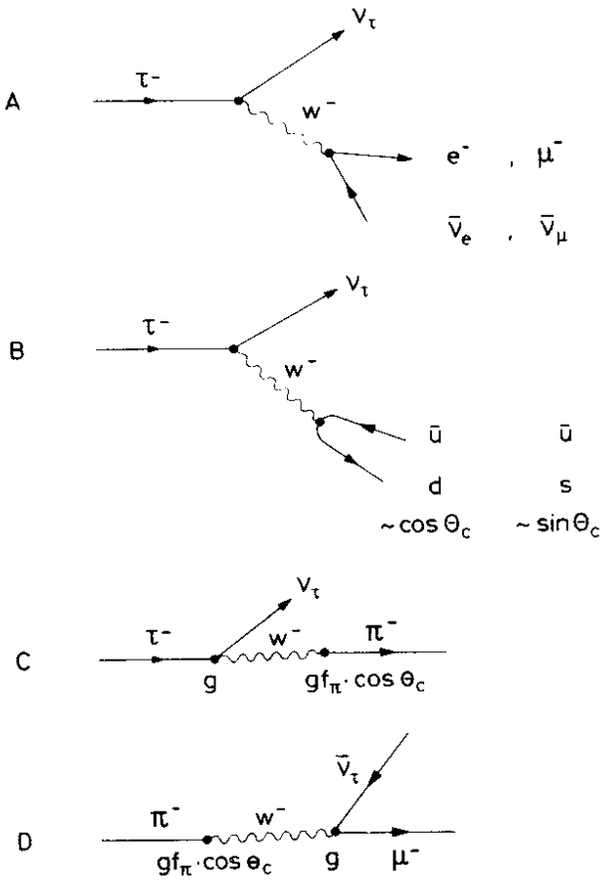

Fig. 9 Decays of the heavy sequential lepton τ.

only first class currents are present; by definition of first class currents.)
To get a statement independent of the latter assumption, the spin parity of the ρπ system was studied. The density distribution in a 3-dimensional Dalitz plot of the masses of the two $\pi^+\pi^-$ combinations and the ρπ system was investigated. Only the $J^P = 1^+$ s-wave and the $J^P = 2^-$ p-wave gave an acceptable description of the data. Fig. 10a shows the mass distribution of the ρπ system together with the expectation from a Monte-Carlo calculation for different partial waves. The p- and d-waves give a very bad account of the data. Only the

$$J^P = 1^+ \text{ s-wave}$$

is acceptable. This proves again the existence of an axial part in the hadronic current. In particular, there are no indications for a 1^- s-wave from second class axial currents.

The ρπ mass distribution is much better described if one assumes a resonance with M = 1 GeV and Γ = 0.475 GeV in the 1^+ s-wave (fig. 10b). This indicates that the observed decay may indeed be due to

$$\tau \rightarrow A_1 \nu \rightarrow \rho \pi \nu .$$

The evidence is not compelling, however.

Since the axial vector current is not conserved, its divergence can also contribute to the hadronic current. Therefore also $J^P = 0^-$ final states are allowed and the τ will decay into νπ.

This decay plays a central role in the discussion of the weak current involved in τ decay since it constitutes the "inversion" of the π decay. It can, therefore unambiguously be predicted from the pion coupling constant f_π (fig. 9c,d).

The relative width is given by[32]

$$\Gamma(\tau\rightarrow\pi\nu) \,/\, \Gamma(\tau\rightarrow e\nu\nu) = 12\,\pi^2\, f_\pi^2\, \cos^2\theta_c / M_\tau^2$$

With $BR(\tau\rightarrow e\nu\nu) = 16.8\,\%$, $f_\pi = 0.129$ GeV/c² and $M_\tau = 1.8$ GeV/c² this yields

$$BR(\tau\rightarrow\pi\nu) = 9.5\,\%.$$

The PLUTO group studied inclusive pion production[33] from the reaction:

$$e^+ e^- \rightarrow \tau\,\tau \begin{cases} \rightarrow \pi\nu \\ \rightarrow \text{1 prong + no photons} \end{cases}$$

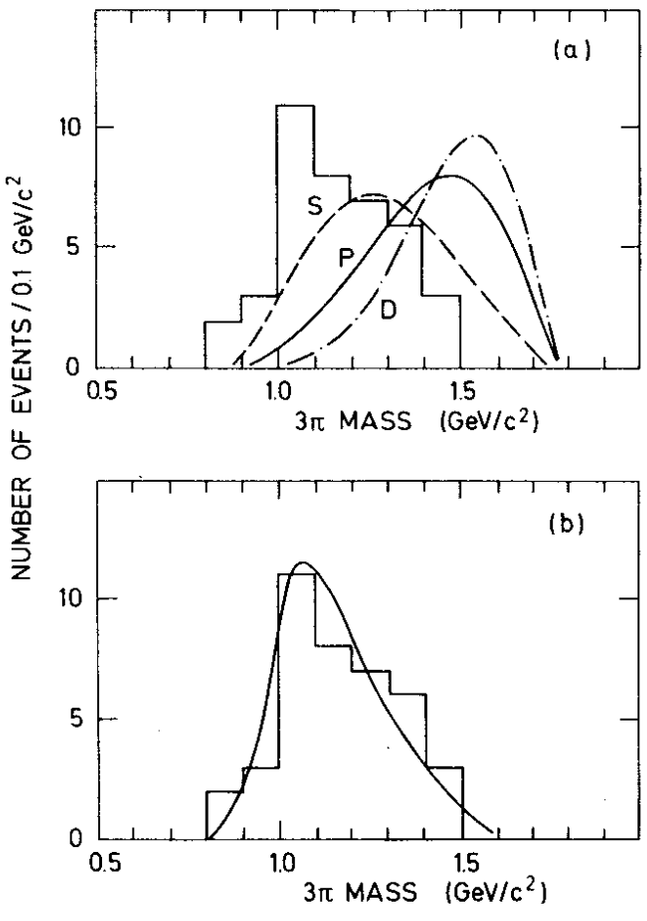

Fig. 10 PLUTO: 3π mass distribution of the decay $\tau \to \rho\pi\nu$.
a) Mass distribution of the 3π system in the ρ band ($0.68 \leq M_{\pi\pi} \leq 0.86$ GeV). The curves are phase-space calculations for different partial waves of the $\rho\pi$ system.
b) The same distribution. The curve is a resonant s-wave with $M_{A_1} = 1.0$ GeV and $\Gamma_{A_1} = 475$ MeV.

32 events of the signal class

$$e^+ e^- \to \text{hadron} + 1 \text{ charged track} + \text{no photon}$$

were seen in the 4 to 5 GeV energy range. On the other hand, only 8.9 ±1.0 events were expected from hadron misidentification, $\tau \to \rho\nu$ decay and hadronic sources. The PLUTO group obtains a branching ratio of

$$BR(\tau \to \pi\nu) = (9.0 \pm 2.9)\ \%$$

with an additional systematic uncertainty of 2.5 %.

The DELCO experiment at SLAC achieved[35]

$$BR(\tau \to \pi\nu) = (8.0 \pm 3.2)\ \%\ \ (1.3\ \%\ \text{additional systematic error})$$

from a study of the reaction $e^+e^- \to e^\pm$ + 1 hadron.

Two other groups at SLAC - SLAC-LBL and MARK-II - obtained very similar results[10]. The present world average of[10]

$$BR(\tau \to \pi\nu) = (8.3 \pm 1.4)\ \%$$

is in good agreement with the theoretical expectation.

c) Summary

Table 3 gives a summary of the experimental knowledge about τ, which is now clearly established as a new heavy lepton with the mass $M_\tau = 1.782\ ^{+.03}_{-.04}$ GeV. All properties of this new particle are as expected for a sequential left-handed lepton with conventional weak coupling to its own massless neutrino. It should be noted, however, that the orthoelectron hypothesis (the neutrino being of the ν_e type) as well as pure V or pure A coupling can not firmly be excluded (table 3).

Till now the new lepton τ has remained a domaine of e^+e^- physics. Within three years, most of its properties have been established. It was the particle that destroyed the four lepton - four quark symmetry (which had just been established) and gave a new impetus to the old puzzle of μ-e universality. Today it is the corner stone of a third generation of quarks and leptons.

2. The b quark

a) The Ypsilon story

Since the discovery of the Ypsilon meson by the Columbia-Fermilab-Stony Brook collaboration at FNAL in 1977[23] (fig. 11) the new particle has been produced in various hadron experiments[36]. The discoverers themselves improved both the statistics and the resolution of their experiment[37]. From these data we have firm evidence for the existence of at least two Y states and some indications of even a third one. The challenge for e^+e^- physics was, of course, to search for these new states as narrow resonances in e^+e^- collisions and thereby reveal their potential nature as bound states of new quarks. Therefore after the announcement of the discovery in June 1977 the PLUTO collaboration proposed in July 1977 to upgrade DORIS to reach the 10 GeV region.

In the original layout of DORIS the beam energy was limited to 4.6 GeV from the magnet design. However, the available high frequency power would have done only for 4.3 GeV. So first of all the power limitations had to be overcome.

Due to synchrotron radiation losses

$$U_{syn} = 88 \frac{E^4\,(\mathrm{GeV}^4)}{\rho(\mathrm{m})}$$

the power consumption

$$W = U_{syn} \cdot e \cdot f \cdot B \cdot (I_+^b + I_-^b) \sim I^b \cdot B$$

rises linearly with the bunch current I^b and the number of bunches B.
On the other hand the luminosity

$$L \sim I_+^b \cdot I_-^b \cdot B \sim (I^b)^2 \cdot B$$

increases quadratically with I^b. Therefore, the most economic way of reaching high energies with sufficient luminosity is a single bunch machine with large I^b. Once a single bunch mode is envisaged, separate rings for electrons and positrons are not needed any more. In addition, changing to a single ring operation one profits from a zero crossing angle. At DORIS one wins a factor of 10 in luminosity as compared to the finite crossing angle of the two-ring mode. Consequently it was decided to transform DORIS into a single ring single bunch machine. Apart from the technical effort of this reconstruction various other problems remained: The magnets were designed for 4.6 GeV and had to be driven

Table 3 Summary of τ parameters. World averages or best values are given

Parameter	Units	Prediction	Exp. Value	Experiments
Mass	GeV/c^2	-	$1.782\ ^{+.003}_{-.004}$	PLUTO, SLAC-LBL, DASP, DESY-Heidelberg, DELCO
Neutrino mass	MeV/c^2	0	<250 (95 % C.L.)	SLAC-LBL, PLUTO, DELCO
Spin		1/2	1/2	PLUTO, DASP, DELCO, DESY-Heidelberg
Lifetime	10^{-13} s	2.8	<23 (95 % C.L.)[+]	PLUTO, SLAC-LBL, DELCO
Michel parameter ρ		0.75 [++]	0.72 ± .15	DELCO
Leptonic branching ratios				
B_e: $\tau^- \to \nu_\tau e^- \bar{\nu}_e$	%	16.8)	16.7 ±1.0	SLAC-LBL, PLUTO, Lead-Glass-Wall,
B_μ: $\tau^- \to \nu_\tau \mu^- \bar{\nu}_\mu$	%	16.4)		Ironball, MPPS, DASP, DELCO
B_μ/B_e		.98	.99 ± .20	SLAC-LBL, PLUTO, DASP
Semihadronic BR				
$\tau^- \to \nu_\tau \pi^-$	%	9.5	8.3 ±1.4	PLUTO, SLAC-LBL, DELCO
$\tau^- \to \nu_\tau \rho^-$	%	25.3	24 ±9	DASP
$\tau^- \to \nu_\tau A_1^-$	%	8.1	10.4 ±2.4	PLUTO, SLAC-LBL
$\tau^- \to \nu_\tau$ + $\geq$3 prongs	%	-26	32 ±4	PLUTO, DASP, DELCO
$\tau^- \to K^- \ldots / \tau^- \to \pi^- \ldots$		.05	.07 ± .06	DASP

[+] In conjunction with upper limits on $\nu_\mu \to \tau$ production this value excludes $\nu_\tau \equiv \nu_\mu$. Similar limits on $\nu_e \to \tau$ do not exist to exclude $\nu_\tau \equiv \nu_e$ (ortho electron hypothesis)[34].

[++] V-A prediction. ρ(V+A) = 0 is excluded, ρ(V or A) = 0.375 disfavoured by the data[10,35].

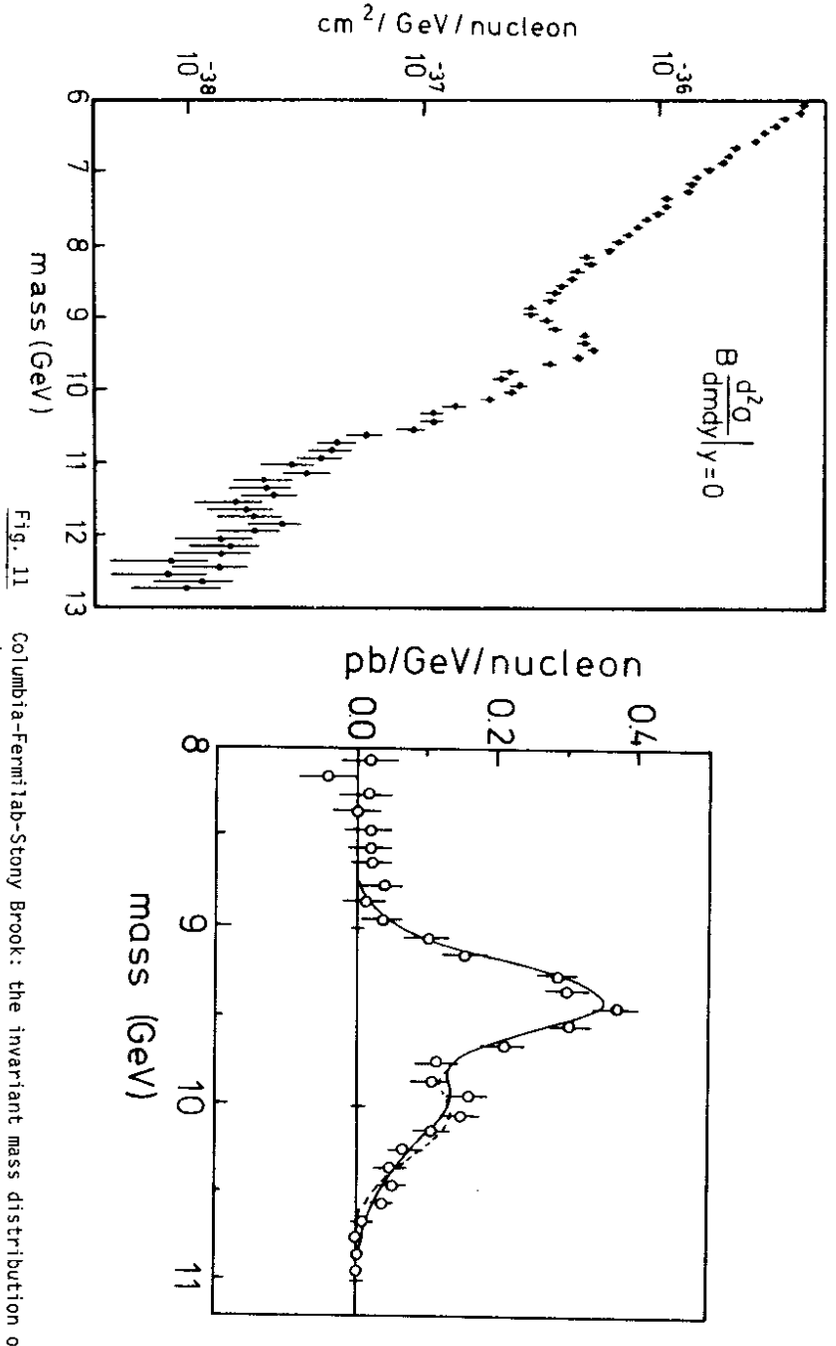

Fig. 11 Columbia-Fermilab-Stony Brook: the invariant mass distribution of $\mu^+\mu^-$ from p + Be → $\mu^+\mu^-$ + X : evidence for Υ and Υ'.

into saturation (~ 5 % at 5 GeV). PETRA cavities had to be introduced to deliver sufficient high frequency power.

In parallel, the PLUTO detector was upgraded. Shower counters were introduced to replace the lead converters. Fig. 12 shows the new detector. The barrel and endcap shower counters consist of lead scintillator sandwiches and cover 94 % of 4 π. This adds to the charged track recognition (87 % of 4 π) in the proportional chambers.

On April 12, 1978, the preparations were finished to start the search. Already on May 2, 1978, thanks also to the precise determination of the mass by the Columbia-Fermilag-Stony Brook collaboration, the Υ was found at DORIS by the PLUTO[38] and DASP2[39] collaborations simultaneously. The original data of this search are shown in fig. 13 which displays the visible cross section in both detectors as a function of energy. A clear signal at 9.46 GeV is seen in both experiments.

From these original data both groups agreed on a mass value of M_Υ = 9.46 ±.01 GeV, an electronic width of Γ_{ee} = 1.3 ±.4 keV and a total width of the resonance Γ_{tot} < 18 MeV. Note that the error on the mass is due to the DORIS calibration uncertainty and the width corresponds to the DORIS energy spread. These values already strongly favoured an interpretation of the Υ being a bound state of a new quark-antiquark pair with a charge of 1/3 [38].

b) Determination of parameters

The immediate issue of e^+e^- physics of the Υ is, of course, a determination of the leptonic and the total width of the resonance. The leptonic width Γ_{ee} can be inferred directly by integrating the hadronic cross section of the resonance according to the formula

$$\frac{M^2}{6\pi^2} \int \sigma_{had}\, dE = \frac{\Gamma_{ee}\,\Gamma_{had}}{\Gamma_{tot}} \approx \Gamma_{ee}$$

assuming $\Gamma_{ee}/\Gamma_{had} \ll 1$. The integral extends to infinitely high energies which in practice means that radiative corrections have to be applied properly. The absolutely normalized results of the PLUTO group[40] are shown in fig. 14. The results of two other experiments, the DASP2 group[42] and the NaJ-lead glass detector[41], which replaced the PLUTO detector after its move to PETRA, are shown in fig. 15.

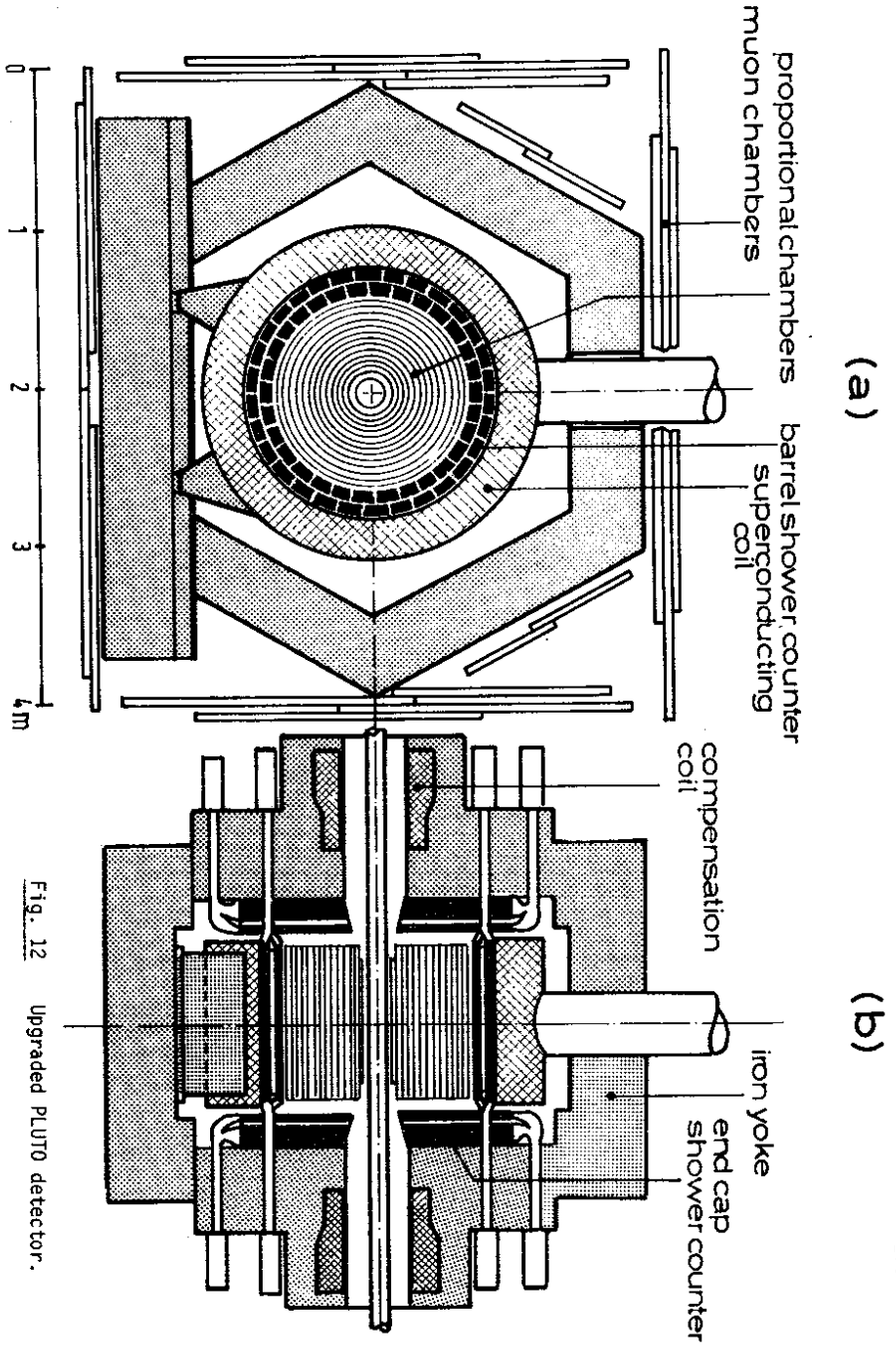

Fig. 12 Upgraded PLUTO detector.

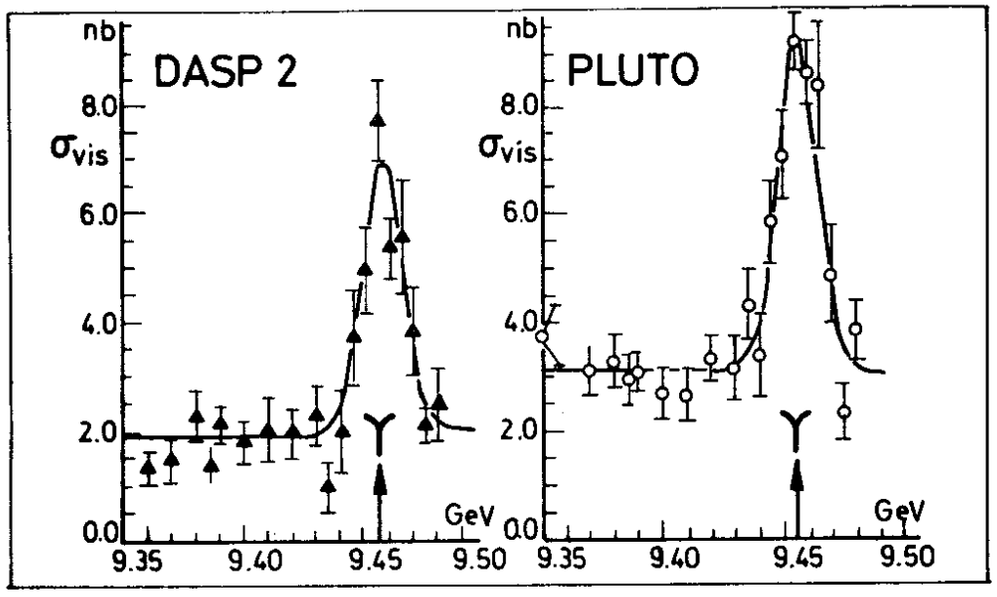

Fig. 13 PLUTO and DASP 2: the original evidence for Υ production in e^+e^- annihilation.

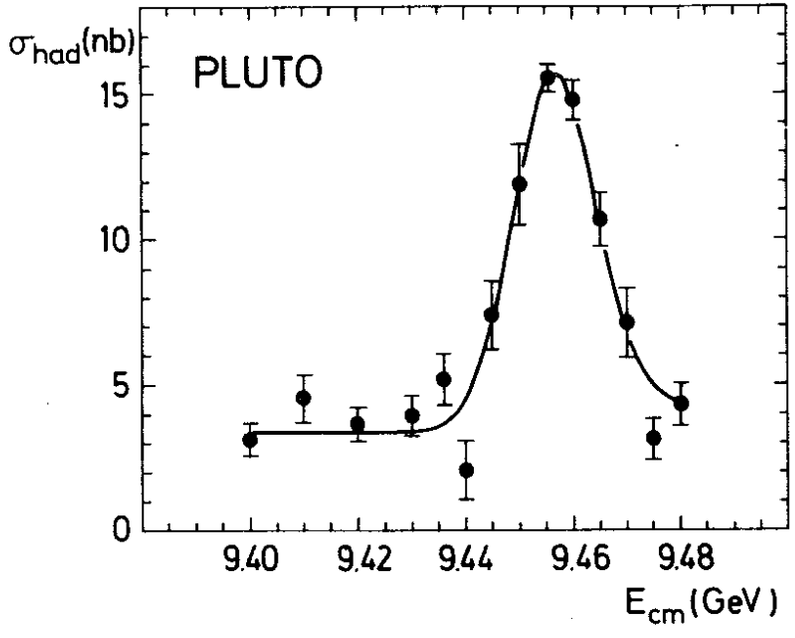

Fig. 14 PLUTO: Absolutely normalized hadronic cross section in the Ypsilon region. The curve is a Breit-Wigner fit including radiative corrections. $\Gamma_{ee}, \Gamma_{tot}$ and the machine resolution are free parameters.

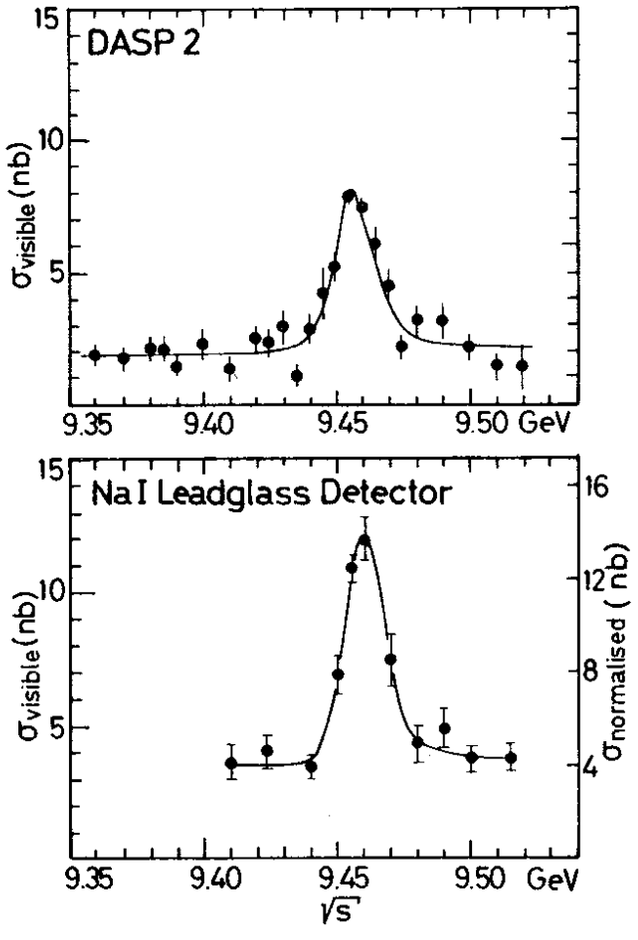

Fig. 15 DASP 2 and DESY-Hamburg-Heidelberg-München collaboration: visible cross section for e^+e^- → hadrons in the Ypsilon region.

(The latter detector was operated by a DESY-Hamburg-Heidelberg-München collaboration.) Their values are not absolutely normalized. For a determination of the leptonic width Γ_{ee} both detectors used the PLUTO value of R at 5 GeV. The results of the three experiments are summarized in table 4.

Table 4 Results on Y(9.46)

	M (Y) (GeV)	Exp. Width (MeV)	Γ_{ee} (Y) (keV)	$B_{\mu\mu}$ (%)	Γ_{tot} (keV)
PLUTO	9.46 ±0.01	17.2 ±0.2	1.33 ±0.14	2.2 ±2.0	>23(2s.d.)
DASP2	9.46 ±0.01	18 ±2	1.5 ±0.4	2.5 ±2.1	>20(2s.d.)
D-H II	9.46 ±0.01	17 ±2	1.04 ±0.28	$1.0^{+3.4}_{-1.0}$	>15(2s.d.)

Mean Values: Γ = (1.32 ±0.09) keV

$B_{\mu\mu}$ = (2.3 ±1.4) %

Γ_{tot} > 25 keV (95 % c.l.)

An attempt was made by the three groups[40-42] to determine the total width of the resonance. To this end one has to measure the μ pair branching ratio $B_{\mu\mu}$ on the resonance. Assuming μe universality, the total width can then be obtained from $\Gamma_{tot} = \Gamma_{ee}/B_{\mu\mu}$. In all three experiments the determination of $B_{\mu\mu}$ suffers from very low statistics. The angular distribution of the PLUTO events[40] is shown in fig. 16. The data are in good agreement with the expectation of $1 + \cos^2\theta$. The values of $B_{\mu\mu}$ obtained from the three experiments are summarized again in Table 4.

Due to the large error on $B_{\mu\mu}$ only lower limits can be given for the total width of the resonance. Even if all values are combined the error is still too large to obtain a two standard deviation upper limit on the total width. Again one can only obtain a lower limit of 25 keV on a 95 % confidence level. (Note that this limit justifies our previous assumption $\Gamma_{ee}/\Gamma_{had} << 1$.) If we take $B_{\mu\mu}$ = 2.3 % at face value we find the 'best' total width of

Γ_{tot} = 57 keV.

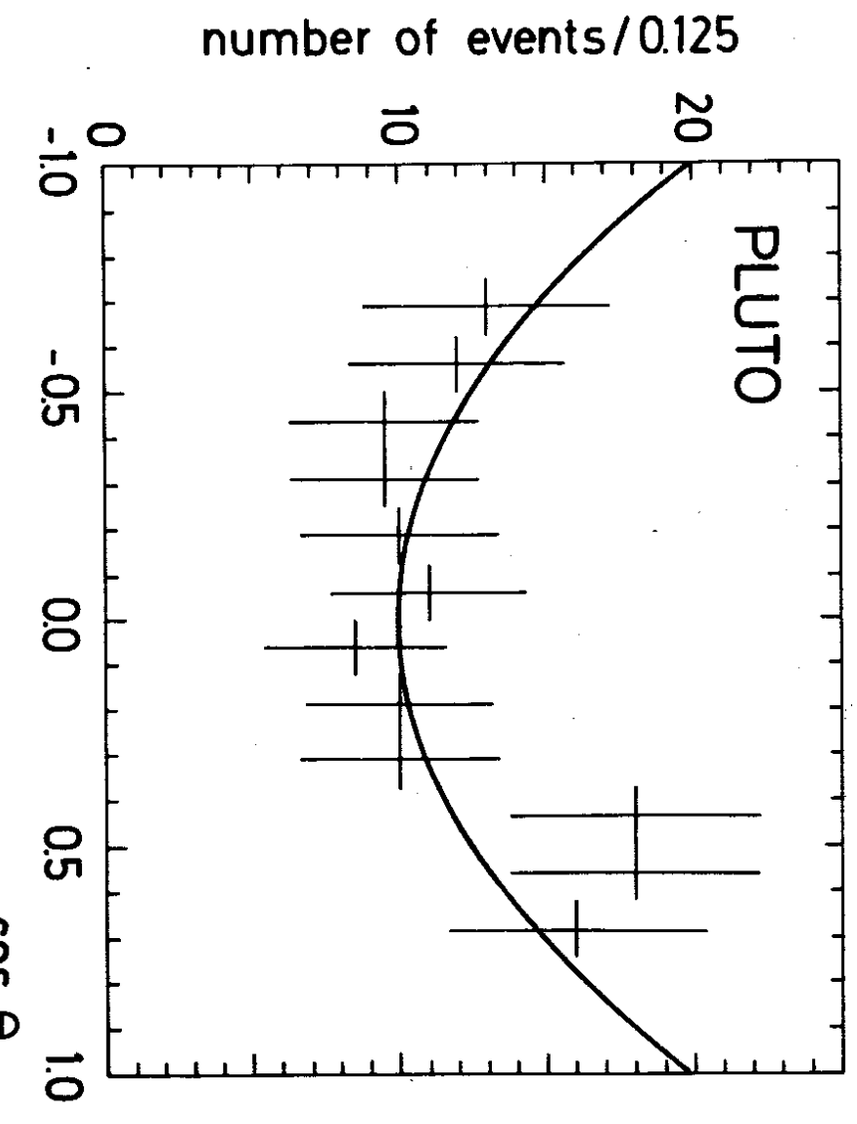

Fig. 16 PLUTO: angular distribution for muon pairs produced in the Ypsilon region. Data on and off resonance are combined. The curve is proportional to $1+\cos^2\theta$.

c) Ypsilon prime

In August 1978 the DASP2 [42] and the NaJ-lead glass groups[41] advanced into the region of 10 GeV to search for the first excitation in the Y family (Y'). Fig. 17 shows their results. There is a resonance structure around 10.02 GeV with a width compatible with the resolution of the e^+e^- machine DORIS. In table 5 the parameters of the Y' as found by the two groups are compiled together with the mean values. A surprising feature of these data is the relatively low mass difference between Y and Y'. In particular $\Delta M(Y) = 558 \pm 10$ MeV is smaller than $\Delta M(\psi) = 589 \pm 1$ MeV.

Table 5 Results on Y'(10.02)

	M(Y') (GeV)	M(Y')-M(Y) (MeV)	$\Gamma_{ee}(Y')$ (keV)	$\frac{\Gamma_{ee}(Y)}{\Gamma_{ee}(Y')}$
DASP2	10.012 ±0.020	555 ±11	0.35 ±0.14	4.3 ±1.5
D-H II	10.02 ±0.02	560 ±10	0.32 ±0.13	3.3 ±0.9
Mean	10.016 ±0.020	558 ±10	0.33 ±0.10	3.6 ±0.8

d) Quark charge and number of Y states

What are the conclusions that can be drawn from these results?
The leptonic widths of the states are $\Gamma_{ee}(Y) = 1.32 \pm 0.09$ keV and $\Gamma_{ee}(Y') = 0.33 \pm 0.10$ keV. Since $\Gamma_{ee} \sim Q_q^2$ is sensitive to the quark charge, a comparison with model predictions may decide on the type of constituent quark[17]. Fig. 18 shows lower bounds on Γ_{ee} for 1/3 and 2/3 charge deduced from rather general assumptions[43]. The measurements indicated in the figure exclude charge 2/3. They coincide nicely with the shaded region indicating the area allowed for $Q_b = -1/3$ in a large class of potential models[43].

Duality arguments[44] predict that the reduced leptonic width Γ_{ee}/Q_q^2 should be mass independent. Fig. 19 shows that this quantity is in fact surprisingly constant up to the Y mass if we assume $Q_b = -1/3$. Note the reduction of error bars since 1978.

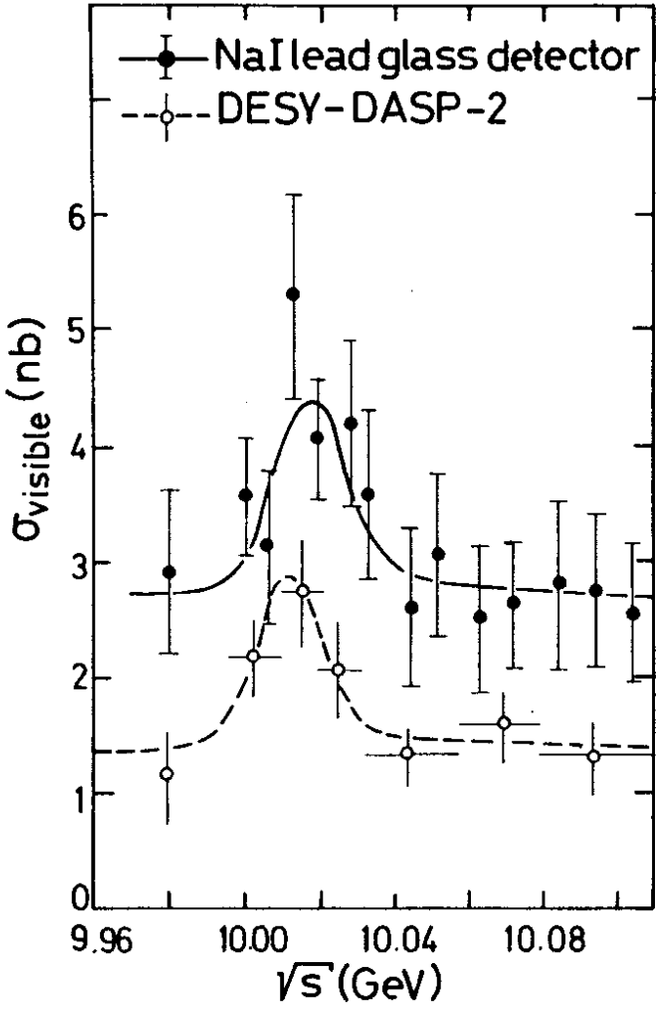

Fig. 17 DASP 2 and DESY-Hamburg-Heidelberg-München collaboration. Evidence for the Ypsilon Prime in e^+e^- annihilation.

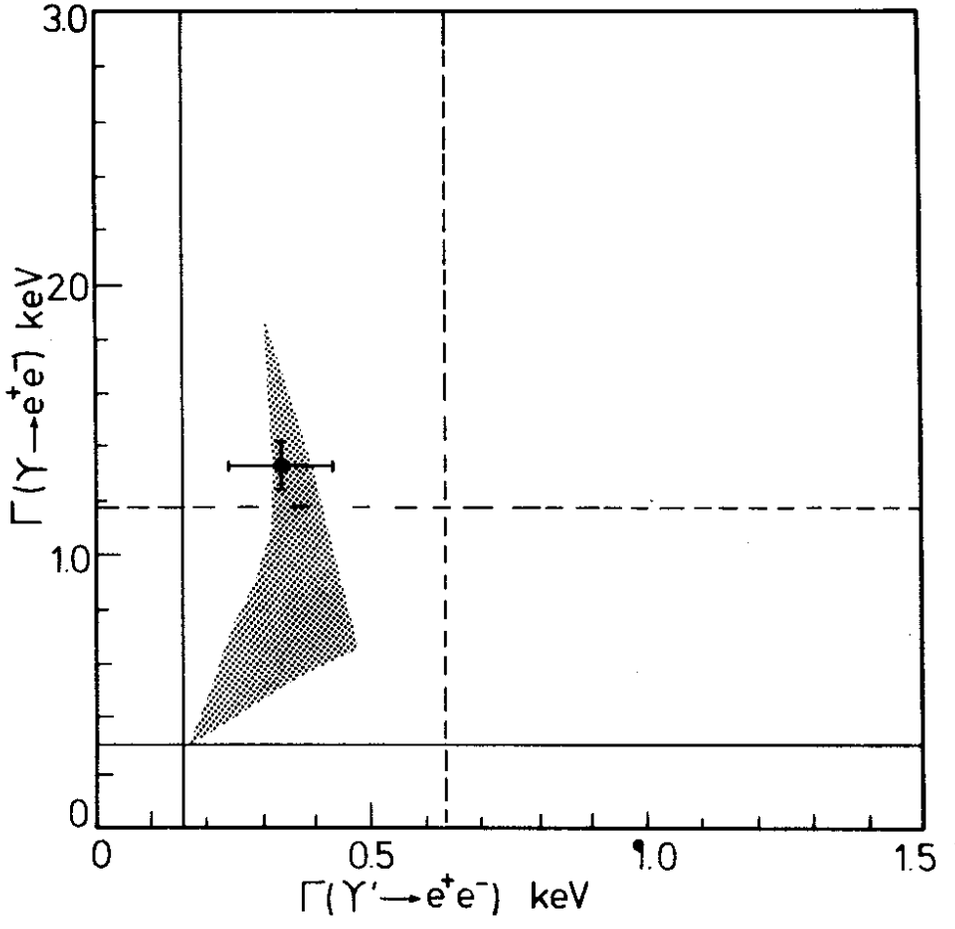

Fig. 18 Lower bounds on Γ_{ee} for Υ and Υ' for different quark charges. The shaded area indicates the charge 1/3 predictions of 20 different potential models. A comparison with the DORIS data shows good agreement with charge 1/3 and excludes charge 2/3.

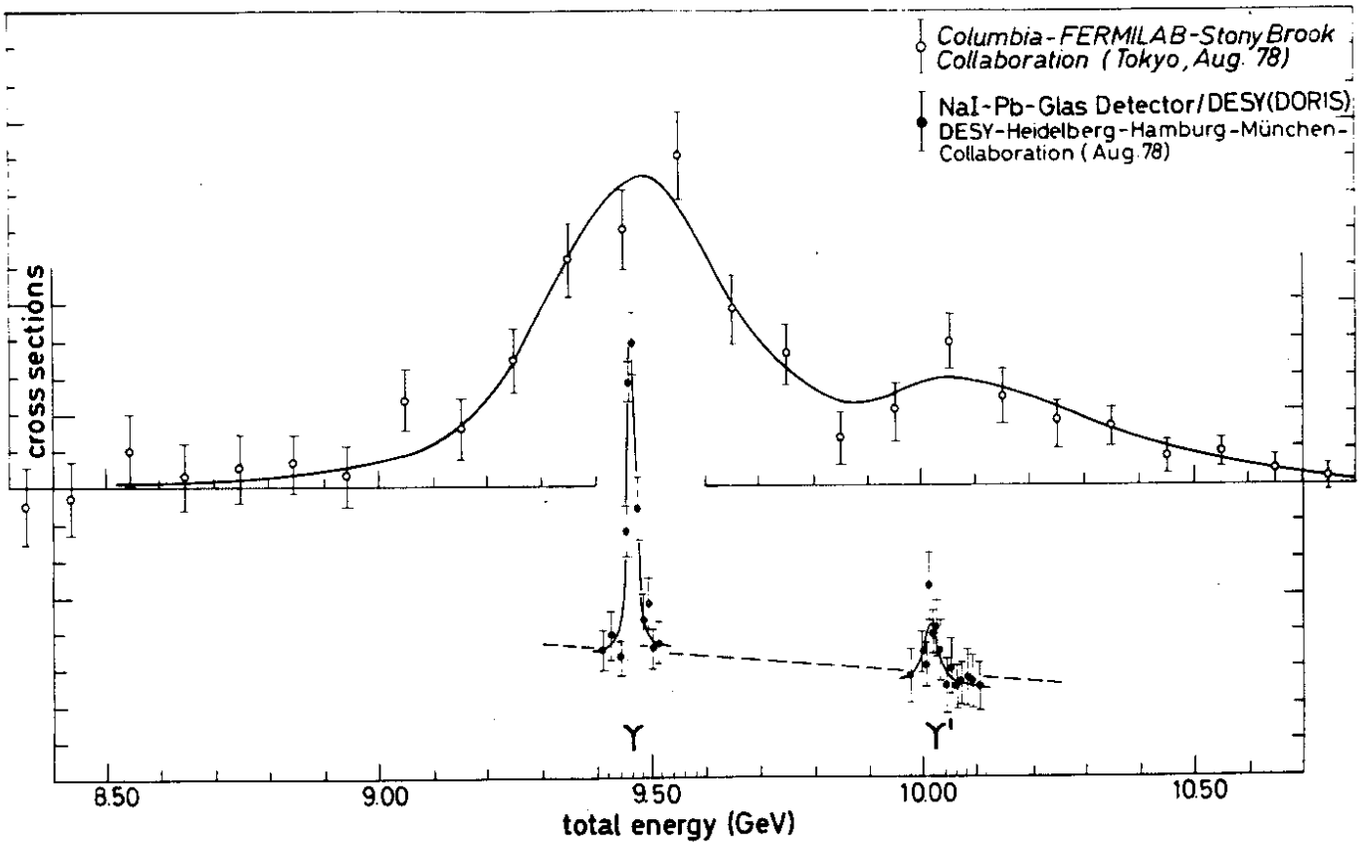

Fig. 20 Columbia-Fermilab-Stony Brook and DESY-Hamburg-Heidelberg-München Collaborations: The Υ family in hadronic and e^+e^- reactions.

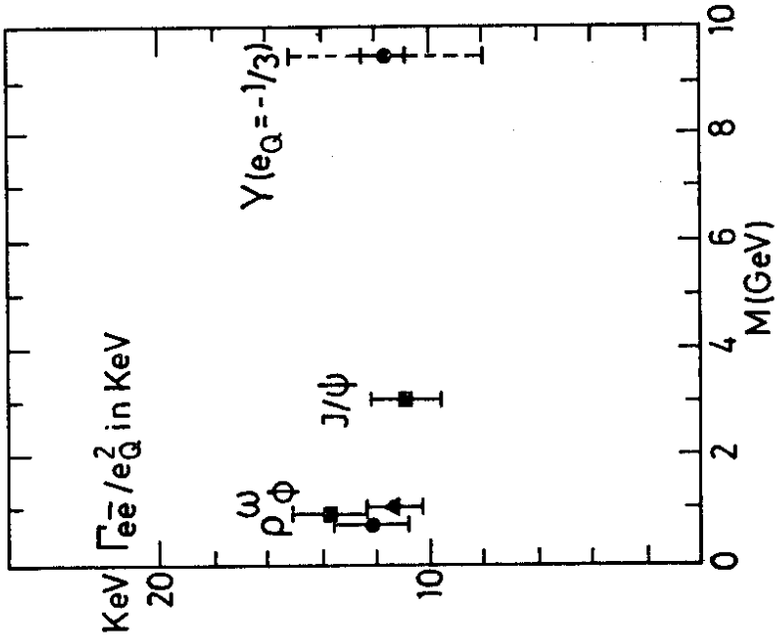

Fig. 19 Reduced leptonic width Γ_{ee}/Q_q^2 for vector meson ground states as a function of mass (dashed error bars: August 1978).

Fig. 20 shows a comparison of the FNAL and DESY data shown at the Tokyo conference in August 1978. The mass difference of M = 558 ±10 MeV is more precise and lower than the one suggested by the Columbia-Fermilab-Stony Brook collaboration. This group, therefore, imposed the DORIS value on a fit of their data[37]. Thus they increased the evidence for a third state in the Y family from 4 to 11 standard deviations. They obtained a mass value of

$$M(Y'') = 10.41 \pm 0.05 \text{ GeV}.$$

e) Summary

In summary we have seen that Ypsilon and Ypsilon Prime are produced as narrow resonances in e^+e^- collisions. Their masses are M(Y) = 9.46 ±0.01 GeV and M(Y') = 10.02 ±0.01 GeV. The leptonic widths are in agreement with a charge 1/3 of the constituent quark and exclude a charge 2/3. The low mass difference improves the evidence for a third Ypsilon resonance in the FNAL data.

Thus there is strong evidence for a b quark, the counterpart of the τ in the proposed third generation of quarks and leptons. However, there is still a long way to go to reveal any detailed properties of this new quark.

What about the sixth components? The τ neutrino is not rigorously proven and t is still waiting for discovery (if it exists).

III. EVENT TOPOLOGY

1. Jets below 9.4 GeV

We have seen in chapter I that the asymptotic behaviour of R is in good agreement with the simple description of the quark-parton model. Let us, therefore, assume that quark pair production really governs the process

$$e^+ e^- \rightarrow \text{hadrons}.$$

In this picture the two quarks should fragment to form two back-to-back jets of particles (fig. 21).

What are these jets like? In the quark-parton model jets are described in a phenomenological way by a fragmentation of quarks with limited transverse momentum with respect to the original quark axis. On the other hand QCD tells us that jets are produced automatically by gluon bremsstrahlung in the framework of perturbative QCD[45]. Since in this process the transverse momentum increases with energy it will eventually win over the quark-parton process once the energy is high enough[46].

For the poor exerimentalist finally a jet is a bunch of particles, which he has to isolate within the limited acceptance and the measurement errors of his detector.

Fig. 22 shows a very clean jetlike event from the PLUTO detector. Two distinct back-to-back bunches of particles are clearly visible. Also the neutral energy of the two jets is clustered and follows the charged energy. Unfortunately, even at these high energies of about 9.4 GeV only few events show a jet structure in such a nice way. Therefore a more realistic random selection of events around 9.4 GeV is given in fig. 23. To reveal any topological structure in these events we certainly need quantitative measures of event topologies.

a) Quantities to measure jets

Several quantities have been proposed to measure jets. I will only use two of them here, namely sphericity[47]

$$S = \frac{3}{2} \min \frac{\sum_i p_{\perp i}^2}{\sum_i p_i^2}$$

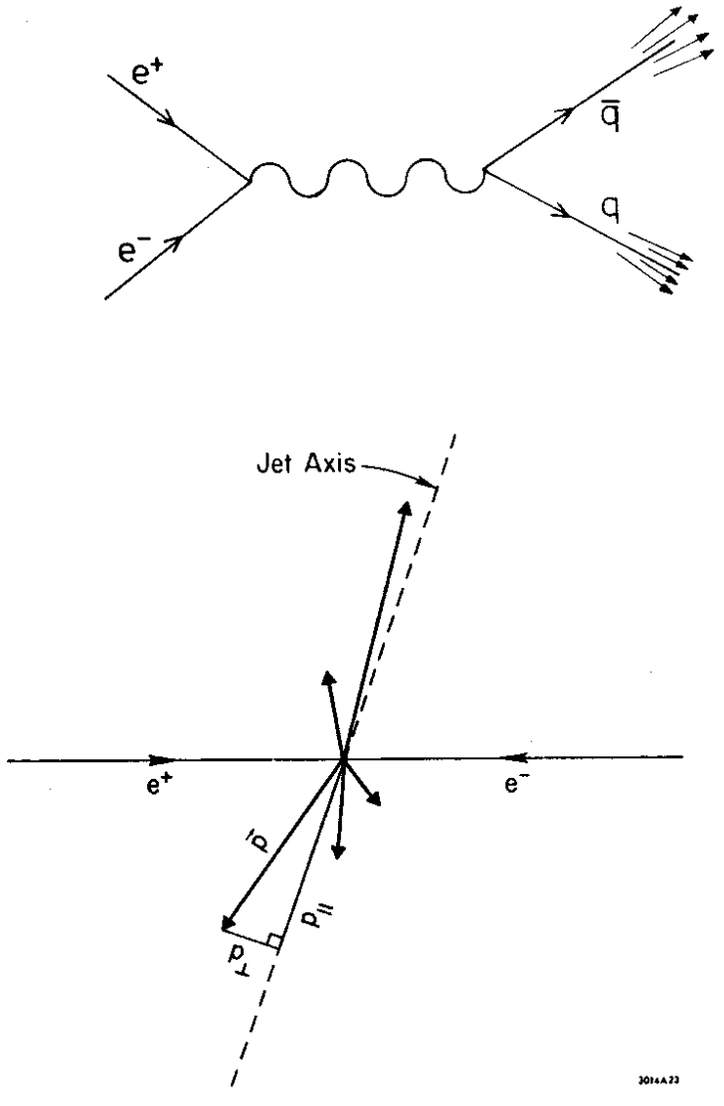

Fig. 21 Definition of quantities used in the jet analysis.

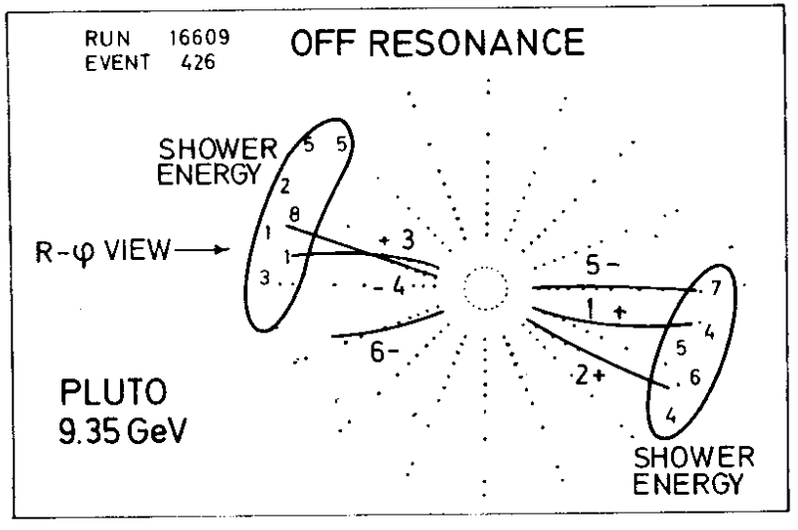

Fig. 22 PLUTO: a non-typical nice jetlike event of E_{CM} = 9.35 GeV.

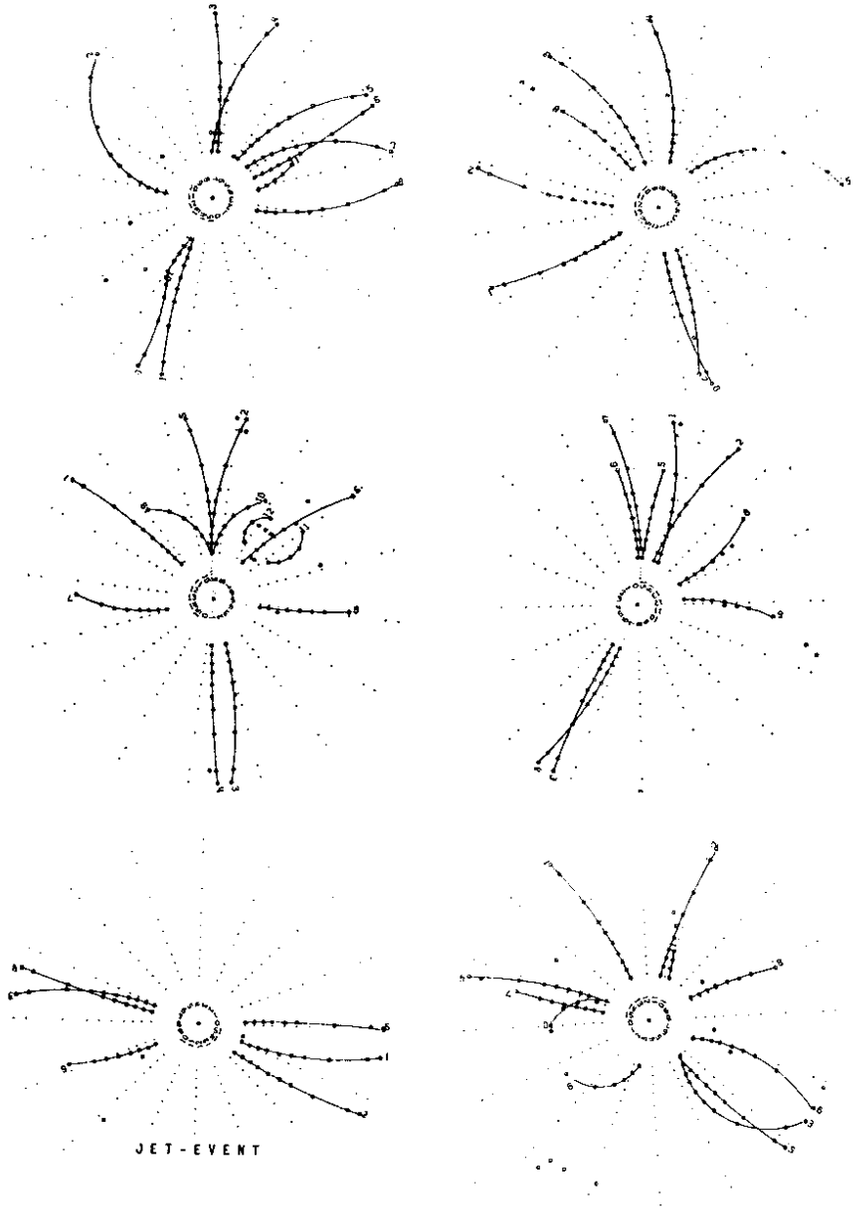

Fig. 23 PLUTO: a random selection of events around E_{CM} = 9.4 GeV.

and thrust[48]

$$T = \max \frac{\sum_i |p_{Li}|}{\sum |p_i|}$$

(This definition is slightly different from the original one, where the sum for p_L runs over one hemisphere only.)

Both quantities simultaneously define the jet axis and give a measure for the topological structure of the event. The axis is found in a variational method by either minimizing the sum of the transverse momentum squared (p_T^2) or maximizing the sum of the absolute longitudinal momentum component ($|p_L|$) with respect to a given axis (fig. 21). Extreme values of the two quantities for isotropic or ideally jetlike events are summarized in table 6.

Table 6 Values for S and T in extreme topologies

Events	S	T
isotropic 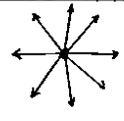	→ 1	→ 1/2
ideally jetlike 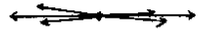	→ 0	→ 1

If we assume that p_T is about constant the quantities <S> or <1-T> will both fall with increasing energy (assuming that the multiplicity is only slowly varying).

Sphericity has the virtue that it can be easily calculated by standard diagonalization methods. It will, therefore, be used in most of the following analysis. However, since the momenta enter quadratically, high momentum particles get a stronger weight in <S>. Also it is not invariant against clustering (multiplicity) of particles. Therefore, theorists dislike it, because it depends on details of the fragmentation. They rather introduced a third jet measure, spherocity[49],

which is linear in the momenta. However, this quantity suffers from discontinuities and, therefore, cannot easily be applied to data analysis (Brandt and Dahmen in ref. 48).

b) SLAC-LBL results

In 1975 the topological structure of charged particles emerging from e^+e^- reactions was studied at SLAC[50]. This analysis covered a c.m. energy range up to 7.8 GeV. The results in terms of sphericity are shown in figs. 24 and 25. We realize a drastic decrease of $\langle S \rangle$ with increasing c.m. energy between 2.4 and 7.8 GeV. These features of the data are in good agreement with a quark-parton model and cannot be described by a simple phase space distribution (figs. 24 and 25). The results were generally taken as first evidence for jets in e^+e^- reactions. In addition it was shown that the jets are governed by limited transverse momentum as expected in a simple quark-parton model. The angular distribution of the jets was found to follow a $1+\cos^2\theta$ distribution as expected for the production of spin 1/2 particles.

c) PLUTO results at DORIS

New results on the subject have become available recently from the PLUTO collaboration[51]. These data cover an even larger energy range from 3.6 to 9.4 GeV c.m. energy.

Like in the SLAC-LBL data results are so far mainly based on an analysis of the charged tracks. Since the momentum resolution is degrading rapidly in the very forward direction only tracks with $\cos\theta$ less than 0.85 have been used. Hadronic events were selected according to their total energy and their charged multiplicity:

$$E_{tot} = E_{neut} + E_{ch} > 0.6\, E_{CM}$$

$$n_{ch} \geq 4$$

The beam gas background is low. It is estimated from events outside the interaction point and subtracted. The remaining background due to various QED processes (mainly e^+e^-, $\gamma\gamma$ processes and τ pair production) is estimated to be of the order of less than 10 %.

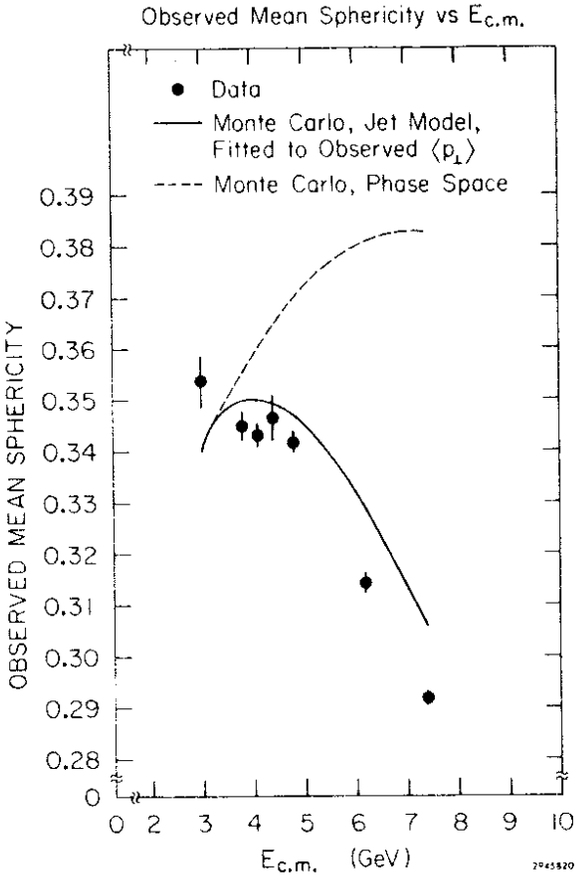

Fig. 24 SLAC-LBL Collaboration: First evidence for jets in e^+e^- annihilation. Observed mean sphericity as a function of energy. The full and dashed line show Monte-Carlo simulations of a jet and phase space model, respecticely.

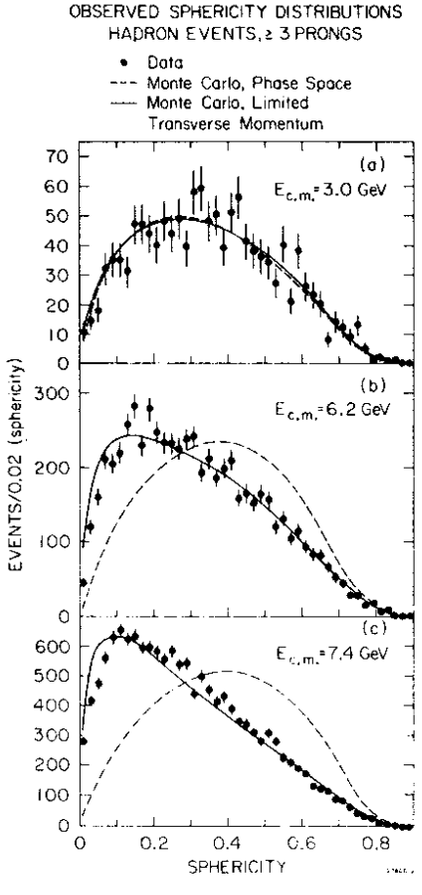

Fig. 25 SLAC-LBL: sphericity distributions observed at E_{CM} = 3.0 GeV (a), 6.2 GeV (b) and 7.4 GeV (c). Data are compared with a jet model (solid curve) and a phase-space model (dashed curve).

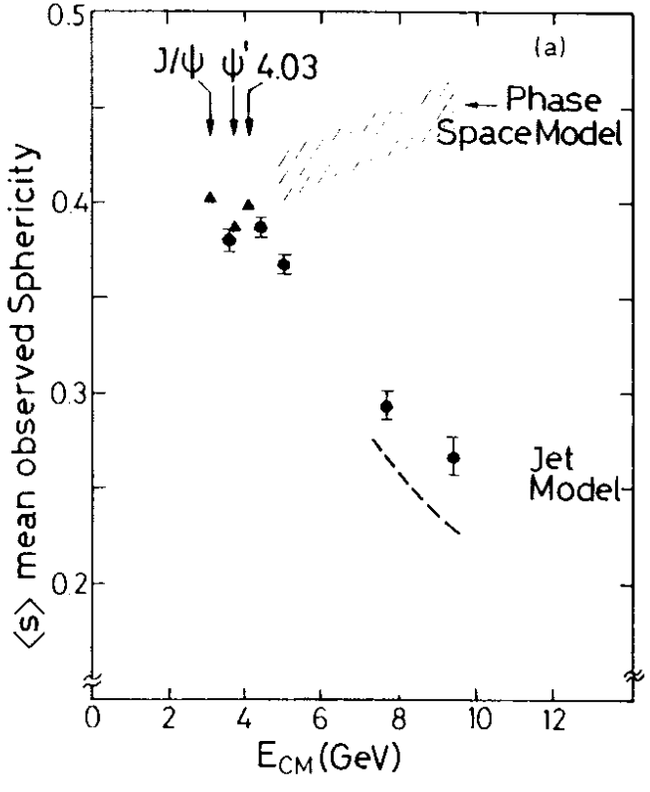

Fig. 26 PLUTO: mean observed sphericity of charged particles (≥ 4 prongs) as a fucntion of E_{CM}. The shaded area represents the phase-space prediction, the dashed curve the two-jet model without radiative corrections.

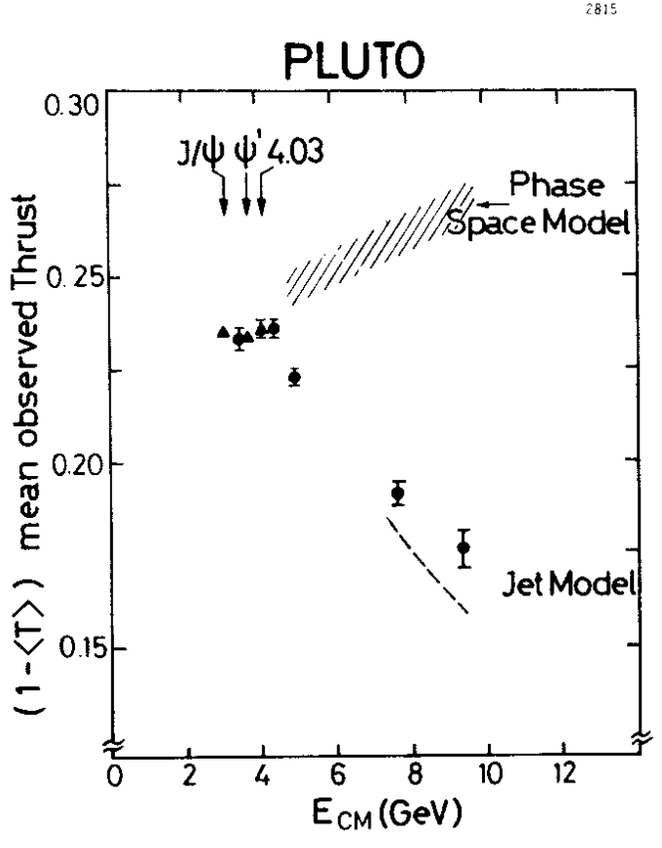

Fig. 27 PLUTO: mean observed thrust as a function of E_{CM} ·<1-T> is plotted for easier comparison with <S>. Model predictions like in fig. 26.

Fig. 26 shows the observed mean sphericity as a function of c.m. energy in the range from 3.6 to 9.4 GeV. <S> decreases drastically with increasing energy. Fig. 27 shows the same trend for <1-T>. Again mean observed values are given. Qualitatively both quantities behave as expected for a jetlike structure of the hadronic final state. To get a quantitative comparison with models the following procedure was applied throughout this section.

- We define a model.
- We generate events according to this model and pass them through a realistic Monte-Carlo simulation of our detector.
- We compare the results of these Monte-Carlo calculations with our observed quantities.

The data were compared with two models.

(1) The phase-space model
The particles were produced according to phase space assuming π production only. The mean charged multiplicity and the neutral energy were adjusted to the experimentally observed values.

(2) Two jet Monte Carlo (Feynman-Field parametrization)
The Feynman-Field model[52] is a parametrization of quark parton jets. The application of this model to e^+e^- reactions is sketched in fig. 28. The dressing of

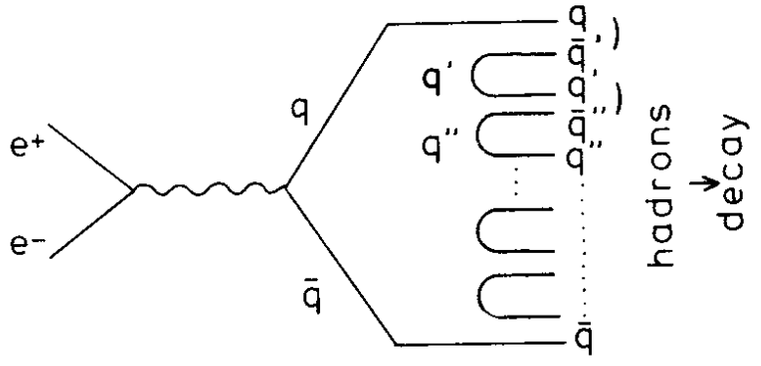

Fig. 28 The fragmentation of quarks from $e^+e^- \to q\bar{q}$ in the Feynman-Field model.

the primary quark antiquark pair proceeds through a chain of other quark antiquark pairs which are picked up from the vacuum. Thus mesons are produced down the chain until all the energy is used up. This process is completely determined by the following assumptions:

Fragmentation function

In each step a probability $f(\eta)$ is calculated that a hadron takes $(1-\eta)$ of the available momentum with it.

The production of $s\bar{s}$ pairs is assumed to be half as likely as $u\bar{u}$ production.

The production of vector mesons and pseudoscalar mesons is assumed to be equally probable.

Finally the decay of all primary hadrons is included in the model. The function $f(\eta)$ is chosen such that the fragmentation function $D(z)$ fits deep inelastic lepton and e^+e^- data. ($D(z)$ describes the momentum distribution of particles along the original quark direction.)

Limited transverse momentum

Particles in the chain of fig. 28 are produced with limited transverse momentum. It is chosen such that the final mean transverse momentum of the decay products is about 330 MeV. This is again adjusted to lepton and e^+e^- data.

With these assumptions all parameters are fixed. The model has been applied without further adjustments. Note that charm production is not included in the present version of the Feynman-Field model.

The results of these two model calculations for sphericity and thrust are given in figs. 26 and 27, respectively. We observe good agreement between the data and the Feynman-Field calculations whereas a simple phase-space description is completely ruled out. The agreement with Feynman-Field may look surprising since charm is not included in the model. However, adding charm has only little effect on $\langle S \rangle$. This can be qualitatively explained by the fact that far above threshold all quark jets behave very similarly. I will come back to this point in the last chapter.

How well is the axis defined?

We have seen that the gross features of our events expressed in terms of sphericity or thrust agree very well with the features of a simple jet model. Be-

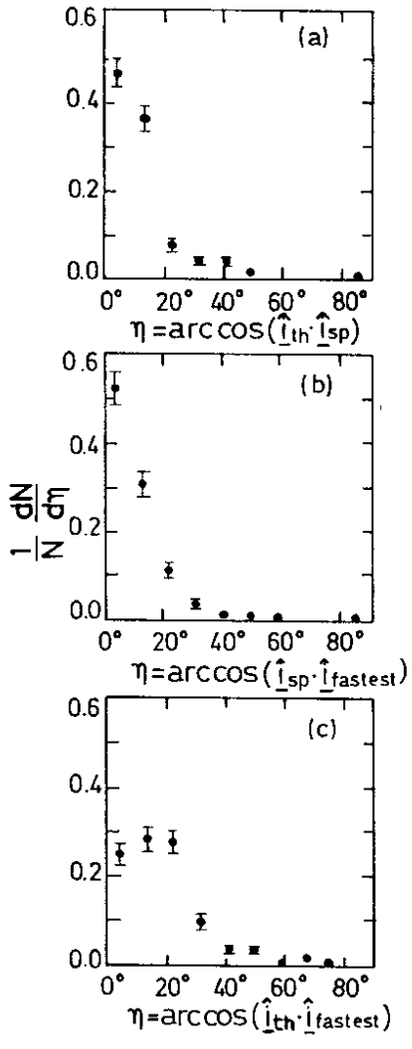

Fig. 29a) PLUTO: the relative angle between the jet axes as defined by thrust or sphericity or the fastest particle in the jet.

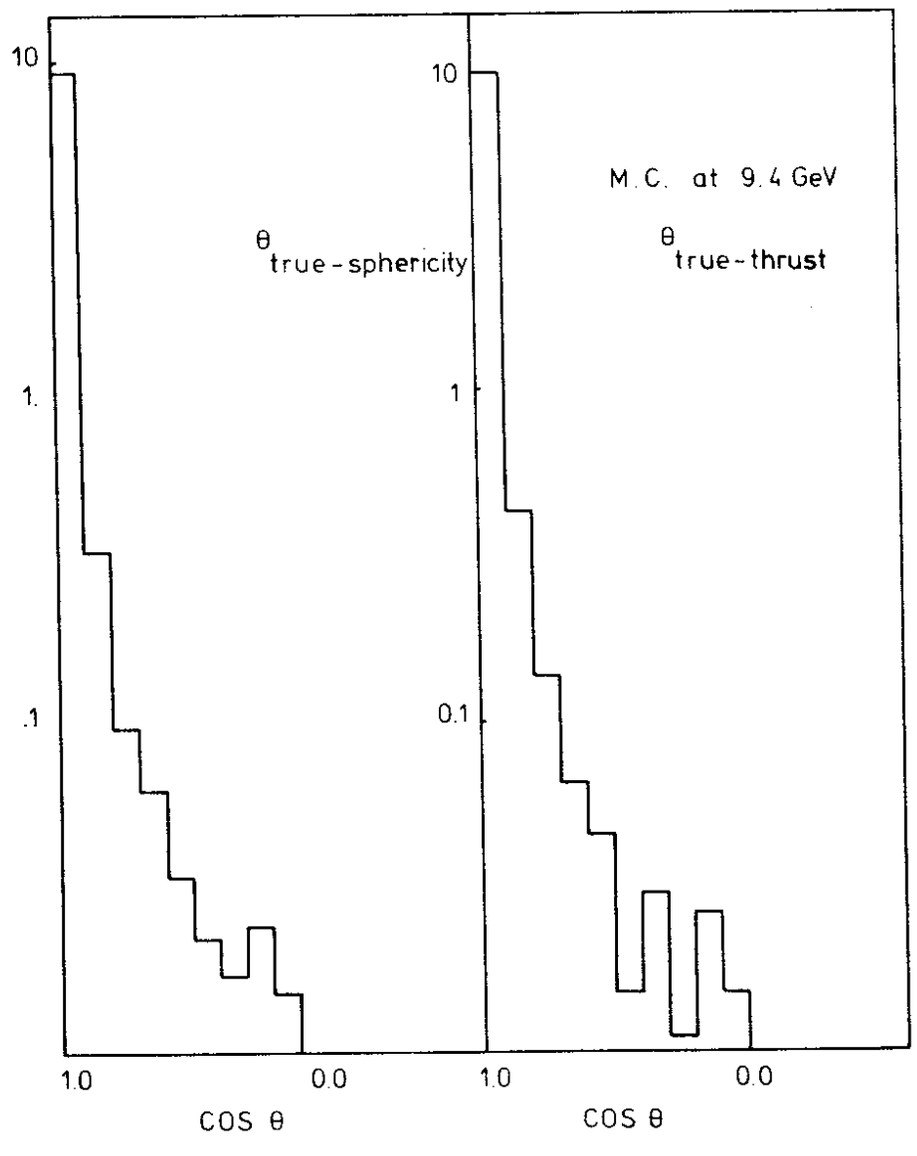

Fig. 29b) Two-jet model calculations: relative angle between the generated quark axis and those defined by thrust and sphericity.

fore we go any further into the description of detailed features of these data we should get an impression how well the jet axis is defined. Fig. 29a shows distributions of the relative angles between the axis as defined by sphericity, thrust or the fastest particle in the jet. The mean width of these distributions is about 15^{o}. This gives a rough estimate of the uncertainty with which the jet axis is defined. Monte-Carlo studies indicate that the relative angle between the original quark axis and the axis defined by sphericity or thrust is even smaller (fig. 29b).

Energy distribution inside a jet

Our next question is whether the neutral and the charged energy flow inside a jet are correlated. Fig. 30 shows the two energy flow distributions with respect to the jet axis (defined by thrust). The data are divided up in different thrust bins. We note that qualitatively the neutral energy distribution follows closely the charged one. In detail there are, however, differences which are most pronounced in the high thrust bin. The excess of charged energy (roughly 20 %) is concentrated at small angles and large thrust. This may just be a reflection of the jet axis being defined by charged particles.

The opening angle of the jets is still rather large. In the two higher thrust intervals the mean half opening angle is 25^{o} and 33^{o} for charged and neutral particles, respectively.

Angular distribution of the jet axis

If jets in $e^{+}e^{-}$ annihilation originate from the production of a pair of quarks the angular distributions of these jets should contain information about the quark spin. Neglecting the quark mass the angular distribution should be $1+\cos^{2}\theta$ for spin 1/2 particles. Fig. 31 shows the angular distribution of the jet axis as defined by thrust for energies of 7.7 and 9.4 GeV. If we fit these data with a function $1 + \alpha \cos^{2}\theta$ we obtain values of $\alpha = 0.76 \pm 0.3$ at 7.7 GeV and $\alpha = 1.63 \pm 0.6$ at 9.4 GeV. Within the large errors these values are consistent with the theoretical prediction of 0.8 and 0.88 at the two energies[53]. These predictions include finite mass effects of the quarks.

p_T and p_L distributions

The basic assumption of the quark-parton model is that the average p_T approaches a limiting value with increasing energy. Fig. 32 shows the mean p_T and mean p_L distributions with respect to the thrust axis as observed in the PLUTO detector.

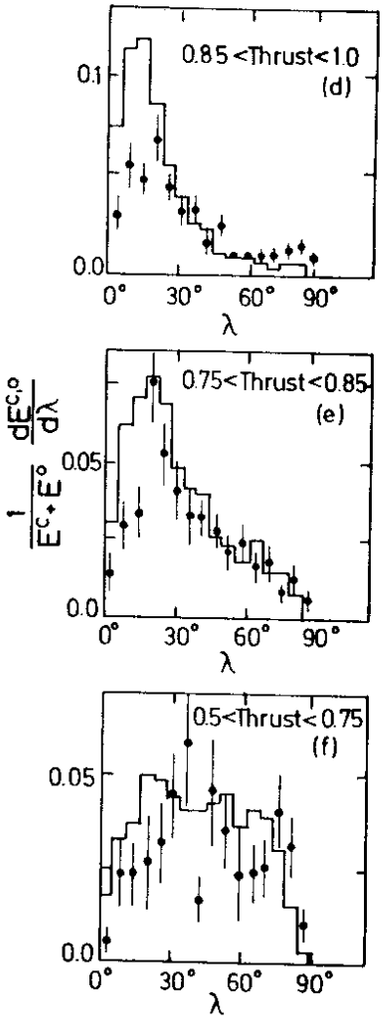

Fig. 30 PLUTO: angular distribution of the energy flow with respect to the thrust axis for three different thrust bins. The charged energy (histogram) and neutral energy (points) are treated separately.

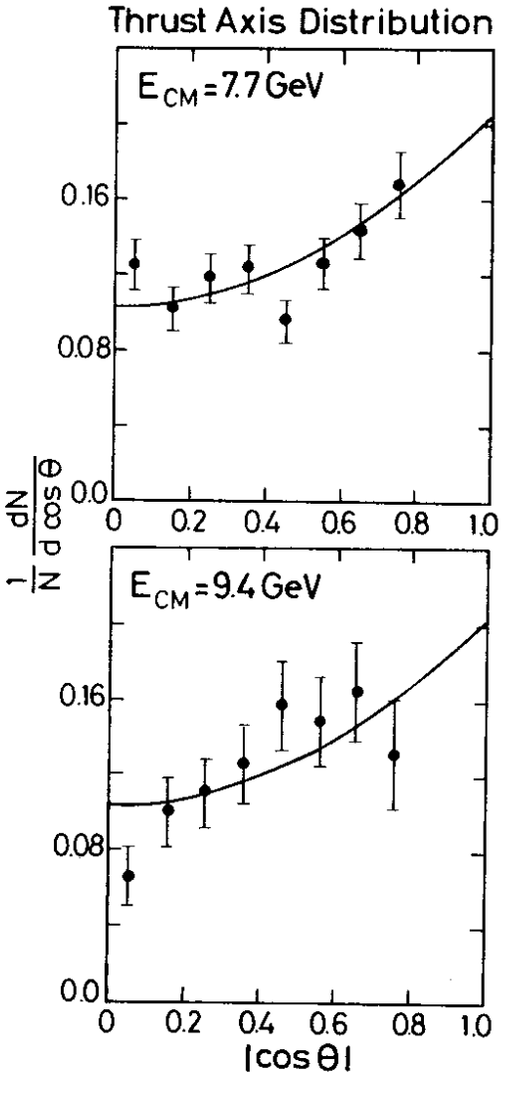

Fig. 31 PLUTO: angular distribution of the jet axis as defined by thrust at 7.7 GeV and 9.4 GeV. The curves are $1+\cos^2\theta$ distributions.

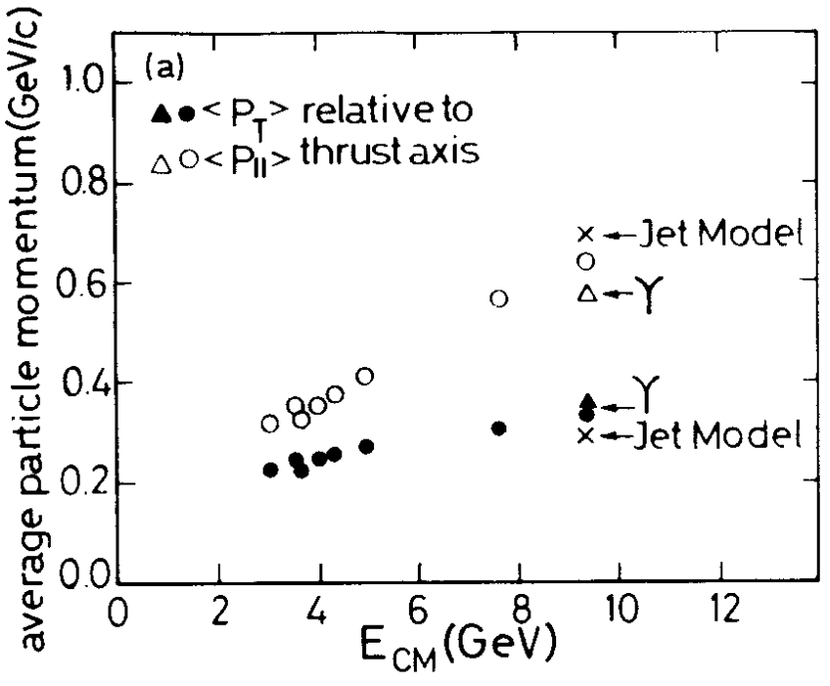

Fig. 32 PLUTO: mean observed p_T and p_L with respect to the thrust axis as a function of c.m. energy. Jet mode calculations and Υ data are given for comparison.

The figure shows indeed that the increase in p_T is slowing down at the highest energies whereas p_L keeps growing nearly linearly. The figure nicely demonstrates again how the jet structure evolves with increasing energy. The half opening angle defined by the transverse and the parallel momentum is 28^0 at 9.4 GeV in good agreement with the value obtained from the energy flow distributions.

Differential distributions and experimental cuts

So far we have only compared gross features of our data like mean observed sphericity and mean observed transverse momentum with different models. We proceed now to differential distributions. At the same time we will try to get a feeling of the effects caused by limited acceptance and measurement errors. We therefore compare our measured values with two kinds of Monte-Carlo predictions:

- Values generated in the Feynman-Field model without passing the events through the detector.
- Distributions after simulating the detector and applying initial state radiative corrections.

Figs. 33 and 34 show the distributions of p_T and S at 9.4 GeV. The comparison with model predictions indicates reasonable agreement with the data once the detector simulation and radiative corrections are applied. However, there is still some discrepancy between model and data at low sphericity values. The comparison between the generated and the final Monte-Carlo distributions shows how far the real distributions are distorted by the detector. The effect is particularly large in the sphericity distribution. Table 7 shows how the mean values of p_T, p_L and S evolve from the generated values to the final ones including corrections. The mean transverse momentum increases only slightly because the distortions in the high momentum part of the distribution get very low statistical weight.

Table 7 The effect of detector resolution, efficiency and radiative corrections on the mean values of p_T, p_L and S. Two jet MC events were generated at 9.4 GeV. All values are calculated with respect to the sphericity axis.

	generated value	including resolution and efficiency	including resolution, efficiency and radiative corrections
$\langle p_T \rangle$	302	317	317
$\langle p_L \rangle$	722	715	655
$\langle S \rangle$	0.20	0.22	0.25

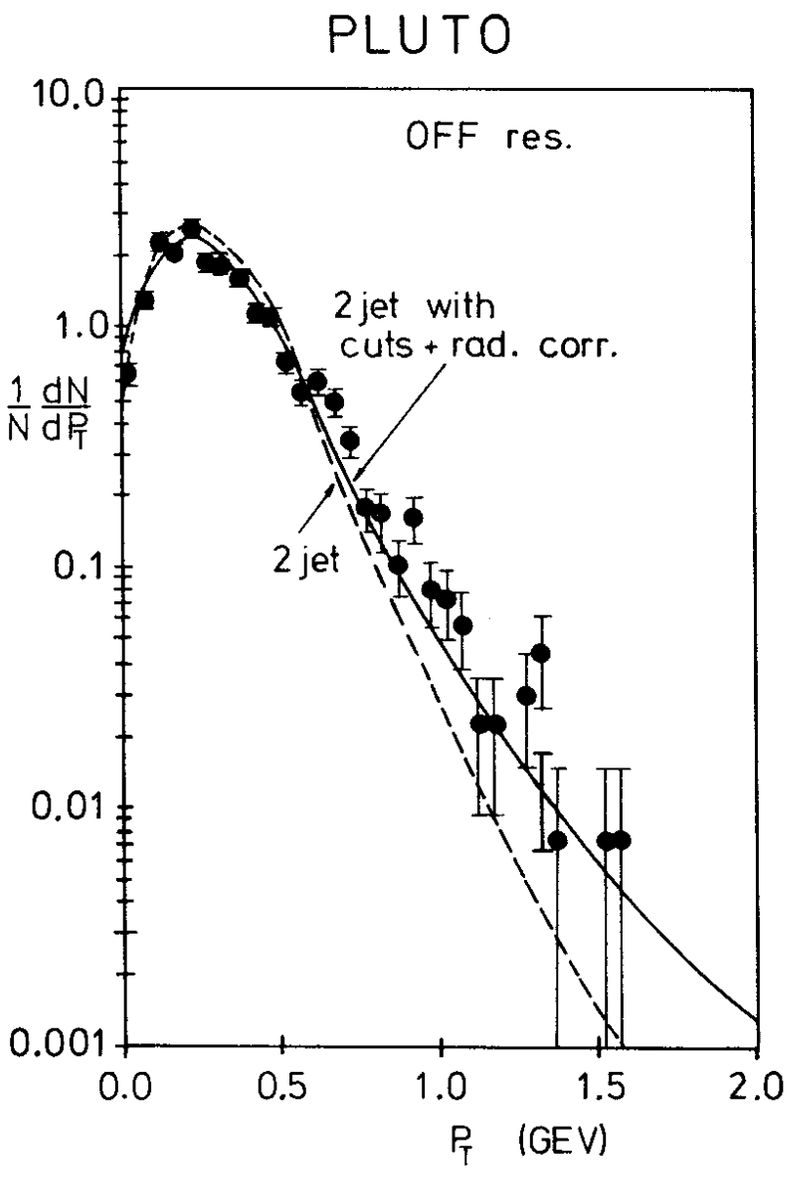

Fig. 33 PLUTO: (preliminary) observed p_T distributions at 9.4 GeV.
a) OFF resonance: the curves are two-jet model predictions including (——) and not including (- -) detector cuts and radiative corrections.

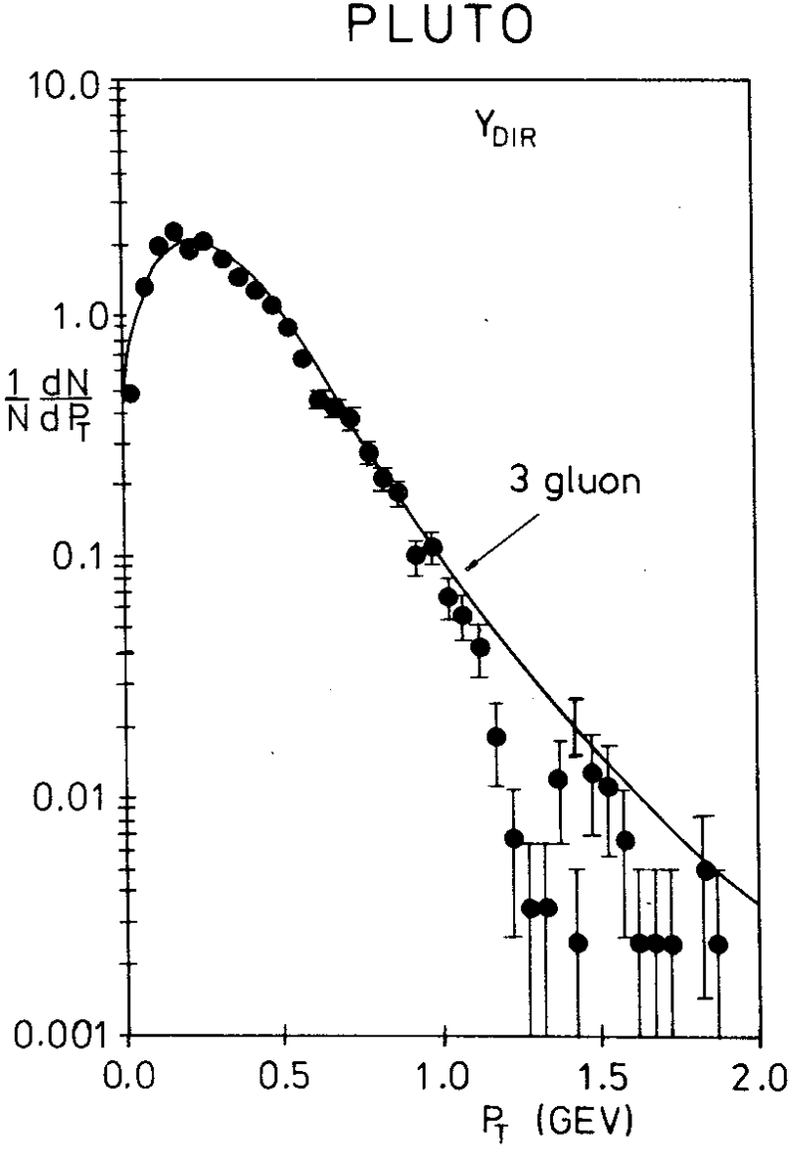

Fig. 33 b) ON resonance: the curve is a three-jet model prediction including all corrections.

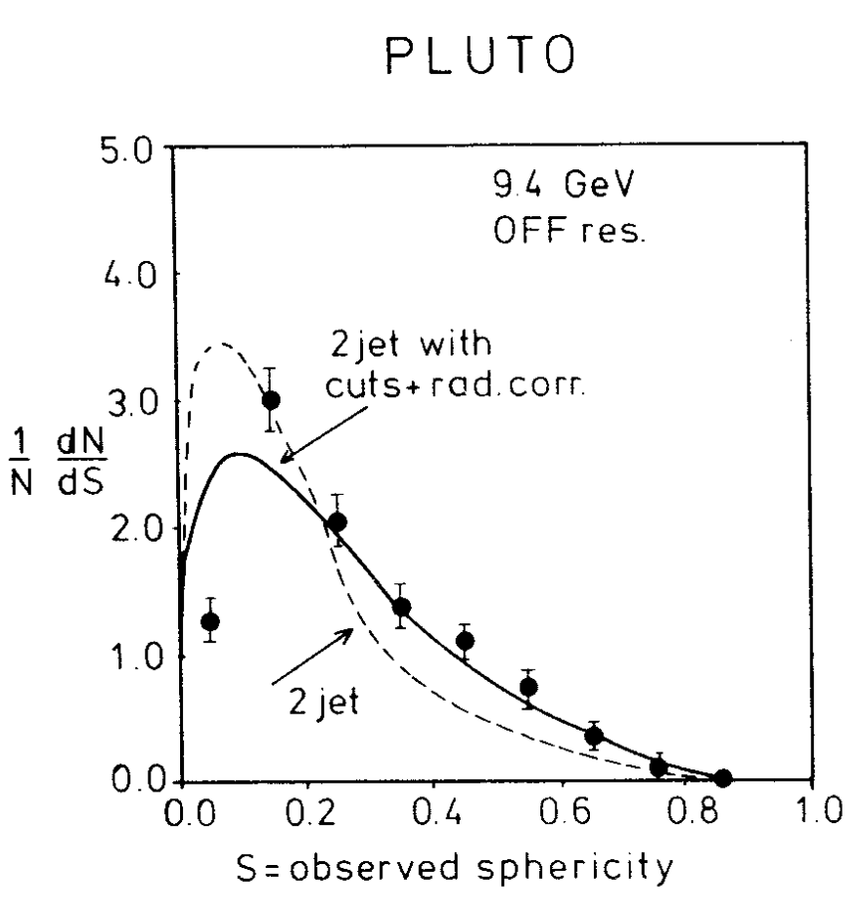

Fig. 34 PLUTO: (preliminary) observed S distributions at 9.4 GeV.
a) OFF resonance: curves as in fig. 33

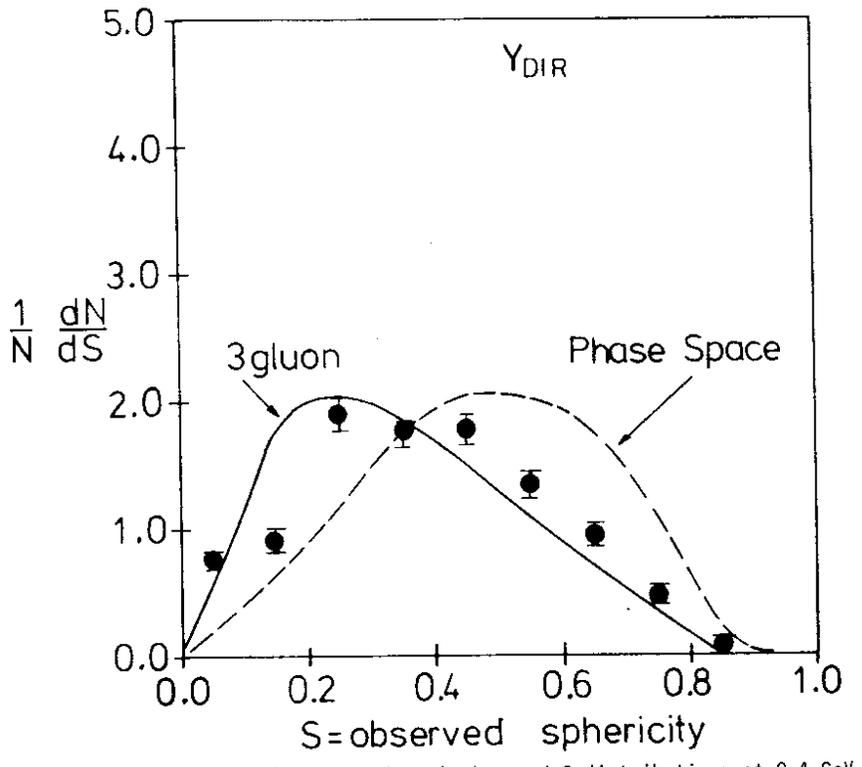

Fig. 34 PLUTO: (preliminary) observed S distributions at 9.4 GeV.
b) ON resonance: curves as in fig. 33

d) Conclusion on jets

The analysis of off-resonance data between 3.6 and 9.4 GeV has shown evidence for quark-parton jets in e^+e^- annihilation into hadrons.

- There is clear (confirming) evidence for the existence of jets with decreasing sphericity.
- Neutral and charged energy are correlated with a common half opening angle of about 30^o at E_{CM} = 9.4 GeV.
- The mean transverse momentum levels off at high energies as expected in the simple quark-parton model.
- The angular distribution of the jet axis is compatible with the production of spin 1/2 particles.

So far we have not discussed any test of QCD gluon bremsstrahlung. I will come back to this point in the last chapter on PETRA data.

2. Y decay topology

In the frame work of QCD a $q\bar{q}$ bound state couples to three gluons. Once the energy of the $q\bar{q}$ state is high enough a fragmentation of these three gluons into jets will become the preferred decay mode (fig. 35a)[7].

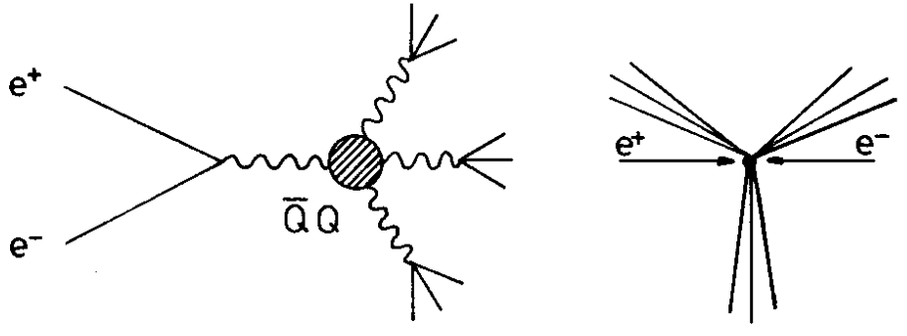

Fig. 35a) Proposed Ypsilon decay into three gluons.

The observation of a three jet structure in the Y decay would therefore be a decisive test on the existence of gluons and the validity of QCD[54-56]. This conjecture leads to the following predictions.

(1) Topological quantities like sphericity and thrust change drastically as one passes through the resonance.

(2) A three jet structure would of course lead to a planar configuration of the events.

(3) Eventually three separated jets may be visible.

Although a possible observation of (1) and (2) may be indicative only (3) could be really decisive. Unfortunately it turns out that an asymmetric partition of energy among the three jets is preferred[54] which leads to a nearly back-to-back structure of the events instead of a symmetric three star structure (fig. 35b).

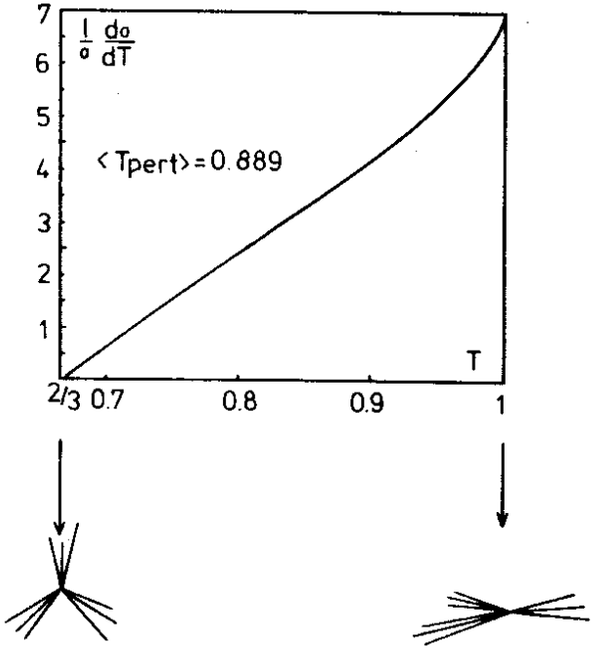

Fig. 35 b) Relative cross section for symmetric and asymmetric three-gluon events.

In addition at the present stage of theory and analysis any interpretation of the data suffers from the following problems.

- The fragmentation of gluons is not known and theoretical predictions are rather vague and controversial[57].
- At the Y resonance the energy of the proposed gluon jets is still very low (about 3 GeV/jet).
- Resonance events can only be separated statistically from the continuum.

a) Experimental procedure

This last point complicates the study of direct Ypsilon decays. The analysis proceeds in three steps.

- Isolate the direct decay mode.
- Define models.
- Compare the uncorrected data with these models.

In this section I will mainly concentrate on experimental results from two groups - the PLUTO collaboration[58] and the NaJ-lead glass experiment[59]. These two experiments are complementary to each other since the first one concentrates on charged particles whereas the second one measures neutral energy. There will not be enough time to discuss the analysis of a third group - the DASP2 collaboration[42] - which measured only particle directions.

Data were compared with three models,

(1) the phase space model,

(2) the two-jet Feynman-Field model,

both defined in section 1, and

(3) a three-gluon jet model,

as described in the following:

The basic assumption of this model is that gluons fragment like quarks[54]. The two ingredients of the model are then:

- A three-gluon matrix element[54,60] for the production of three massless gluons through an intermediate virtual photon.
- A fragmentation of the gluons with limited p_T. The mean p_T is adjusted to fit the two-jet data at 9.4 GeV below the resonance (at comparable jet energies). The charged multiplicity and neutral energy is adjusted to the Y data.

b) PLUTO data

In the resonance region three terms contribute to the hadronic cross section σ_{on} (fig. 36): the continuum contribution denoted as σ_{off}, the one-photon or vacuum polarization term denoted as $\sigma(\Upsilon)$ and finally the direct decay mode of the Y into hadrons (σ_{dir}). The terms σ_{off} and $\sigma(\Upsilon)$ both show the characteristics of two-jet production discussed in the previous section. Only the direct decay term σ_{dir} is expected to show the features we are looking for.

Although it will turn out that there are large differences between these contributions there is no clean way to separate them from each other event by event. The extraction of σ_{dir} has therefore to be done on a statistical basis. From all differential distributions in the resonance region appropriately normalized distributions of the corresponding off-resonance data are subtracted:

$$\sigma_{dir} = \sigma_{on} - \sigma_{off} - \sigma(\Upsilon) = \sigma_{on} - \sigma_{off}\left(1 + \frac{\sigma_{\mu\mu}^{on} - \sigma_{\mu\mu}^{off}}{\sigma_{\mu\mu}^{off}}\right)$$

The normalization of the off-resonance data is calculated from the relative luminosities on and off resonance and from the PLUTO measurements on the muon branching ratio $B_{\mu\mu}$ (see chapter II).

1872 events on resonance and 470 events off resonance enter into the final analysis. This corresponds to a total integrated luminosity of 396 nb^{-1} in the whole 9.4 GeV energy region[58]. The subtraction method described above leaves about 1250 events for the direct decay contribution. Fig. 37a shows the mean observed thrust of these events. For comparison also the unsubtracted Ypsilon data and the off-resonance data are given. We observe a drastic change of topology as one passes through the resonance (see insert in fig. 37a). We can, therefore, draw a first conclusion on the two-jet mechanism which describes the data outside the resonance: This process is certainly excluded as a major contribution to the direct Y decay.

What about the three-gluon decay? Fig. 37b shows a detailed comparison with our three models (phase space, three gluon and two jet decay). The complete data (fig. 37b) and the break down into multiplicity classes (fig. 37c) are both in good agreement with the three-gluon Monte Carlo[61]. The data are in disagreement with the two-jet description and the phase-space model although the latter is only about 2 to 3 standard deviations away. Fig. 37c shows that the relative values of data and models are nearly independent of the charged multiplicity.

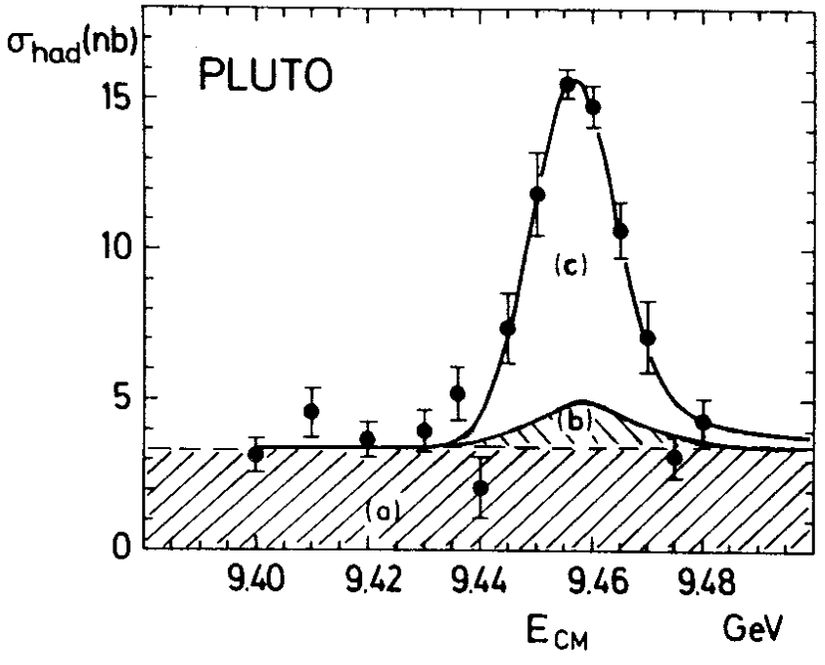

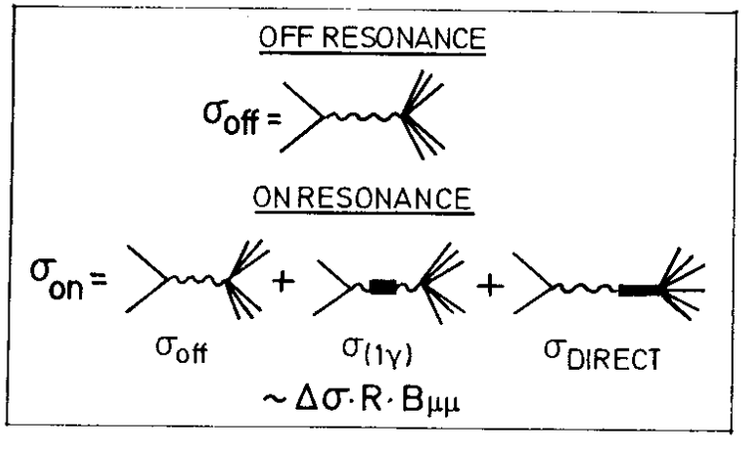

Fig. 36 Off and on resonance contributions to the annihilation cross section.
(a) = σ_{off}, (b) = $\sigma(1\gamma)$, (c) = σ_{DIR}

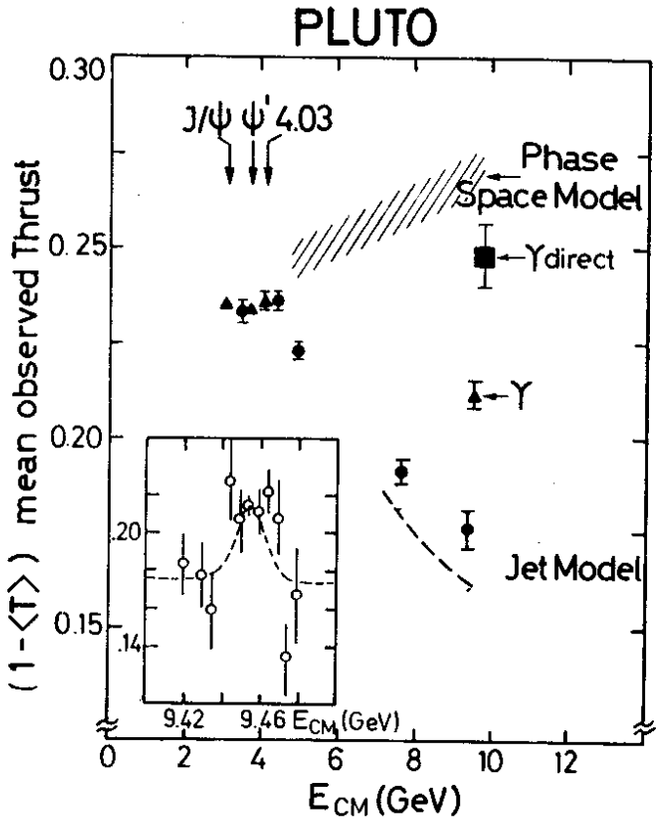

Fig. 37 PLUTO: observed mean thrust and sphericity for charged particles including the Ypsilon.
a) observed mean thrust

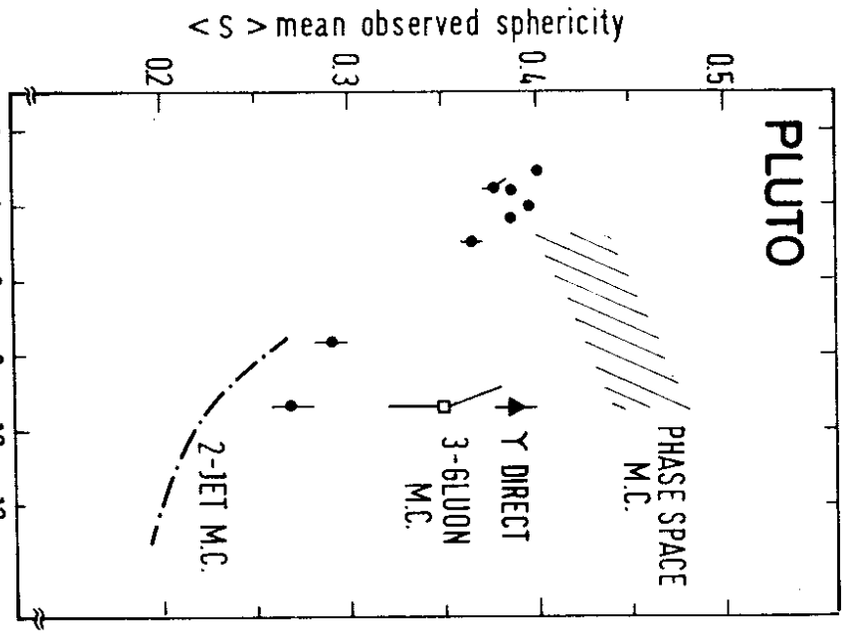

Fig. 37 b) observed mean sphericity. The predictions for phase-space, two-jet and three-gluon models are indicated

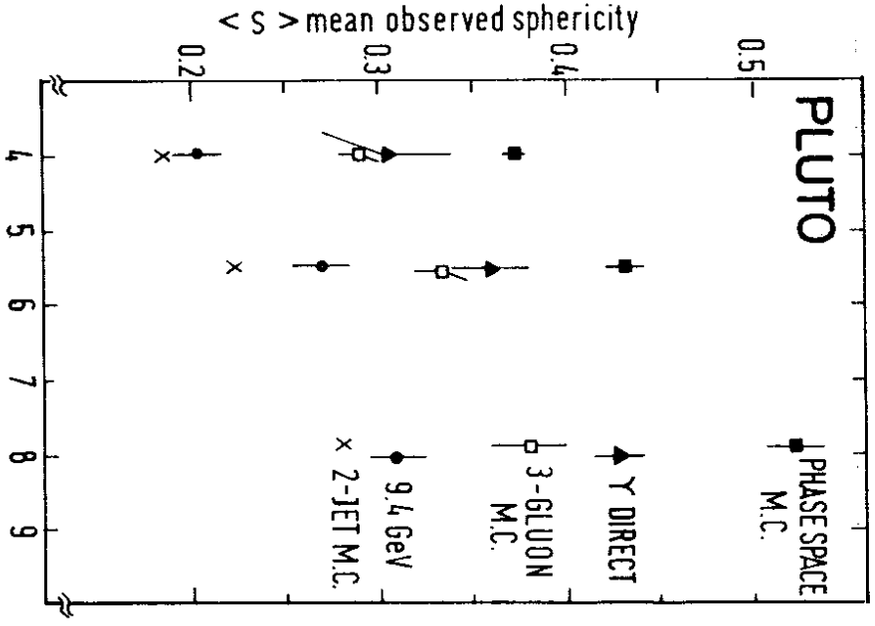

Fig. 37 c) data on and off resonance compared to model prediction: breakdown into multiplicity classes.

In particular this excludes that the change in sphericity is merely a reflection of a change in multiplicity.

Being encouraged by the reasonable agreement of the mean sphericity with a three-gluon description let us proceed to a detailed comparison of differential distributions with the models. Fig. 34b shows the differential sphericity distribution on resonance. The p_T distributions on and off resonance are compared in fig. 33a and b. Again we realize good agreement between the resonance data and a three-gluon jet model. A comparison of fig. 33a and b shows that the p_T distribution changes little as one crosses the resonance.

The angular distribution of the sphericity axis for the direct Y decay is shown in fig. 39. It agrees well with the shape of $1 + 0.39 \cos^2\theta$ predicted from the Ypsilon decay into massless spin 1 gluons[54].

Fig. 38 shows the mean p_T as a function of x_L on and off resonance. x_L is the scaled longitudinal momentum along the jet axis. Both distributions show a clear indication of the 'seagull' effect. The trend of the data is again correctly described by the two models although the increase of mean p_T at intermediate x_L is again overemphazised by the three-gluon model.

In conclusion we see that the overall features of the on-resonance data are reasonably well described by a three-gluon model where the gluons are assumed to fragment like quarks. In particular all observed quantities show strong differences in comparing on- and off-resonance data. These differences are correctly described by a two-jet Monte Carlo off resonance and a three gluon Monte Carlo on resonance. On the other hand the three-gluon model does not yield a quantitative agreement with all features of the data. In particular details of the p_T distributions are not correctly described by the model. Taking the rough nature of this model this is of course not surprising. For instance, since the model was adjusted to the data outside the resonance it automatically contains important charm contributions. In QCD these contributions are not expected on the Y (compare section 2e). But even if this effect might explain some of the differences between the model and the data we are certainly not yet in a position to really test the details of the gluon-fragmentation functions.

c) NaJ-lead glass detector data

As a second example I want to discuss the results from the DESY-Hamburg-Heidelberg-Munich collaboration[59]. This group took data at the upgraded DORIS storage

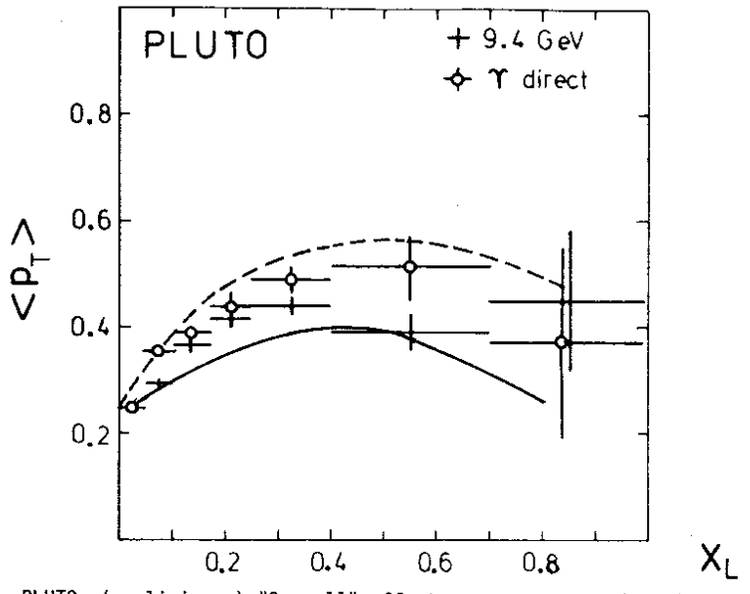

Fig. 38 PLUTO: (preliminary) "Seagull" effect - mean p_T as a function of x_L (scaled momentum parallel to the jet axis: $x_L = p_L/E_b$). The model predictions for two jets (——) and three gluons (- - -) are displayed for comparison.

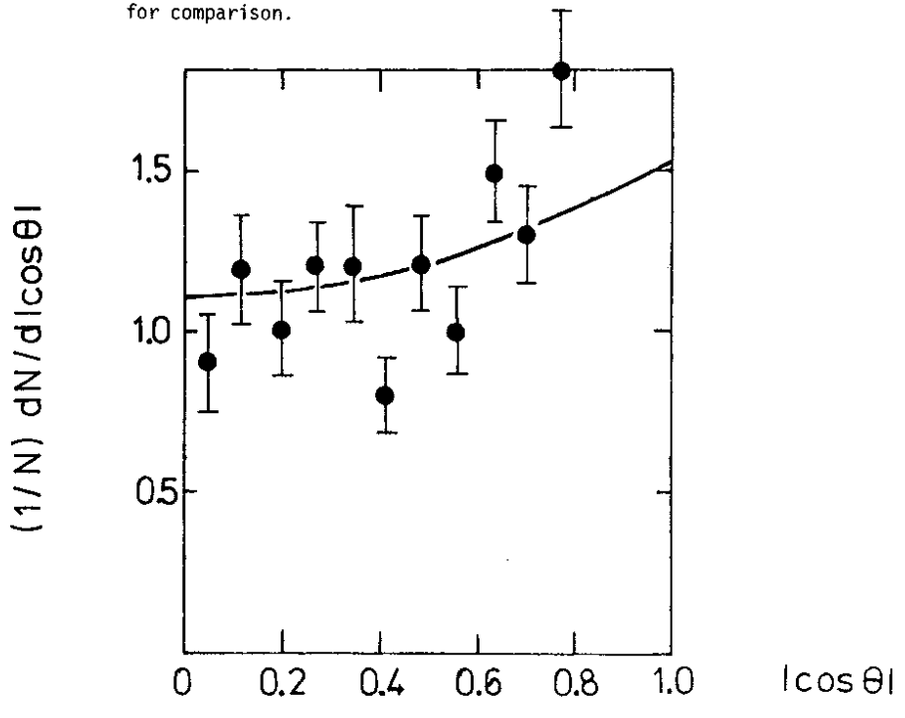

Fig. 39 PLUTO: angular distribution of the sphericity axis on resonance. The curve is proportional to $1 + 0.39\ \cos^2\theta$ [54].

ring using the NaJ-lead glass detector of the DESY-Heidelberg collaboration. The device consists of a nonmagnetic inner detector with four layers of drift chambers surrounded by NaJ and lead glass shower counters which cover 94 % of 4π. The topological analysis in this experiment is based on the energy deposited in the shower counters. Thus a large fraction of the neutral energy enters into the analysis, whereas only about one third of the charged energy is counted by minimum ionizing losses. Like for the PLUTO data observed quantities are shown and compared with different models.

Figs. 40 and 41 show the observed sphericity distributions on and off resonance for the Υ and for the Υ', respectively. The off-resonance data and the direct terms of the resonance data are compared with the three models mentioned in the previous section. Again there is a clear distinction on- and off-resonance in both cases. The resonance data are in agreement with a three gluon model. On the other hand the data are not sensitive to the small differences between the three-gluon model (full curve) and the phase-space model (dashed curve).

d) Tests of coplanarity

We have seen in the previous sections that the event topology does in fact change as one passes from the continuum to the Υ resonance. It was also shown that differential distributions of particle momenta and topological measures like sphericity and thrust change in the way expected from QCD. Being encouraged in particular by the good agreement of the data with our three-gluon Monte Carlo let us, therefore, proceed to a more detailed test of the proposed coplanarity of the events.

To this end we introduce a generalized three-dimensional sphericity in the following way[50]: let us look at the expression

$$T_{\alpha\beta} = \sum_i (\delta_{\alpha\beta}(p^i)^2 - p^i_\alpha\, p^i_\beta)$$

defined in analogy to the inertia tensor. If we diagonalize this expression we obtain the Eigenvalues λ_k which correspond to the three main axes of the event in momentum space (fig. 42). If we order these Eigenvalues such that

$$\lambda_1 \geq \lambda_2 \geq \lambda_3$$

then λ_3 closely resembles our well known sphericity definition

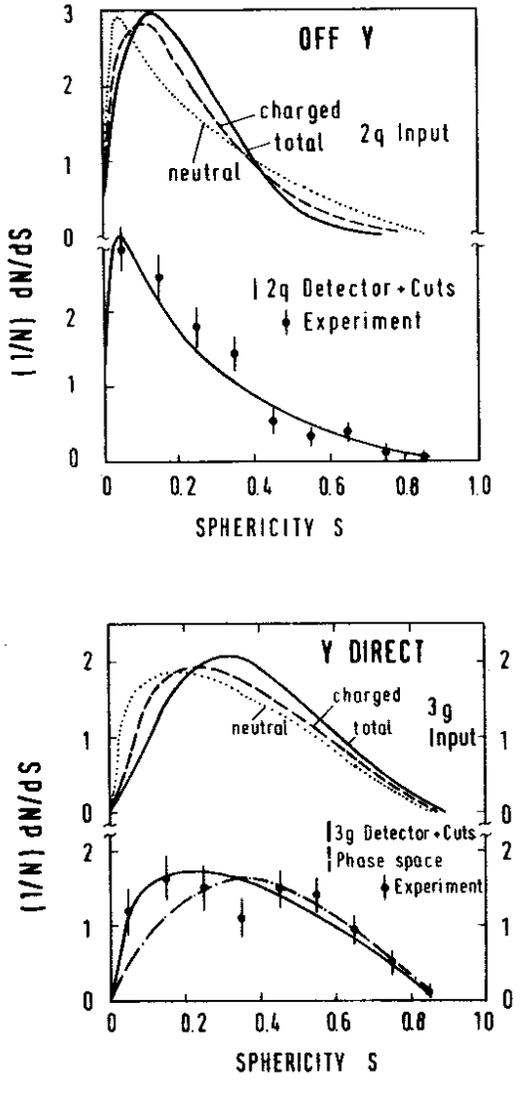

Fig. 40 NaJ-lead glass detector: observed sphericity distributions in the Υ region. OFF resonance data are compared to a two-jet model, Υ DIRECT data to three jet (——) and phase space (– –). The upper curves show the composition of the models (generated values).

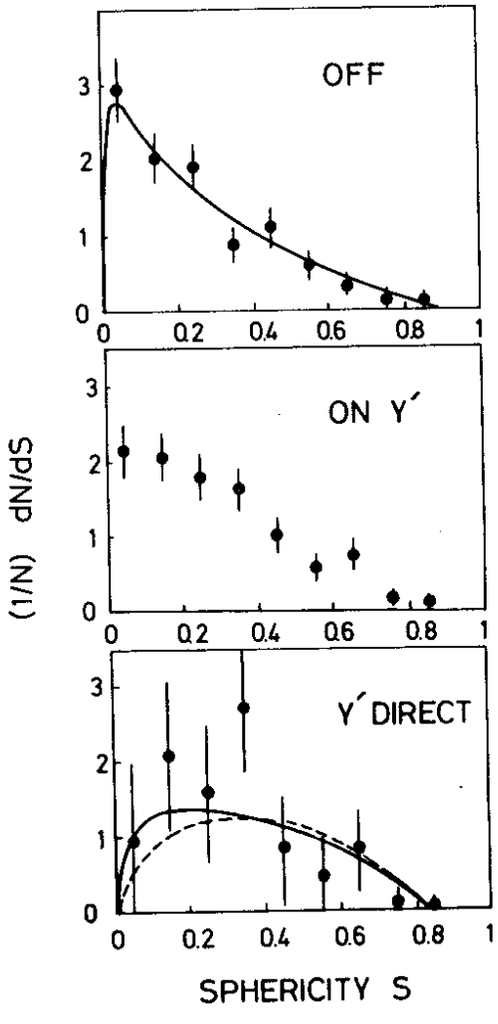

Fig. 41 NaJ-lead glass detector: observed sphericity distributions in the Υ' region. Curves defined as in fig. 40.

$$\lambda_3 = \frac{\sum_i (p_1^i)^2 + (p_2^i)^2}{\sum (p^i)^2} = \frac{\sum (p_T^i)^2}{\sum (p^i)^2} \quad ; \quad S = 3\,\lambda_3(\lambda_1 + \lambda_2 + \lambda_3)$$

The physical meaning of λ_3 is again best understood from an analogy with the inertia tensor. λ_3 points into the direction of the smallest inertia moment in momentum space. To measure the flatness of events we have to study the other two Eigenvalues in particular λ_1 which points into the direction of the smallest extent of the event in momentum space.

It is convenient to define the following quantities[58,62] (fig. 42):

$$Q_k = 1 - \frac{2\,\lambda_k}{\lambda_1 + \lambda_2 + \lambda_3} = \frac{1}{2}\,\frac{\sum_i (p_k^i)^2}{\sum_i (p^i)^2}$$

Q_k points into the same direction as λ_k, however, it measures the sum of the momentum components parallel to the axis λ_k. Consequently the Q_k are ordered in a rising sequence

$$Q_1 \leq Q_2 \leq Q_3$$

for a falling sequence of λ_k. We define now a triangle plot in analogy to a Dalitz analysis where the two perpendicular axes measure Q_1 and $(Q_3 - Q_2)/\sqrt{3}$ (fig. 43). Since Q_1 measures the shortest extension of the event in momentum space, planar events will be characterized by small Q_1 values. Such events will then congregate near to the $(Q_3\text{-}Q_2)$-axis. The extrem topologies of a sphere, a disk and a jet will fall onto the vertices A, B and C in the Q_k triangle, respectively.

The Q_k values are calculated diagonalizing the sphericity tensor for each event. All events are then entered into their position in the Q_k triangle plot. Continuum and vacuum polarization terms are subtracted statistically from these three-dimensional distributions in the same way as described in section 2b. The result is shown in fig. 43., together with Monte Carlo distributions.

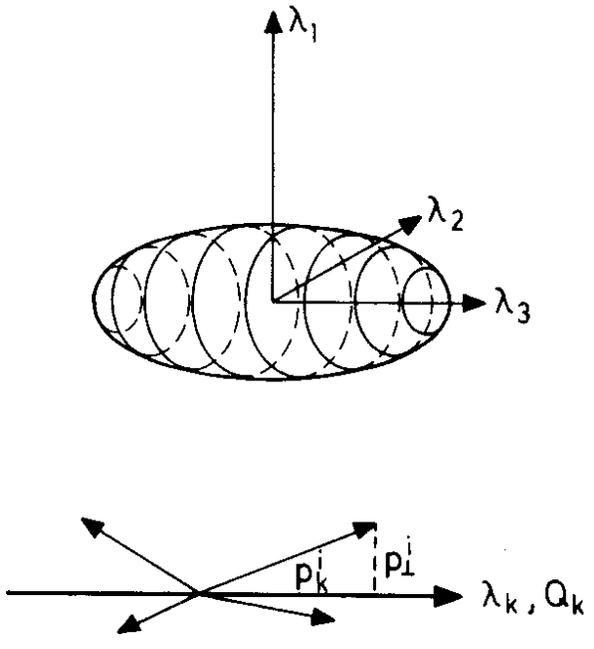

Fig. 42 The sphericity tensor in analogy to the inertia tensor. Definition of λ_k, Q_k.

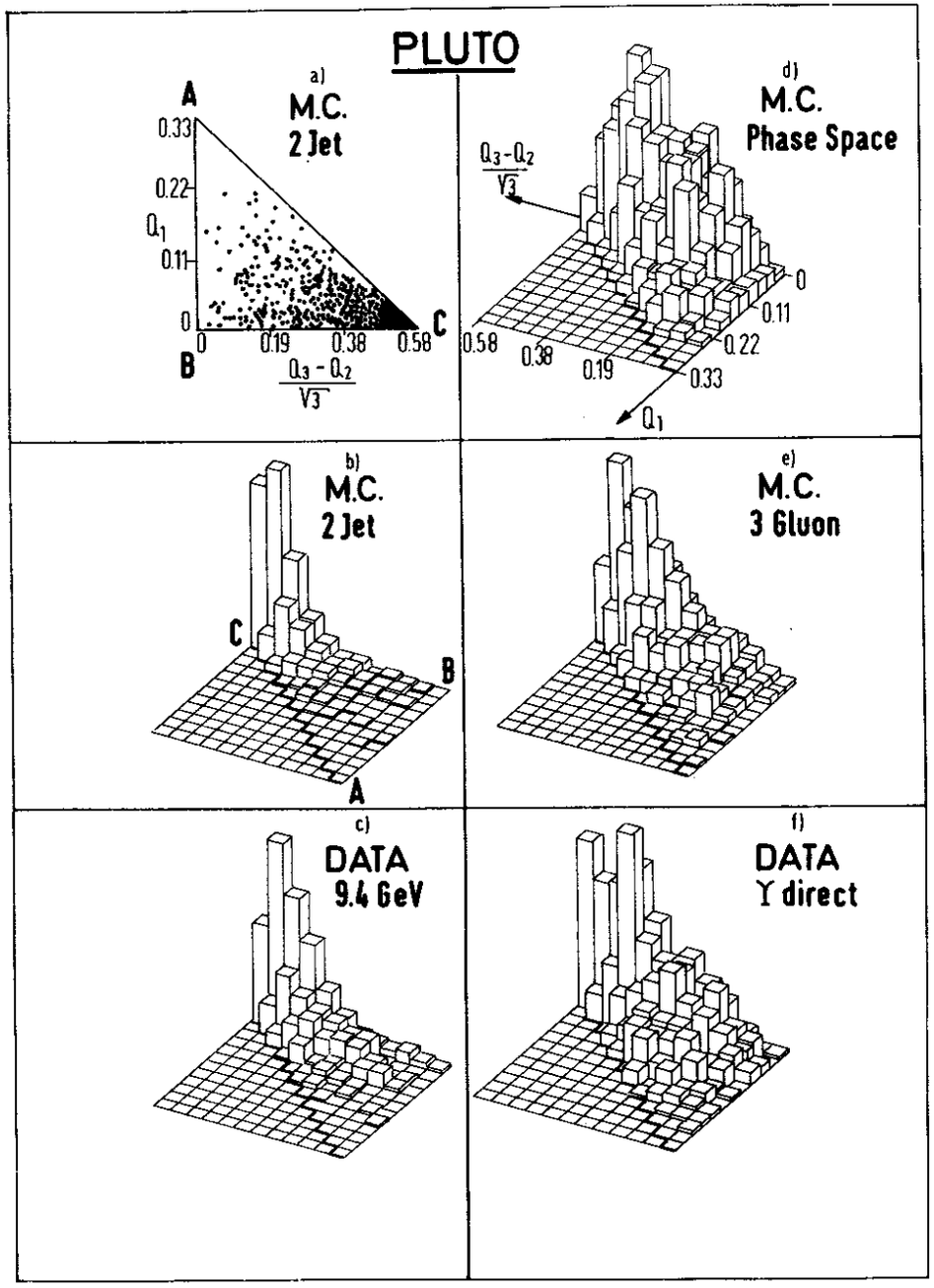

Fig. 43 PLUTO: triangle plots of the momentum space configuration. Q_1 is plotted versus $(Q_3 - Q_2)/\sqrt{3}$. Data are compared with the three models of two jets, three jets and phase space. The vertices A, B, C correspond to perfect sphere, disc and two jet structures.

The off-resonance data are indeed concentrated in the corner C which corresponds to a jet topology. The two-jet Monte Carlo shows a very similar distribution.

The data on resonance also show a peak in the jet corner. However, there is a broad distribution along the (Q_3-Q_2)-axis as expected for a planar configuration. There are very few events only in corner B. This shows that a very symmetrical planar event structure is infact very rare as expected in a three-gluon decay mechanism. The observed increase towards a jetlike configuration is qualitatively expected from the abundant asymmetric three-gluon jets. These events tend to exhibit a two-jet structure in the direction of the two most energetic gluons. A quantitative comparison with the three-gluon model (fig. 43e) shows remarkable agreement with the data. On the other hand, a phase space Monte Carlo distribution as shown in fig. 43d has a broader nonplanar extension than the data.

For a more quantitative comparison we study the projection onto the Q_1 axis. Fig. 44 shows the mean Q_1 as a function of energy for the off-resonance and the on-resonance data. A comparison with the three models shows again that the off-resonance data agree well with the two-jet Monte Carlo description whereas the on-resonance data are in good agreement with the three-gluon Monte Carlo.

In the framework of a sphericity study Q_1 measures the planarity of an event through a sum over the squared momentum component outside the event plane. The corresponding measure in the thrust or spherocity frame work has been coined acoplanarity[46]

$$A = 4 \min \{ (\sum_i |p^i_{out}|)/\sum_i |p_i|) \}^2 .$$

Like in the thrust definition the acoplanarity is based on a measurement of the absolute value of the momentum component perpendicular to the event plane. A direct measurement of the flatness of an event is given by the mean momentum component which points outside the event plane. We denote this quantity p_{out} and define it with respect to the plane given by the Q_1 direction. The mean value of p_{out} is plotted in fig. 45. Again the comparison with our models shows good agreement of the off-resonance data and a two-jet Monte Carlo and of the on-resonance data and a three-gluon Monte Carlo.

Table 8 summarizes all topological quantities measured at the PLUTO and the NaJ-lead glass detector. It shows an impressive agreement in all variables between

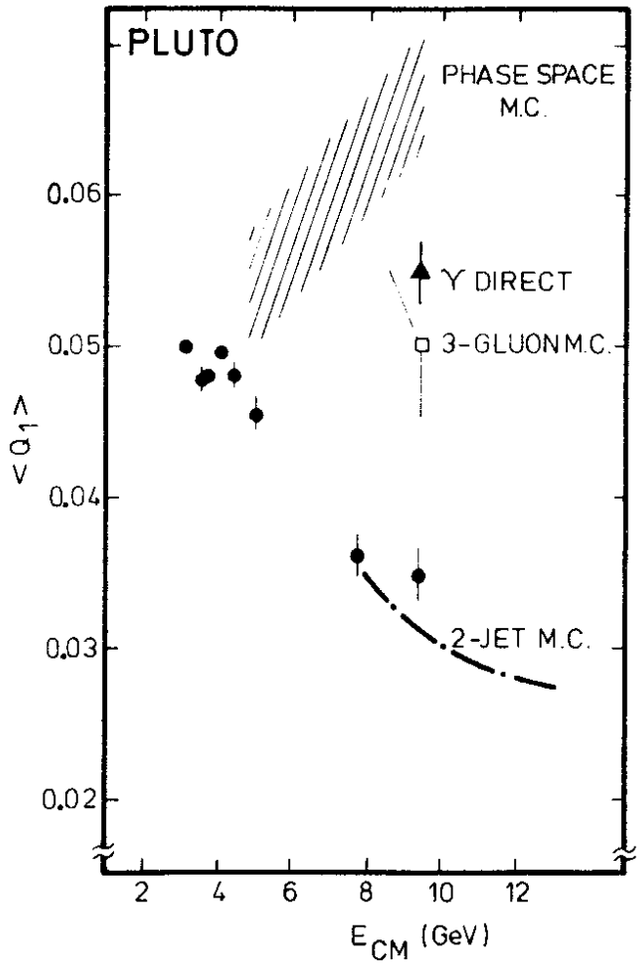

Fig. 44 PLUTO: mean observed Q_1 as a function of energy.

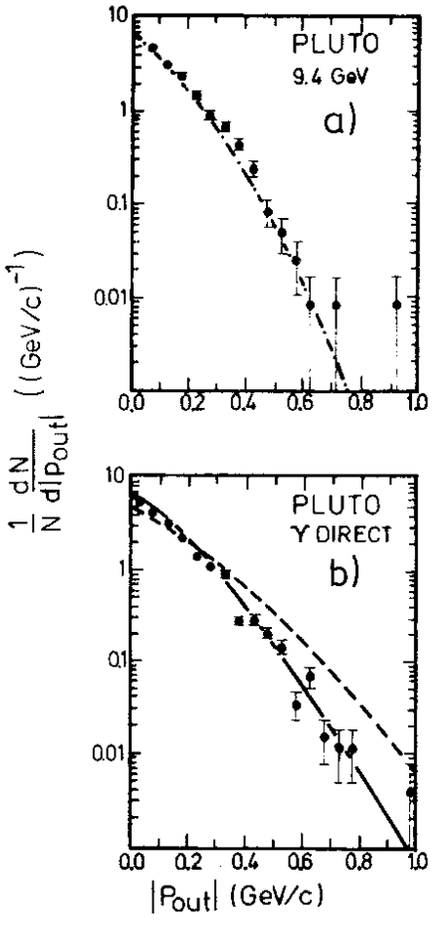

Fig. 45 PLUTO: p_{out} distributions with respect to the Q_1 plane in the 9.4 GeV region.

a) OFF resonance, compared with the two-jet model

b) ON resonance, compared with the three-jet (——) and the phase-space (- -) model

the off-resonance data and the two-jet Monte Carlo on one side and the direct Y data and the three-gluon Monte Carlo on the other side. For a detailed comparison we have to look at the error bars. The errors given for the data in table 8 are statistical only. The errors on the Monte Carlo calculations are estimates of the systematic uncertainties which arise from the adjustment of model parameters to experimental data. Taking these errors all values on resonance agree with the three-gluon Monte Carlo within about 1 standard deviation.

We notice, however, that also the phase-space Monte Carlo generally differs by no more than two standard deviations. Only the mean p_{out} value shows a clear difference of more than three standard deviations.

e) Further tests of the three-gluon model

So far we have seen that the topological structure of events on the Y resonance is in good agreement with a three-gluon decay model. In particular we get satisfactory agreement with the data assuming that gluons and quarks fragment the same way. In this section I want to study whether the mean multiplicity and the K^0_S production observed on and off resonance are in agreement with our conceptions.

Rapidity and multiplicity

Fig. 46 shows the observed rapidity distributions with respect to the sphericity axis for off- and on-resonance data. Both distributions clearly exhibit a plateau in the fragmentation region very similar to secondary particles from hadron collisions[63-65]. A detailed comparison of the on- and off-resonance data shows some very remarkable features.

- The plateau region is wider in the off-resonance data than in the on-resonance data.
- We can readjust the data in such a way that they coincide in the fragmentation region. A plateau lengthening of the order of 0.7 in rapidity becomes particularly clear.
- The plateau is higher on than off resonance. Quantitatively we get 4.2 particles per unit rapidity on resonance and 3.0 particles per unit rapidity off resonance.

In our simple picture these oberservations are readily explained at least qualitatively. Since the energy of two jets off resonance is larger than the mean energy of three jets on resonance the resulting plateau length is larger. The

Table 8 Observed mean values for different measures of event topology

	M. C.	DATA		M. C.		
	two jet	9.4 GeV	Y direct	three gluon	phase space	
<S>	0.22	0.27 ±0.01	0.39 ±0.01	0.35 ±0.03	0.46 ±0.02	PLUTO group[58]
$\langle Q_1 \rangle$	0.030	0.036 ±0.002	0.056 ±0.003	0.050 ±0.005	0.067 ±0.005	
$\langle p_{out} \rangle$	0.115	0.118 ±0.003	0.129 ±0.003	0.140 ±0.006	0.177 ±0.006	
<T>	0.84	0.82 ±0.01	0.76 ±0.01	0.76 ±0.01	0.73 ±0.01	
<A>	0.084	0.099 ±0.005	0.15 ±0.01	0.14 ±0.01	0.16 ±0.01	
			Y direct			NaJ-lead glass detector[59]
<S>	0.26	0.23 ±0.01	0.37 ±0,01	0.36	0.40	
<T>	0.79	0.82 ±0.01	0.74 ±0.01	0.74	0.72	
			Y' direct			
<S>	0.25	0.25 ±0.01	0.32 ±0.04	0.34		
<T>	0.80	0.82 ±0.01	0.77 ±0.02	0.75		

The data are compared with three different models. Errors indicated at the experimental values are statistical only, whereas those on the models include estimates of the systematic uncertainties in determining the model parameters. M. C. values are without radiative corrections.

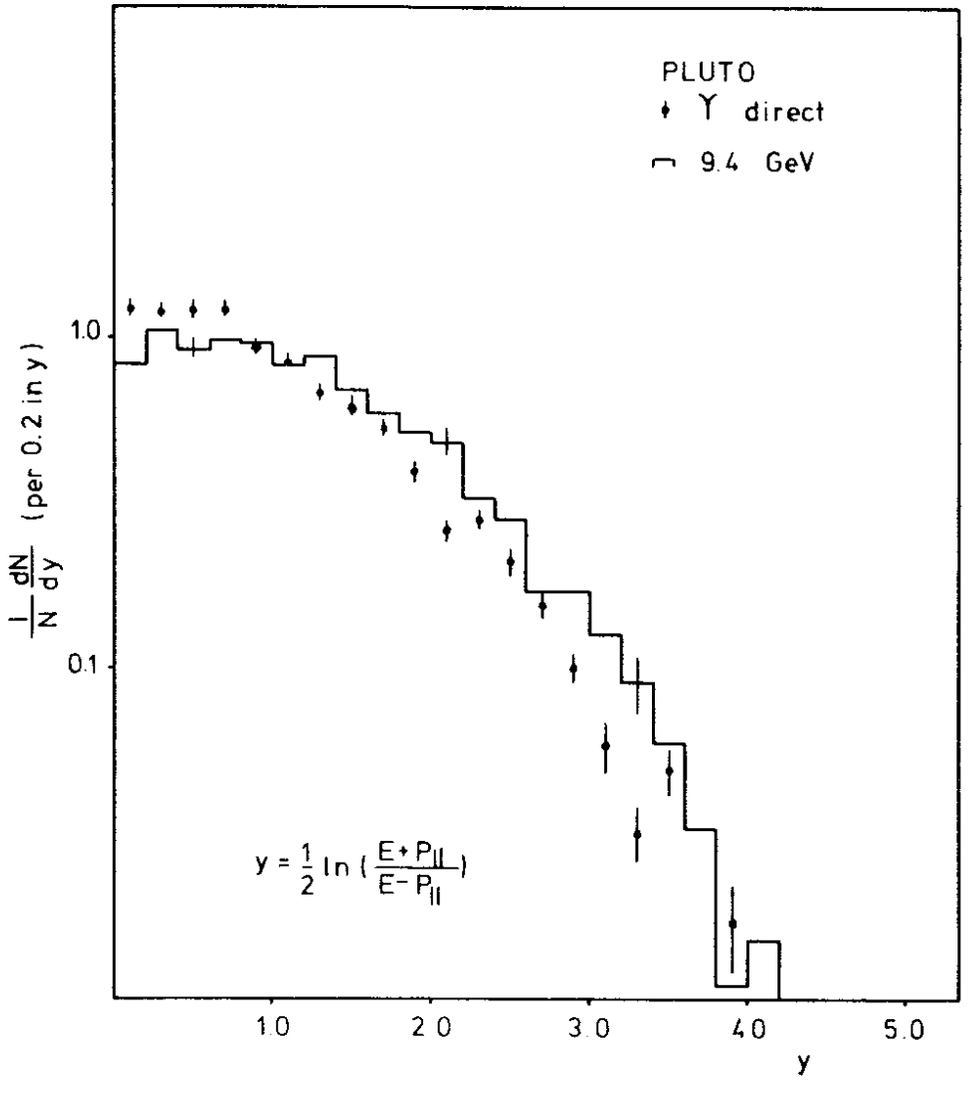

Fig. 46 PLUTO: (preliminary) observed rapidity distribution with respect to the sphericity axis on and off resonance.

observed lengthening of 0.7 is well explained by the expected logarithmic increase with energy. Even the relative heigth of the rapidity plateau corresponds roughly to the naive expectation of three to two. As we remember from hadron physics a plateau in the rapidity distribution results in a logarithmic increase of the mean multiplicity. To estimate the mean multiplicity[66] of the off- and on-resonance data we simply assume that the mean multiplicity is the sum over all jet multiplicities. If the jet multiplicites increase like

$$\langle n_{CH} \rangle_{jet} \simeq a \cdot \ln E_{jet} + b$$

we get for the off-resonance data

$$\langle n_{CH} \rangle_{off} \simeq 2 \cdot a \cdot \ln E_{CM}/2 + 2\,b.$$

With the additional simplifying assumption that all three jets have an energy of $E_{CM}/3$, we get on resonance

$$\langle n_{CH} \rangle_{on} \simeq 3 \cdot a \cdot E_{CM}/3 + 3\,b.$$

We compare this with the corrected values of the mean charged multiplicity as obtained in the PLUTO collaboration

$\langle n_{CH} \rangle_{off} = 6.3 \pm 0.4$ $\qquad$ $\langle n_{CH} \rangle_{on} = 8.0 \pm 0.3$

and the rapidity plateaus of 3 (= 2a) and 4.2 (= 3a) particles per unit rapidity off and on resonance. We observe reasonable consistency within the errors for

$a \simeq 1.4$, $\qquad$ $b \simeq 1.0$.

An increase of the mean (uncorrected) multiplicity from 6.44 ±0.14 to 7.2 ±0.18 has also been observed by the NaJ-lead glass detector[59]. The numbers correspond to observed charged particles and photon conversions with no acceptance corrections.

To conclude the observed multiplicities and rapidity distributions are in good agreement with our three-gluon model.

K^0_S production

Electron-positron annihilation shows a strong increase in K production[67] as one crosses the charm threshold at about 4 GeV. Above this energy most of the K's

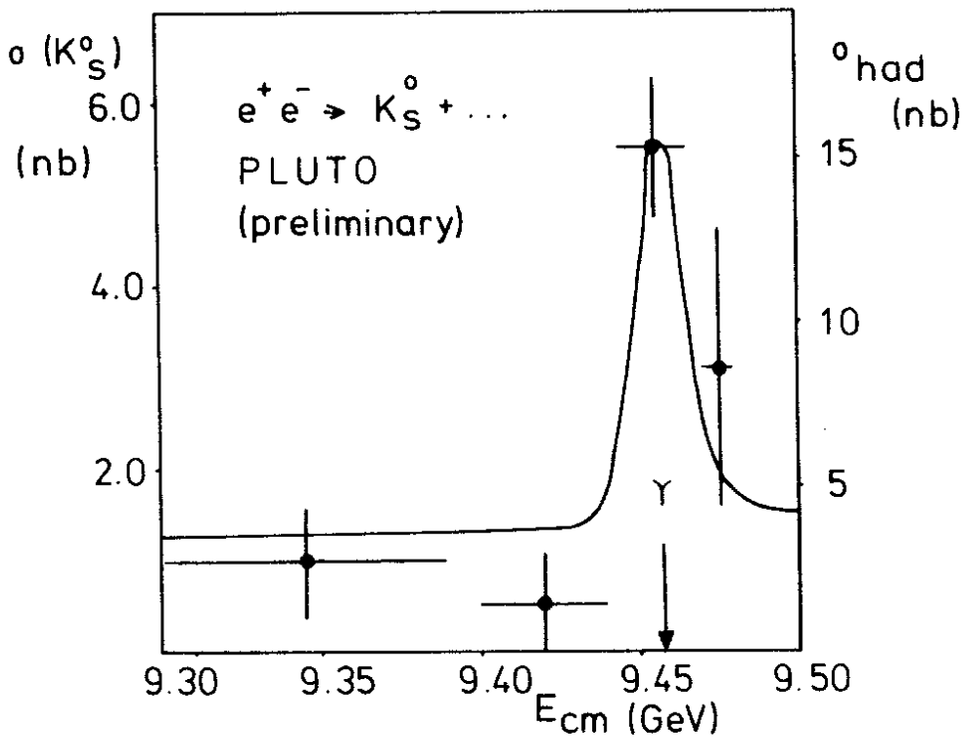

Fig. 47 PLUTO: (preliminary) inclusive K^0_S production in the Y region. The total cross section is shown for comparison.

can be attributed to charm decays. In the QCD picture Y decays into massless gluons. Charm production mediated by gluons

$$g \rightarrow c\bar{c}$$

should be strongly suppressed because of the c quark mass[68]. From these arguments one would therefore not expect any additional K^0_S production as one crosses the resonance.

The experimental result from the PLUTO group[69] (fig. 47) shows, however, a very strong increase. With the appropriate scaling of fig. 47 one may conclude that the inclusive K^0_S production is proportional to the total cross section. At first sight this may suggest that the same production mechanism for K^0_S is at work on resonance as off resonance. This would, of course, contradict QCD.

On the other hand QCD does infact predict another source for K^0_S production on the Y resonance. Since gluons are flavour blind they should in first approximation couple with equal strength to u, d and s quarks. Therefore, on the average one gluon per event produces an $s\bar{s}$ pair. Thus to a very simple approximation one would expect half a K^0_S per event in the direct Y decay. From fig. 47 we conclude that indeed about 0.4 K^0_S per event are produced on the Y. The decisive test, however, whether the observed K^0_S production is really due to this mechanism and thus conformal with QCD predictions can only come from a further check on the suppression of charm production.

f) Conclusion

Off-resonance data between 3.6 and 9.4 GeV

e^+e^- annihilation off resonance shows a clear two-jet structure which is getting more and more pronounced with higher energies. In first approximation there is good agreement between the data and a naive quark-parton model (Feynman-Field parametrization). In the next lecture I will return to some necessary refinements of the model.

Ypsilon data

All aspects of the data like topology, particle distributions and multiplicity are in fair agreement with a naive three-gluon model prediction in which the gluons fragment like quarks. The observed excess in K^0_S production can be interpreted from the flavour blindness of gluons. The data definitely rule out two

jets as a prominent source for Y decays. A simple phase-space distribution gives a bad description of the data. In most variables which have been considered so far the phase space is, however, not excluded by more than 2 standard deviations. Therefore, further work is necessary and in progress to obtain definite statements about QCD. In particular, the neutral energy will be included into the analysis of the PLUTO data.

IV. FIRST PETRA RESULTS

In this chapter I am going to describe experimental results which have been obtained very recently on the new e^+e^- storage ring PETRA[5]. PETRA is the first of a new generation of storage rings entering into the 30 GeV c.m. energy region. Since it came into operation only a couple of months ago I will spend some time on describing the machine and the first generation of experiments.

1. The Machine

The history of PETRA is summarized in table 9. It may be interesting to realize that the submission of the proposal coincides historically with the discovery[14] of J/ψ in November 1974. It took less than a year until the machine was authorized on October 20, 1975. Again one year later in Autumn 1976 decisions were taken on the first round of experiments[70]: PLUTO[71], MARK J[72], CELLO[73], JADE[74] and TASSO[75]. In the following one and a half years the construction of PETRA and of the five experiments went ahead. In July 1978 already - less than three years after authorization - an electron beam was stored and accelerated in the machine. In Fall 1978 and beginning of 1979 first physics runs could be scheduled and take data sucessfully. During these first physics shifts three detectors were installed in the machine: PLUTO, MARK J and TASSO.

Fig. 48 shows a bird's view of the DESY site with the storage ring PETRA. PETRA - Positron-Electron-Tandem-Ring-Accelerator - is an e^+e^- storage ring designed for a maximum beam energy of 2 x 19 GeV. Its diameter is about 800 m. In the present configuration all other DESY machines are used to fill the new PETRA storage ring. Two linear accelerators produce electrons and positrons. The positrons are preaccelerated to 2.2 GeV in the DESY synchrotron and then stacked into the DORIS storage ring. After accumulation they are reinjected into the DESY synchrotron and, like the electrons, accelerated to their final injection energy of 6.5 GeV. At this energy particles are injected into the PETRA tunnel where they are stacked. Typical currents of several mA are then circulating in the PETRA storage ring and can be accelerated to their final energy. Contrary to the original design of DORIS, PETRA is a single ring few bunch machine. Depending on the number of experimental areas which have to be served, the number of bunches per beam varies between one and four. Some relevant figures on the PETRA performance[76] in January 1979 are summarized in table 10.

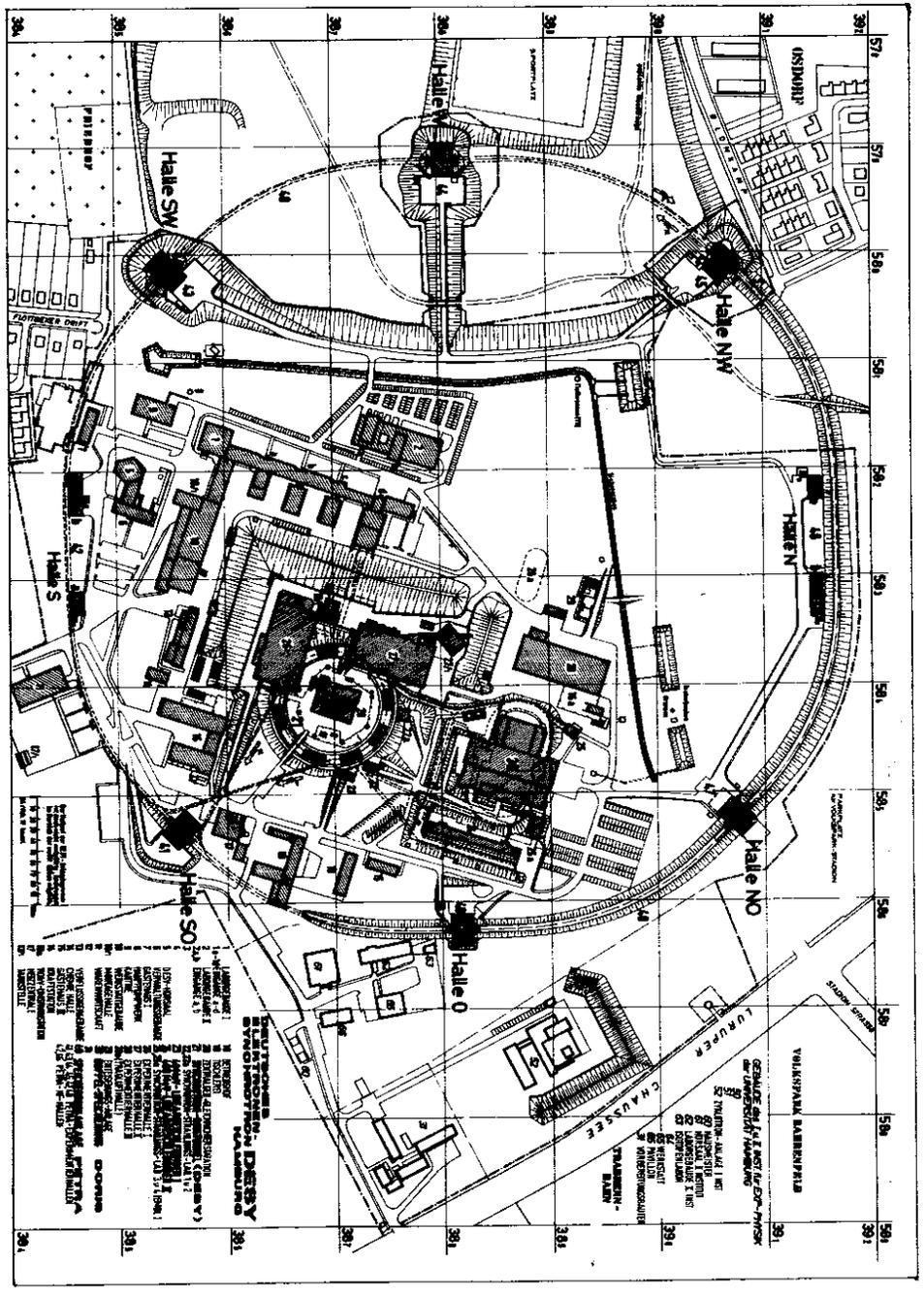

Fig. 48 The e^+e^- storage ring PETRA.

Table 9 History of PETRA

	Proposal submission November 1974
1975	Authorization Oct. 20, 1975
1976	Proposal up - date Begin of tunnel construction Call for experimental proposals
	Decisions on first round of experiments
1977	Ring tunnel and halls are completed, begin of magnet install. e^+ injection through first octant
	e^- injection through second octant
1978	e^- beam storage July 15, acceleration to >11 GeV July 30 Luminosity measurements Sept. 15 installation of 3 detectors in interaction regions
	first physics runs at 2×8,5 GeV
1979	Shut - down, installation of 4th detector + PIA Physics runs at high energies

Table 10 PETRA performance (by January 1979)

Parameter	Accomplished values	Comments
- Lifetime	5 ./. 8 h	design: 9 h; improving
- Bunch length	11.4 mm (r.m.s.)	no bunch lengthening
momentum spread	0.065 MeV p^2 (r.m.s.)	p = beam momentum in GeV
energy resolution	0.023 MeV E_{CM}^2 (r.m.s.)	E_{CM} = c.m. energy in GeV
- Single bunch current	$\leq$ 18 mA	design: 20 mA
- Energy per beam	$\leq$ 11.1 GeV	in March more than 15 GeV have been reached
- Luminosity at 2x8.5 GeV max.	1.2×10^{30} cm^{-2} s^{-1}	2 x 2 bunches; design value
typical	0.5×10^{30} cm^{-2} s^{-1}	(2 x 4 bunches) 1.4×10^{31} cm^{-2} s^{-1}
tune shift ΔQ	0.015 ./. 0.025	design 0.06
number of bunches	2 x 2	design 2 x 4

The accomplished values for the single beam lifetime, the bunch length, and the single bunch current are close to the design figures. A maximum beam energy of 11.1 GeV could be obtained. (Meanwhile after introducing additional cavities more than 15 GeV were reached.) This indicates that there are no principle obstacles to reach 30 GeV c.m. energy.

In the light of possible resonance searches it is important to note that the design value for the momentum spread of 6.5×10^{-5} GeV x p^2 (p in GeV) was observed. This guarantees an energy resolution of σ = 2.3 MeV at 10 GeV and 21 MeV at 30 GeV c.m. energy. The best luminosity which was obtained at 2 x 6.5 GeV was 1.2×10^{30} cm^{-2} x^{-1}. Compared to the designed luminosity of 1.4×10^{31} cm^{-2} s^{-1} this is still a factor of 10 too low. To understand this discrepancy in detail let us look again at the followong expression for the luminosity:

$$L \sim (\Delta Q^2) \cdot B \cdot \varepsilon_x \sim E^4$$

The number of bunches for the measured luminosity was two whereas four were assumed for the design luminosity. This explains a trivial factor of 2. The remaining difference is due to the tune shift ΔQ. Whereas ΔQ = 0.06 was assumed

Fig. 49 PETRA development

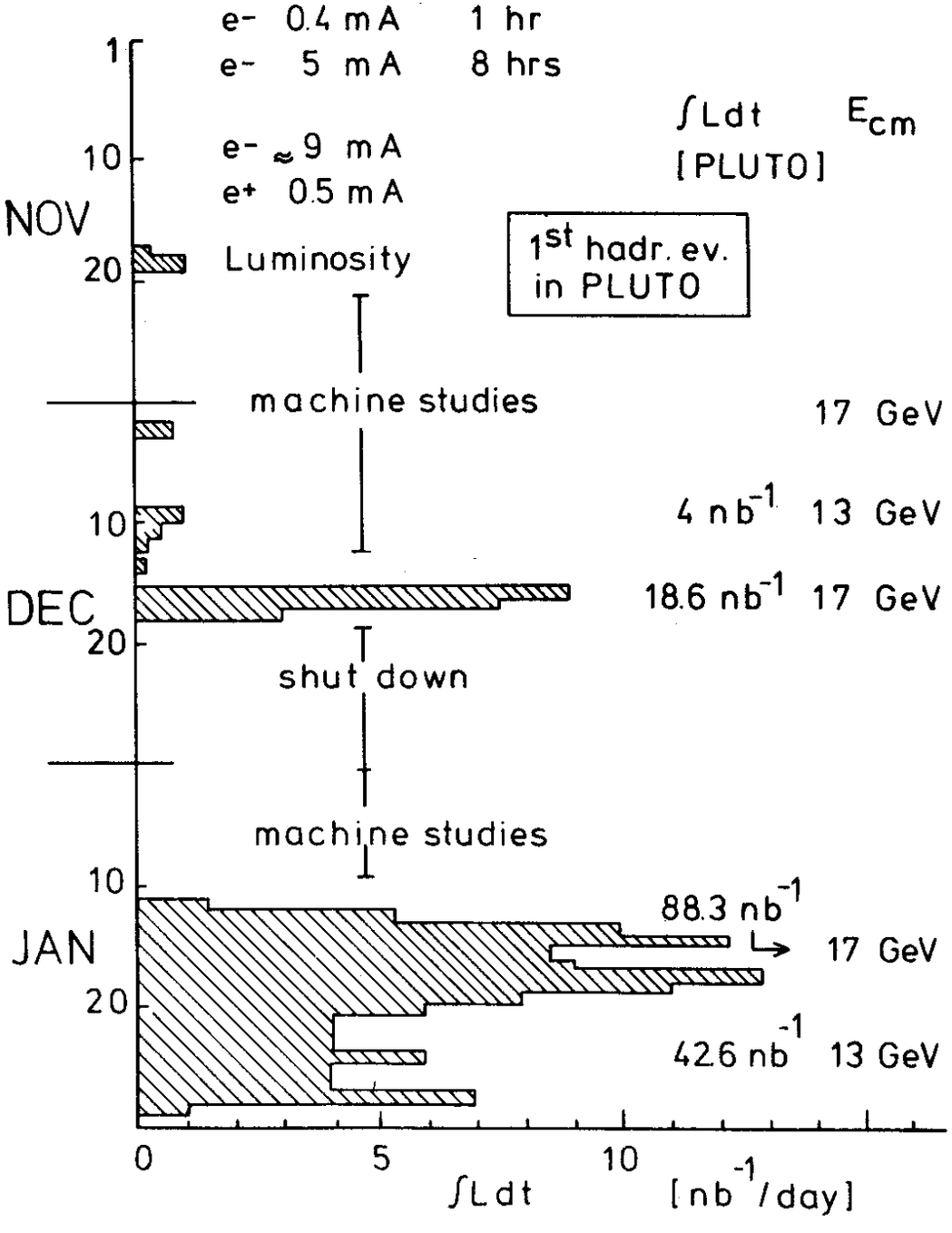

in the design, the accomplished values so far were only 0.025 under optimum conditions and 0.015 typically.

To appreciate these numbers one should certainly not forget that the mean luminosity of about 0.5×10^{30} was reached after a few months of machine studies only. Fig. 49 shows again the development of the luminosity during November 1978. It was then when the first hadronic event was observed in the PLUTO detector. The figure shows the rapid improvement in luminosity delivered to the experiments. Note also that the mean luminosity at 17 GeV was higher than at 13 GeV, as expected.

2. First round detectors

The first experiments at PETRA were primarily motivated by the possible discovery of new degrees of freedom, in particular the proposed new quarks[77] b and t and may be even further quarks and leptons. As already discussed in the first lecture an appropriate handle on new flavours is the total cross section

$$\frac{\sigma_{had}}{\sigma_{\mu\mu}} = R = 3 \times \sum_q Q_q^2 .$$

In addition topological quantities like sphericity or thrust may be even more important looking for new thresholds. Any first round experiment should be in a position to measure these quantities. Therefore, a good detector should have a large acceptance for charged and neutral particles. For the topological studies good energy resolution both for charged and neutral particles is desirable. As we will see in the last section of this chapter, two photon processes become increasingly important at larger energies. To discriminate against these processes a good measurement of the total hadronic energy is indispensable. Of course, this also ensures good discrimination against beam gas, beam wall and synchrotron radiation background.

I will briefly describe the three experiments which have taken data during the first PETRA run. Fig. 50 shows the detector PLUTO in its proposed final configuration at PETRA. All components were ready and tested by November 78 when the first data taking started. In addition to the DORIS configuration which has already been described in chapter II mainly two new components have been added.

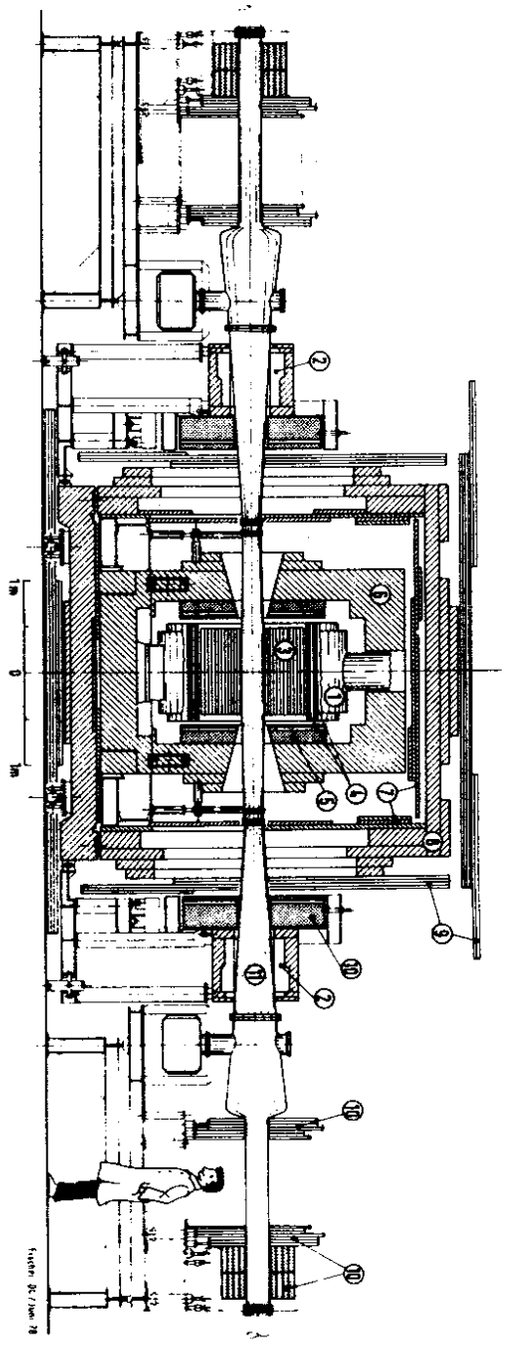

Fig. 50 The PLUTO detector in its PETRA configuration (Aachen-Bergen-DESY-Hamburg-Maryland-Siegen-Wuppertal Collaboration).

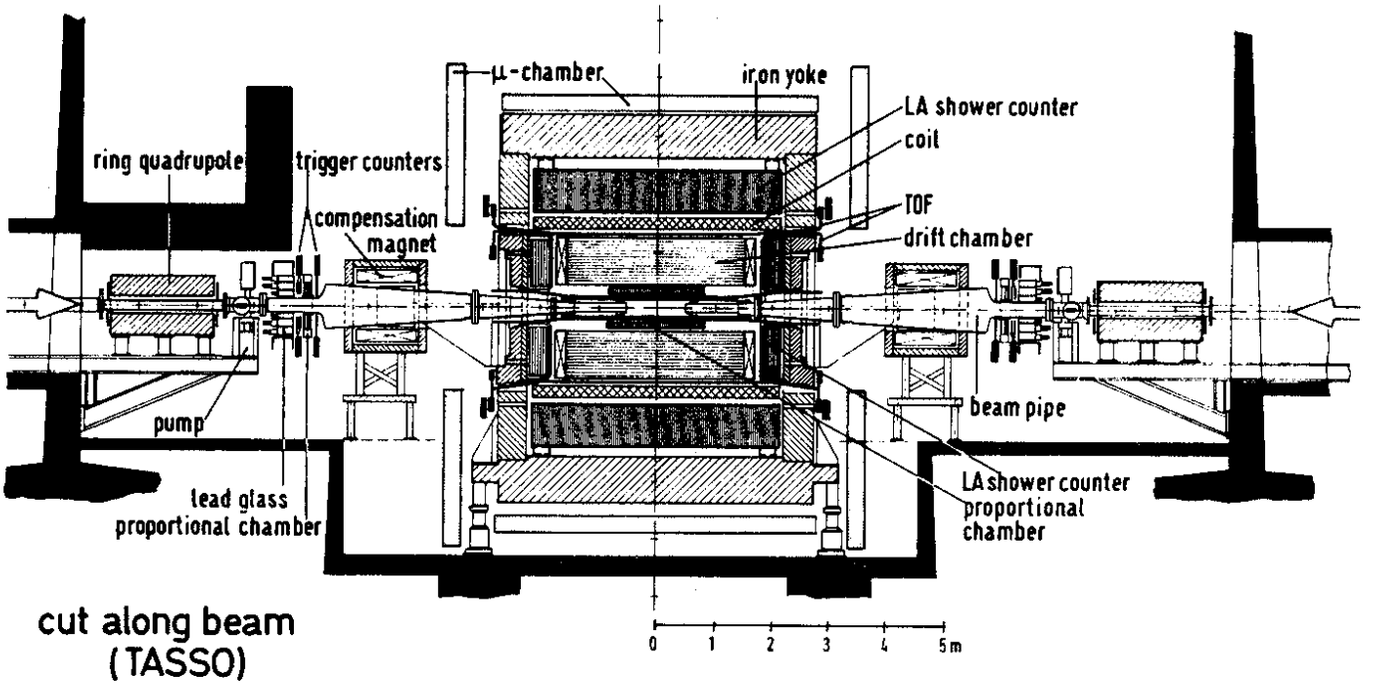

Fig. 52 The TASSO detector (Aachen-Bonn-DESY-Hamburg-IC London-Oxford-Rutherford-Weizman-Wisconsin-Collaboration). Only the magnet with the central detector was installed for the January run.

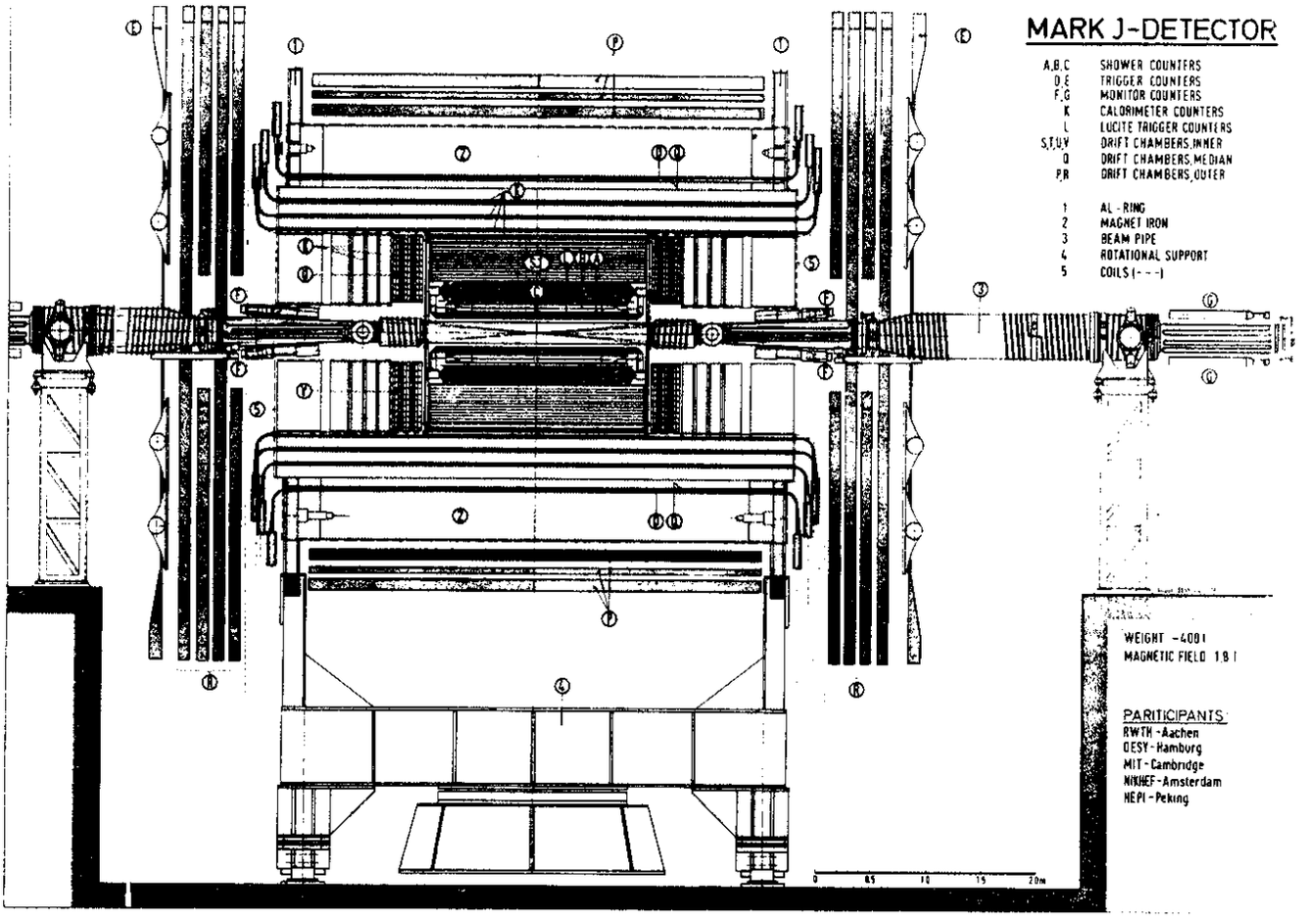

Fig. 51 The MARK J detector (Aachen-DESY-LAPP-MIT-NIKHEF-Peking collaboration). The endcaps were still missing in the January run.

The magnet yoke has been surrounded by additional iron to provide a total iron thickness of 1 m for muon filtering. Large area drift chambers have been mounted outside the new iron house. The complete setup will provide a muon detection over 83 % of 4π with a punchthrough and decay probability of less than three percent up to a muon momentum of 5 GeV.

Two forward spectrometers provide electron detection in the angular region between 25 and 250 mrad. Each spectrometer contains a small angle tagger covering the angular range up to 68 mrad. It consists of a fine segmentes array of lead glass blocks and two sets of proportional chambers. The remaining angular range is covered by the large angle tagger which uses a lead scintillator sandwich preceeded by a layer of proportional tubes. The energy resolution in the SAT and the LAT is 11 $\%/\sqrt{E}$ and 13 $\%/\sqrt{E}$, respectively. The forward spectrometers are important mainly for two reasons. They extend the range for Bhabha scattering down to 25 mrad which is particularly needed for monitor purposes and they serve as tagging devices for two photon reactions. The importance of this will become clear in the course of this chapter.

Fig. 51 shows the Mark J detector[72]. It was built for the dedicated purpose of measuring weak-electromagnetic interference through μ pair production at high energies[78,79]. The whole apparaturs is therefore rotatable in θ and ϕ. Essentially the setup consists of a central electromagnetic shower detector ($\sigma/E = 14\ \%/\sqrt{E}$) surrounded by a hadron calorimeter. Several layers of track chambers are inserted between these two calorimeters. For muon detection the hadron calorimeter is surrounded by additional iron which is covered by sets of multilayer drift chambers. For momentum analysis of the muons the iron can be magnetized. The January data were taken without magnetic field. Also the endcaps of the detector were still missing during that period.

Fig. 52 shows a sideview of the TASSO detector[75]. Until January only the central detector consisting of a drift chamber, the time-of-flight system, the magnet and the top and bottom μ counters were installed. The data I will report here were essentially obtained from the magnetic detector. A warm coil provides a solenoide field of .5 Tesla. The field volume of 4.5 m length and 2.7 m diameter is filled with a large cylindrical drift chamber with 15 sense wire plances, 9 radial and 6 with a stereo angle of $\pm 4^{\circ}$ to determine the z direction. A single wire resolution of 200 microns (rms) is projected which will yield a momentum resolution of .7 % x p (rms). So far $\leq$230 microns have been reached.

Background and rates

For a mean luminosity of 3×10^{29} we expect a hadronic rate of

$$\dot{N}\ (\text{hadronic events}) = L \cdot R \cdot \sigma_{\mu\mu} \simeq 0.5 \times 10^{-3}/\text{s} .$$

This is to be compared with a trigger rate of

$$\dot{N}\ (\text{fast trigger}) \simeq 10^{3}/\text{s}$$

which is dominated by beam gas interactions and off momentum particles. A comparison of these two numbers may give the most vivid impression of the experimental difficulties which are encountered in e^+e^- experiments. The enormous data reduction factor of 10^6 to 10^7 is usually accomplished in a multistep trigger and data analysis chain. In the PLUTO detector, for example, the fast trigger rate is typically some kHz. This is to be reduced to a few Hz of events which are written on magnetic tape. The reduction is done in three steps, a fast trigger, a slow trigger[80] and a filter in the on-line computer. These raw data are still dominated by background with a considerable portion of cosmic events. 3 to 4 orders of magnitude in data reduction are then still left to the off-line analysis.

3. Results

a) QED processes

In this section I will concentrate on the QED process

$$e^+ e^- \rightarrow e^+ e^- .$$

(The statistics on muon pair production at PETRA is still meager, within the limited statistics the MARK J data are consistent with QED expectations.) The cross section for Bhabha scattering is given by

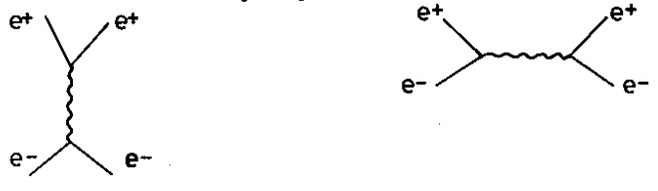

$$\frac{d\sigma}{d\Omega} = \frac{\alpha^2}{2s}\left\{\frac{q'^4+s^2}{q^4}+\frac{2\,q'^4}{q^2 s}+\frac{q'^4+q^4}{s^2}\right\}, \qquad q^2 = -\,s\cos^2\theta/2 \qquad q'^2 = -\,s\sin^2\theta/2$$

where the first term corresponds to the spacelike and the last term to the timelike contribution. The intermediate term describes the interference. I want to discuss two important aspects of Bhabha scattering: The high rate forward scattering is a convenient monitor reaction since it is governed by small q^2 where QED is known to hold. The large angle Bhabha scatters can be used to check the validity of QED at high q^2.

Bhabha scattering as monitor reaction

Bhabha scattering is experimentally defined by a time coincidence between two colinear pairs of showering particles having the energy of the cirbulating beam. Fig. 53 shows the angular distribution in the small angle tagger for a subsample of the PLUTO data[81]. The solid line shows a fit with the QED expectation. The relative normalization of the QED curve and the data determines the integrated luminosity of this data sample. Although this looks very simple and safe at first sight there are several sources for systematic errors.

Since the SAT is mounted close to the beam pipe it suffers from accidental coincidences of off-momentum particles under bad beam conditions. Because the QED function is very steep in forward direction ($\sin^{-4}\theta/2$) the normalization is extremely sensitive to a precise knowledge of the position of the SAT. Additional uncertainties come from an interplay of collinearity, energy cuts, and radiative corrections.

To get a handle on these possible systematic errors the SAT data were compared with e^+e^- large angle scattering in the central detector. Fig. 54 shows the result of the central detector Bhabha scattering. The QED expectation from the SAT measurements is indicated by the full curve. It agrees with the measurement to within 6 %. Therefore a 10 % systematic error on the luminosity measurement is a conservative estimate.

A vertex distribution of Bhabha events in the central detector is shown in Fig. 55. The background is apparently low (less than 1 %). This figure provides us with a valuable extra information on machine parameters. From the width of the

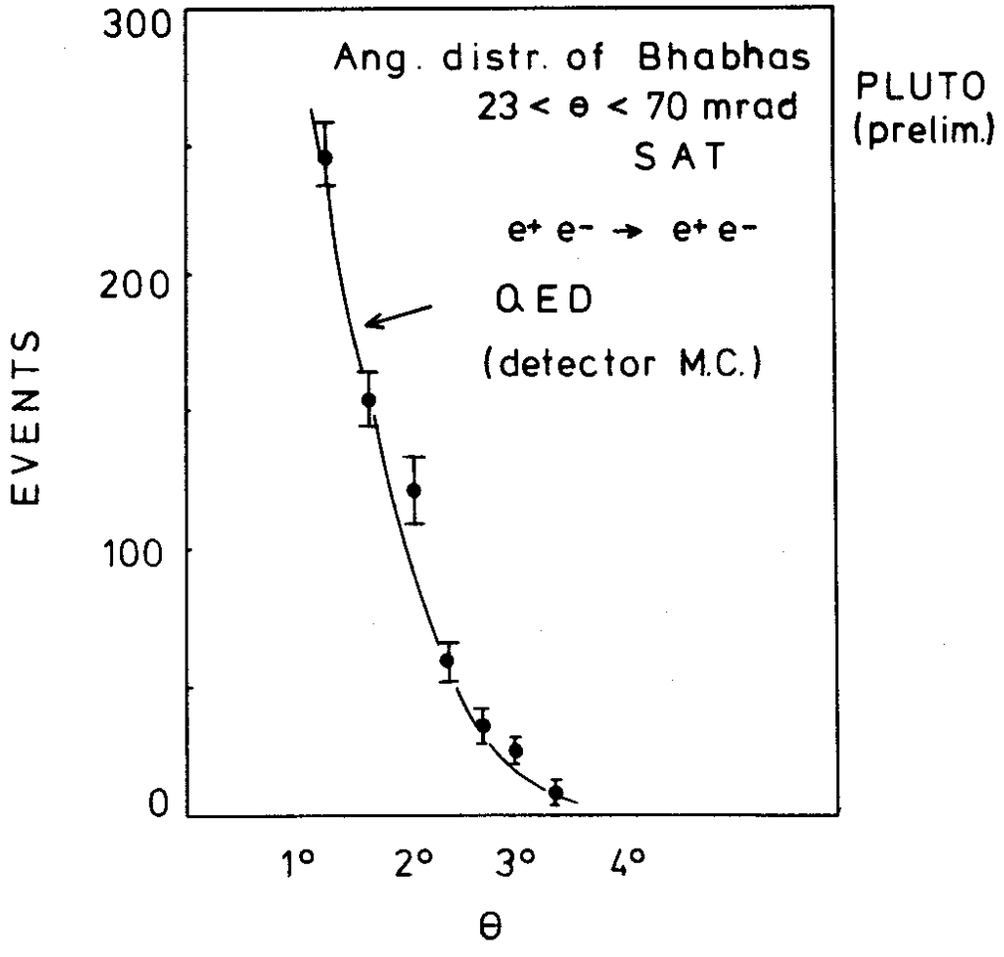

Fig. 53 PLUTO: (preliminary) angular distribution of small angle Bhabha events in the small angle tagger (SAT).

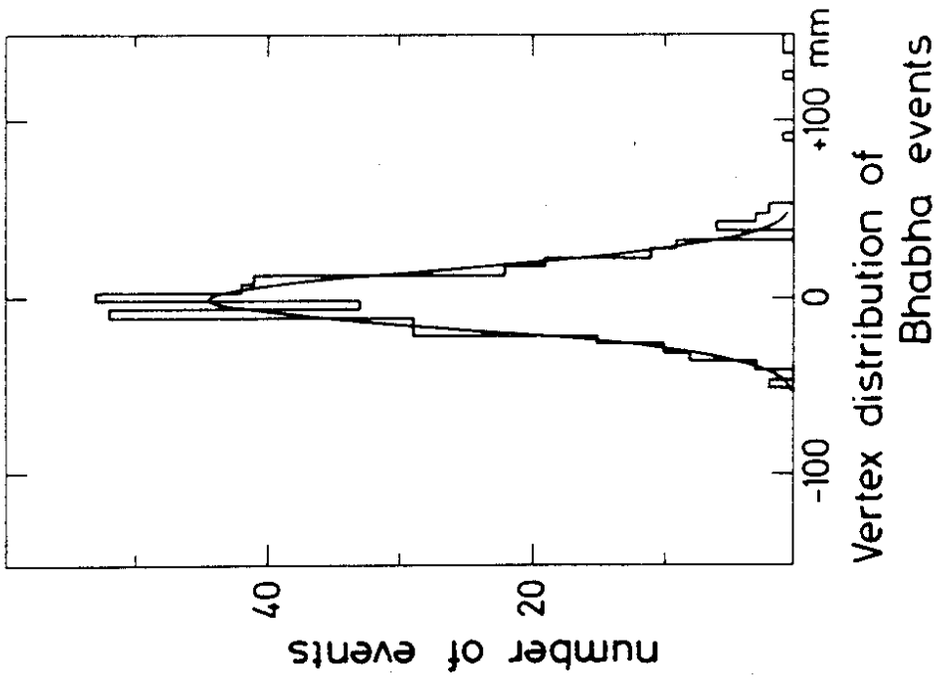

Fig. 55 PLUTO: Vertex distribution of Bhabha scatters in the central detector.

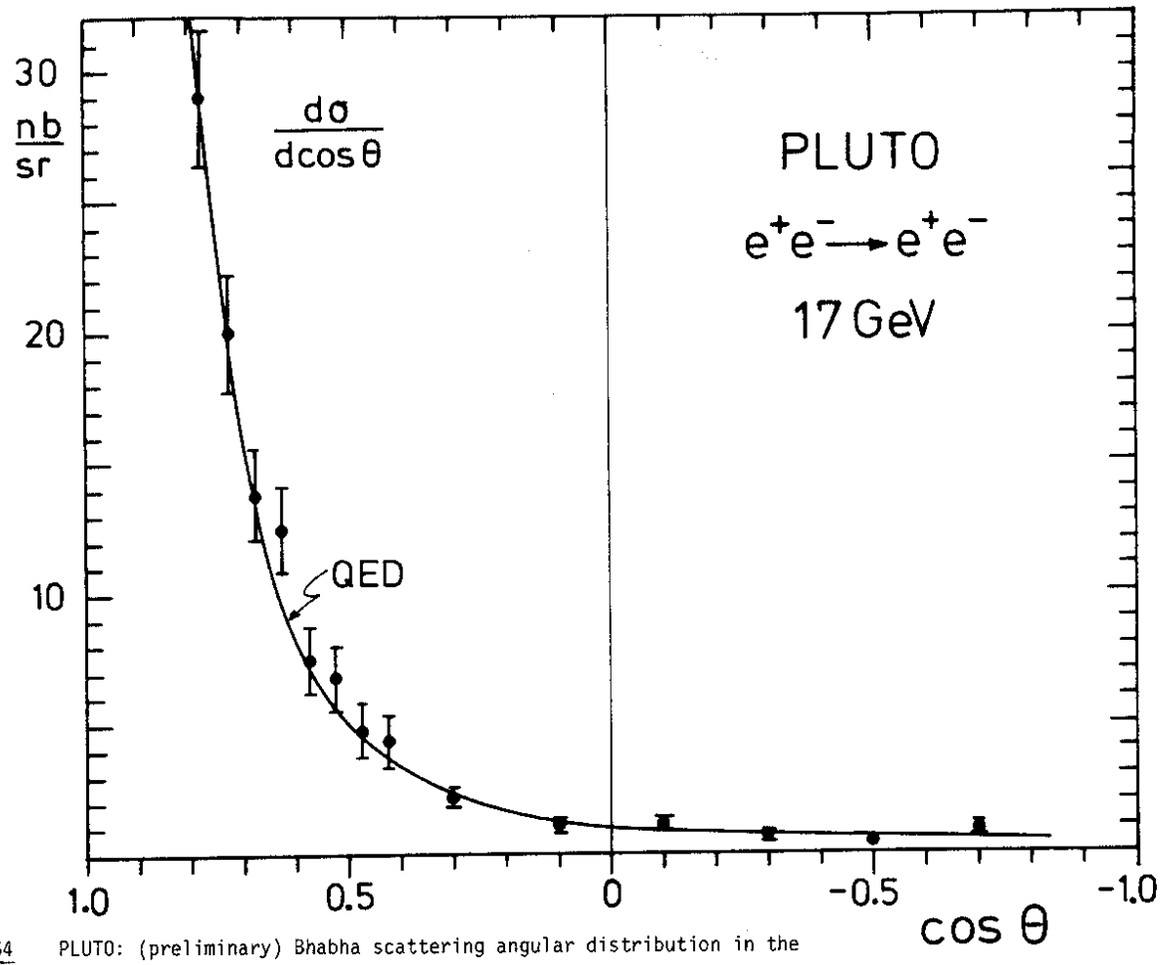

Fig. 54 PLUTO: (preliminary) Bhabha scattering angular distribution in the central detector (barrel + endcap). The curve indicates the QED extrapolation from the SAT, including all radiative corrections.

distribution one can determine the length of the circulating bunches experimentally. The result is σ = 11.8 ±.5 mm. This is in agreement with results from machine studies (σ = 11.4 mm) and corresponds to the theoretical expectation. From this bunch length a momentum resolution per beam of $6.5 \cdot 10^{-5}$ GeV · p (rms; p in GeV) can be inferred (compare table 10).

QED check

In the above argument on a check of the luminosity it has been tacitly assumed that QED holds even for large q^2. To quantify this statement let us introduce formfactors in the differential cross section for e^+e^- scattering[82].

$$\frac{d\sigma}{d\Omega} = \frac{\alpha^2}{2s}\left\{\frac{q'^4 + s^2}{q^4}\,|F(q^2)|^2 + \frac{s^4}{q^2\,q'^2}\,\mathrm{Re}(F(q^2)\,F^+(q'^2))\right.$$

$$\left. + \frac{q^4 + s^2}{q'^4}\,|F(q'^2)|^2\right\}$$

$$F(q^2) = 1 \mp q^2/(q^2 - \Lambda_\pm^2)$$

There are different ways of introducing deviations from QED. Accordingly the exact definition and physical interpretation of Λ is model dependent. In the context of this experimental lecture Λ with the above definition is mearly used as a parametrization to quantify possible limits on QED.

All three experiments[83-85] at PETRA have made an attempt to determine the cut-off parameters from their Bhabha scattering data. Table 11 summarizes the results. For comparison also the best values known so far from SLAC[86] have been given. All values were obtained fitting the experimental data with the above parametrization of the cross section and taking into account radiative corrections[87]. The PLUTO result[84] was deduced from the data shown in fig. 54 the angular distribution of the MARK J data[83] from which the cut-off parameters were calculated is shown in fig. 56.

In conclusion we can say that QED holds even at these high energies. Thus the cut-off parameter can be pushed as high as 40 GeV.

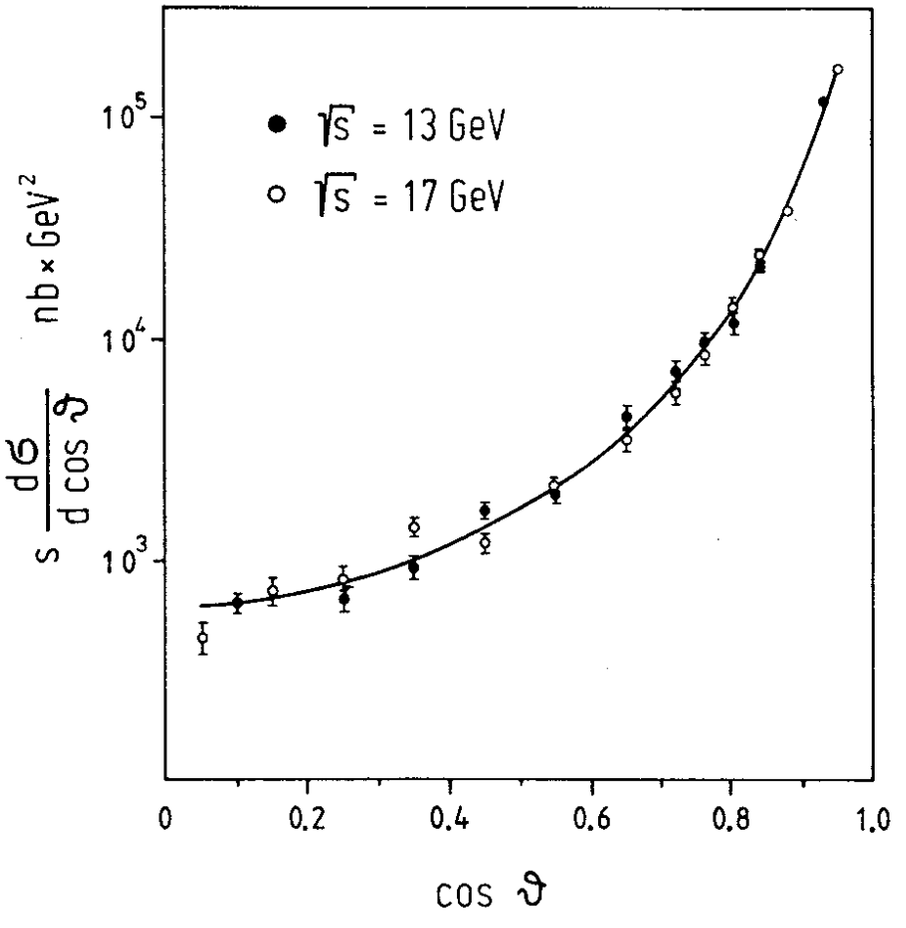

Fig. 56 MARK J: angular distribution of Bhabha scattering at 13 and 17 GeV. The curve is a common QED fit to the data including all radiative corrections.

Table 11 QED cut-off parameters assuming equal timelike and spacelike formfactors

$F(q^2) = 1 \mp q^2/q^2-\Lambda_{\pm}^2$.[+]

95 % C.L. lower limits for Λ_+ and Λ_- are given.

Experiment		Λ_+ (GeV)	Λ_- (GeV)	Ref.
SLAC	1974	14.4	22.8	86
	1975[+]	15	19	86
	1976	33.8	38.0	86
MARK J		26	38	83
PLUTO[+]	(preliminary)	39	42	84
TASSO	(preliminary)	29	34	85

[+] In the limit $\Lambda^2 \gg q^2$ $F(q^2)$ can be written

$F(q^2) = 1 \pm q^2/\Lambda_{\pm}^2$

This parametrization has been applied to the data of the MARKI and PLUTO detector.

b) Total cross section

Entering a new region of energy the PLUTO, MARK J and TASSO groups made an attempt to measure the total cross section[81,88,89]. It has been emphazised already in the first chapter why this quantity is of particular interest in e^+e^- reactions. Any increase in $R = \sigma_{had}/\sigma_{\mu\mu}$ would indicate new flavours. To determine R the theoretical value of $\sigma_{\mu\mu}$ is taken while σ_{had} is measured experimentally:

$$\sigma_{had} = \frac{N}{\varepsilon \cdot \int L\, dt}$$

The total number of observed hadronic events N has been normalized to the integrated luminosity as described in the previous section.

The event acceptance ε is obtained by Monte Carlo studies. Events are generated according to the Feynman-Field parametrization and passed through a realistic model of the detector. Of course, the larger the acceptance the less does ε depend on details of the model. The typical acceptance of the three detectors is of the order of 70 to 80 %. The systematic errors of the total cross section measurements are mainly due to acceptance and luminosity uncertainties.

The number of hadronic events N has to be separated from a background of cosmic rays, QED events of the e and μ type, beam gas, beam losses, synchrotron radiation and so on. Let me remind you again that this background is about 6 to 7 orders of magnitude higher than the events rate of about 1 event per hour under the January running conditions. The event selection criteria are based on a combination of energy and track requirements. In the PLUTO detector[81] for example at least 2 charged particles and a neutral energy deposition of more than 0.3 x E_{CM} was required. Very similar criteria were applied in the MARK J detector[88]: at least 2 hadron showers with at least 1 track pointing to the vertex and a total energy of more than 10 GeV. Since no photon measurement was available in the TASSO detector[89] the track requirements had to be sharpened: at least 3 tracks originating from the vertex.

Fig. 57 demonstrates the quality of event selection in the PLUTO detector. The neutral energy is plotted against the event vertex on the beam axis. It shows that after the neutral energy cut only very little beam gas background remains in the sample. This background can be estimated from the tails outside the interaction region. Fig. 58 shows an example of a hadronic event in the detector PLUTO - by the way the first hadronic event observed at PETRA.

The results of the three detectors are summarized in table 12. The differences in integrated luminosity are due to the fact that not all detectors were operational during the full time of data taking. The radiative corrections quoted are for the hadronic cross section only. Radiative corrections to the monitor are included in the quoted luminosities. Estimated beam gas background is very low in all three experiments. Residual $\gamma\gamma$-contributions to the observed number of these calculations have been cross checked with the measured two-photon events which I will discuss at the end of this chapter. The final

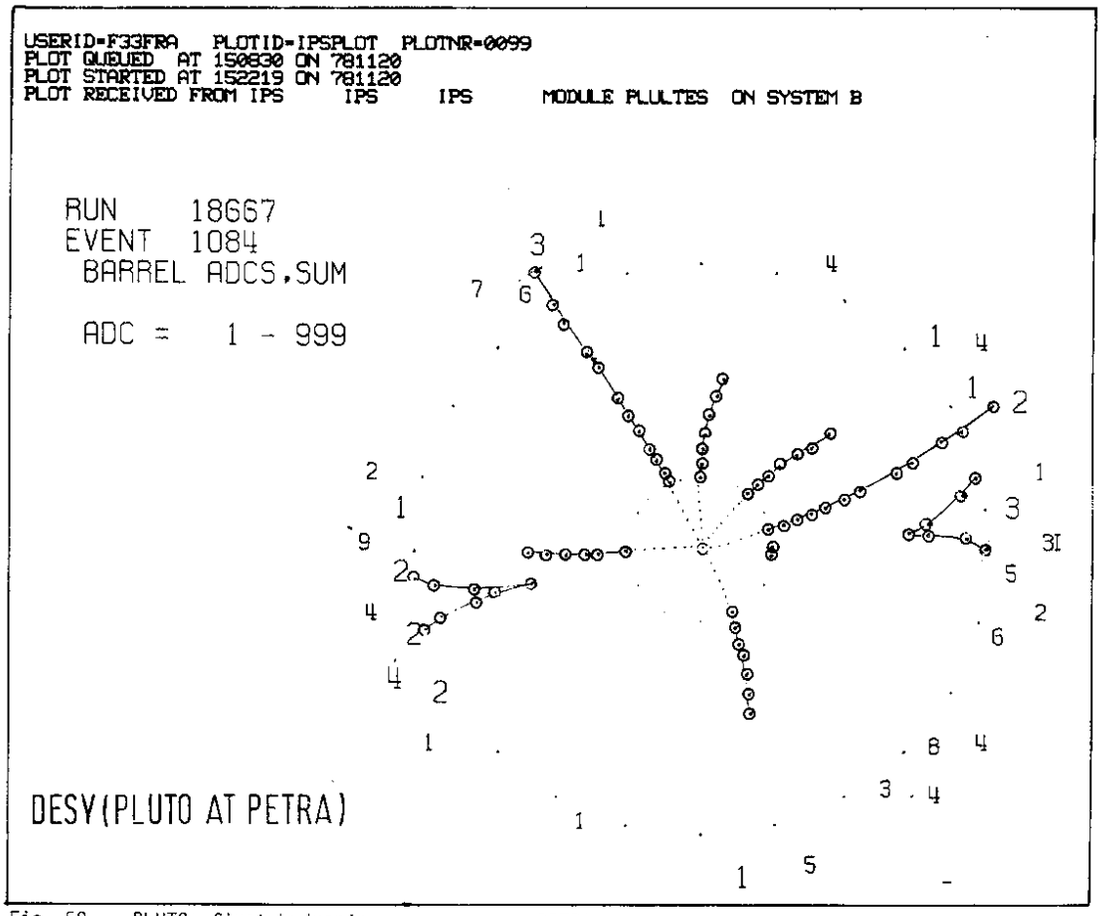

Fig. 58 PLUTO: first hadronic event seen at PETRA.

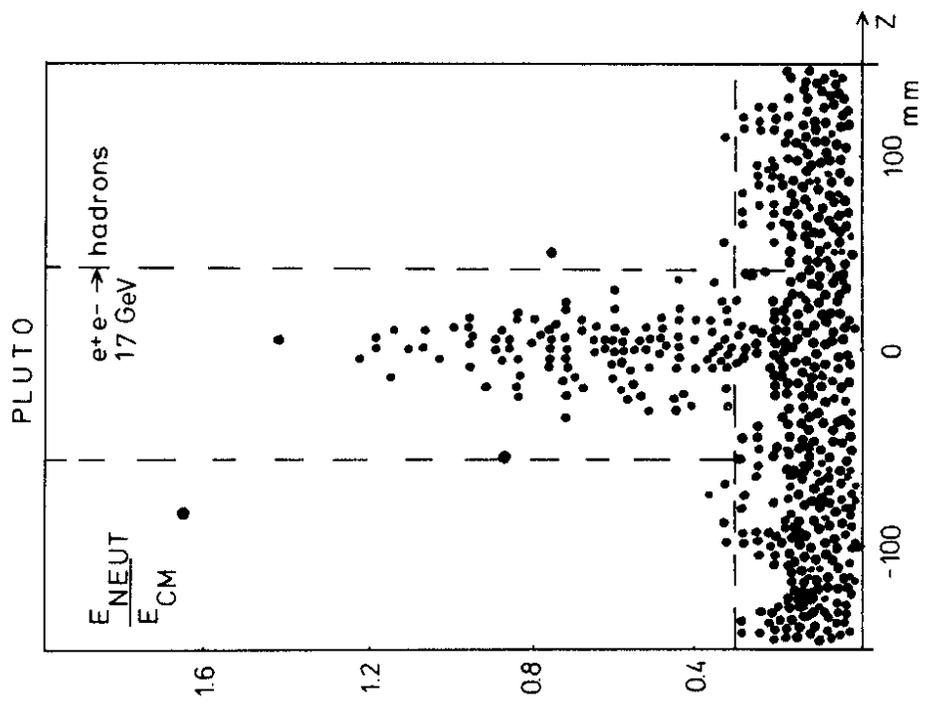

Fig. 57 PLUTO: event selection demonstrated in a two dimensional plot of neutral energy vs. event vertex along the beam axis.

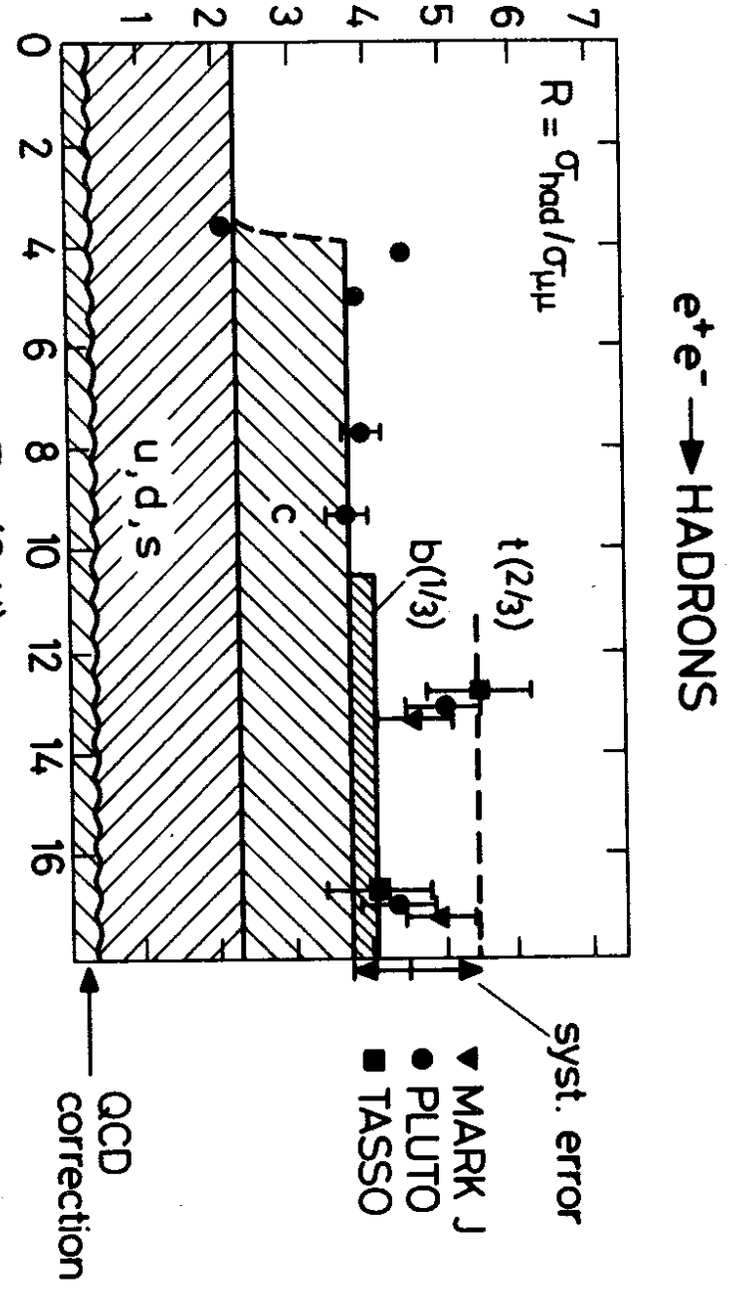

Fig. 59 PLUTO, TASSO, MARK J: measurement of $R = \sigma_{had}/\sigma_{\mu\mu}$ at 13 and 17 GeV. The PLUTO data below 10 GeV are given for comparison. The expectations for different flavours are indicated.

Table 12 Total cross sections at 13 and 17 GeV

	PLUTO[81]		MARK J[88]		TASSO[89]	
E_{CM} (GeV)	13	17	13	17	13	17
Acceptance ε (%)	72	72	79	79	77	78
$\int L\,dt$ (nb^{-1})	42.6	88.3	45	60	29.6±3.0	39.2±3.5
Radiative corrections (%)	-10	-10			- 8	- 8
Estimated bg (ev.)	< 1	< 1	< 1	< 1	) 3	) 1.5
Estimated $\gamma\gamma$ (ev.)	6	13	a few %	a few %	)	)
hadronic events (ev.)	96	108	83	68	75	40.5
$R = \frac{\sigma(hadr.)}{\sigma_{\mu\mu}}$	5.0±0.5	4.3±0.5 (τ excluded)	4.6±0.5	4.9±0.6	5.6±0.7	4.0±0.7 (τ excluded)
Estimated systematic errors	20 %	20 %	±0.7	±0.7	20 %	20 %

number of hadronic events and the values of R are given in the table. The estimated systematic errors are of the order of 20 %. Fig. 59 shows a plot of the measured values of R together with the measurements of PLUTO below 9.5 GeV. The different levels of R expected for the old quarks and possible new contributions from 1/3 and 2/3 charged quarks are indicated.

We can draw the following conclusions:

- Above 9.5 GeV there is certainly room for an increase of R corresponding to a $b\bar{b}$ threshold. It is unlikely that this new quark b has a charge of 2/3 although this cannot be excluded due to the large systematic errors. (compare also the evidence for $Q_b = -1/3$ given in chapter II.)

- Assuming that the systematic errors cancel in the relative measurement between 13 and 17 GeV we can exclude any new charged 2/3 thresholds coming up between these two energies.

c) Event topology

Events in e^+e^- annihilation exhibit a jet structure outside the resonances. As shown in chapter III this two jet topology becomes more and more pronounced if one increases the energy. In first approximation the event topology below 10 GeV is fairly well understood in the simple quark fragmentation model. As the energy increases two additional effects are expected.

Thresholds

As one crosses a threshold of new flavour production the decay of new heavy quark pairs will contribute to the event topology[46]. The sphericity of these weakly decaying slow quarks will be comparatively large[90]. Consequently the mean sphericity will increase. Under favourable conditions (near threshold) the new contributions might even be separable.

QCD jets

As Sterman and Weinberg[45] pointed out the effect of gluon emission in the quark pair production leads to a natural broadening of the energy flow in the final state[91-93]. The effect which is analogous to QED radiative corrections can be calculated in the first order QCD (fig. 60).

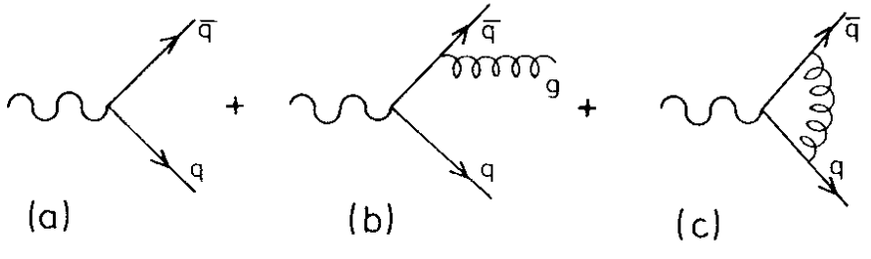

Fig. 60 Contributions to the annihilation cross section in first order QCD.

At large energies this effect should lead to a broadening of the jet fragmentation. One prediction is therefore that the mean transverse momentum of the jets should increase with energy.

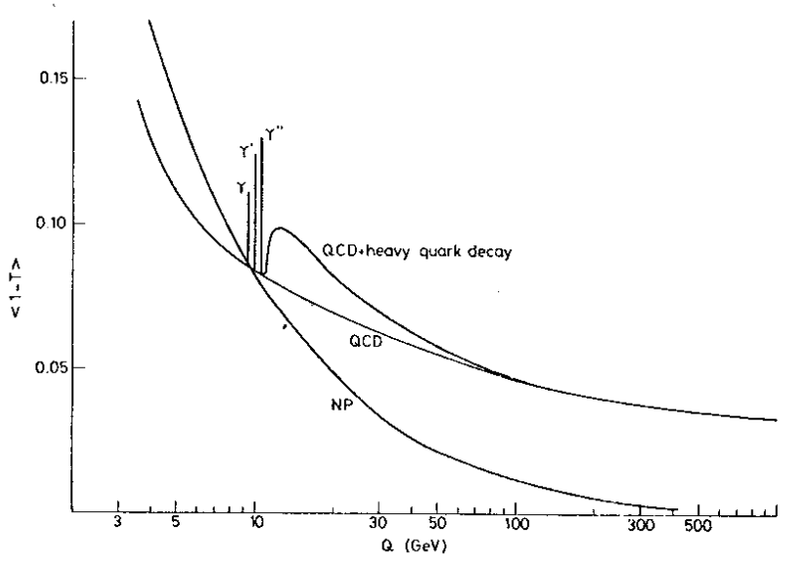

Fig. 61 Theoretical expectation for three contributions to the event topology: first order QCD, fragmentation (NP) and heavy quarks (from ref. 45).

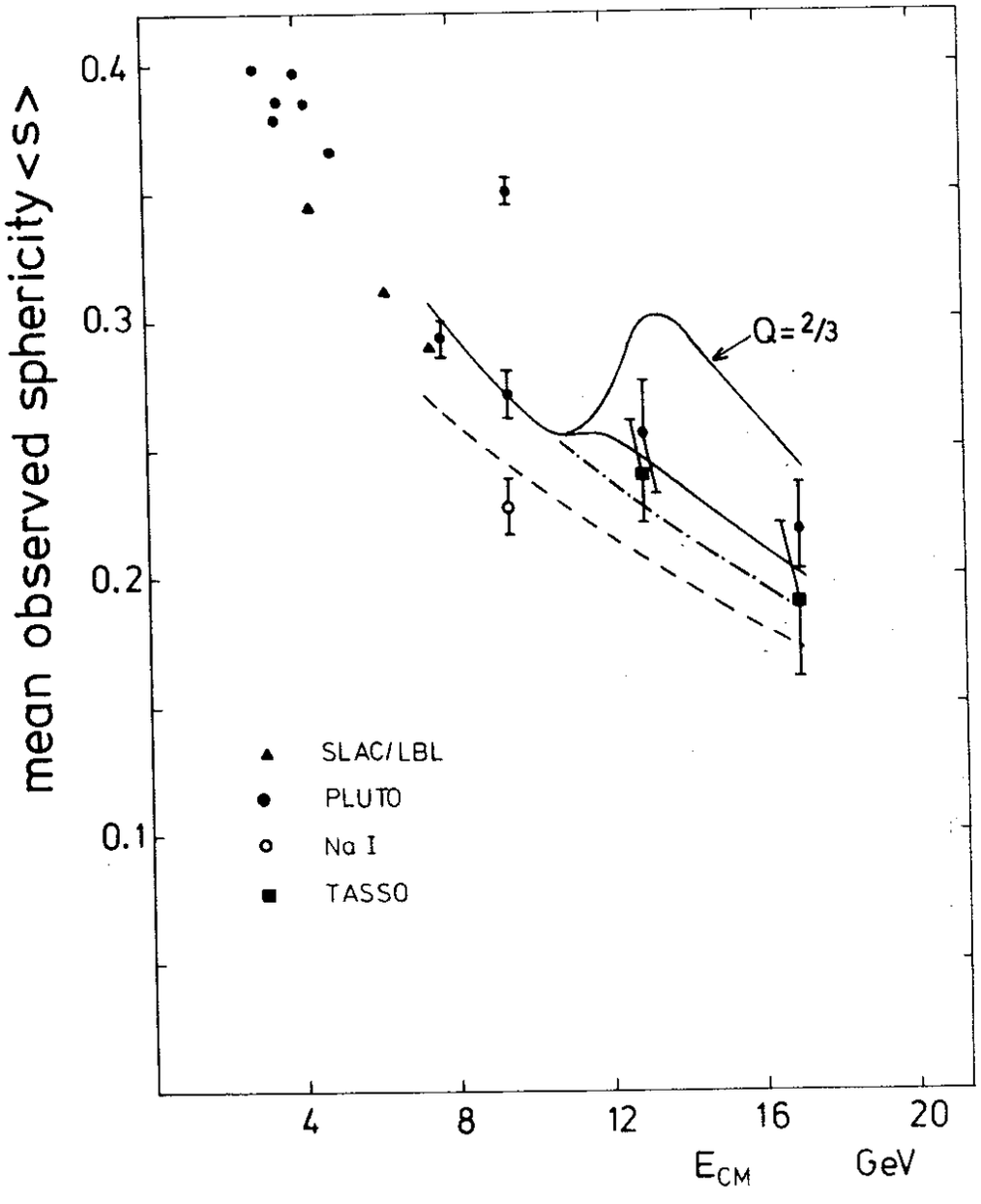

Fig. 62 SLAC-LBL, PLUTO, TASSO and NaJ-lead glass: mean observed sphericity as a function of energy. The dashed line indicates the simple two-jet model (Feynman-Field). Inclusion of charm and bottom leads to the dash-dotted and full curves[90]. A charge 2/3 contribution is indicated.

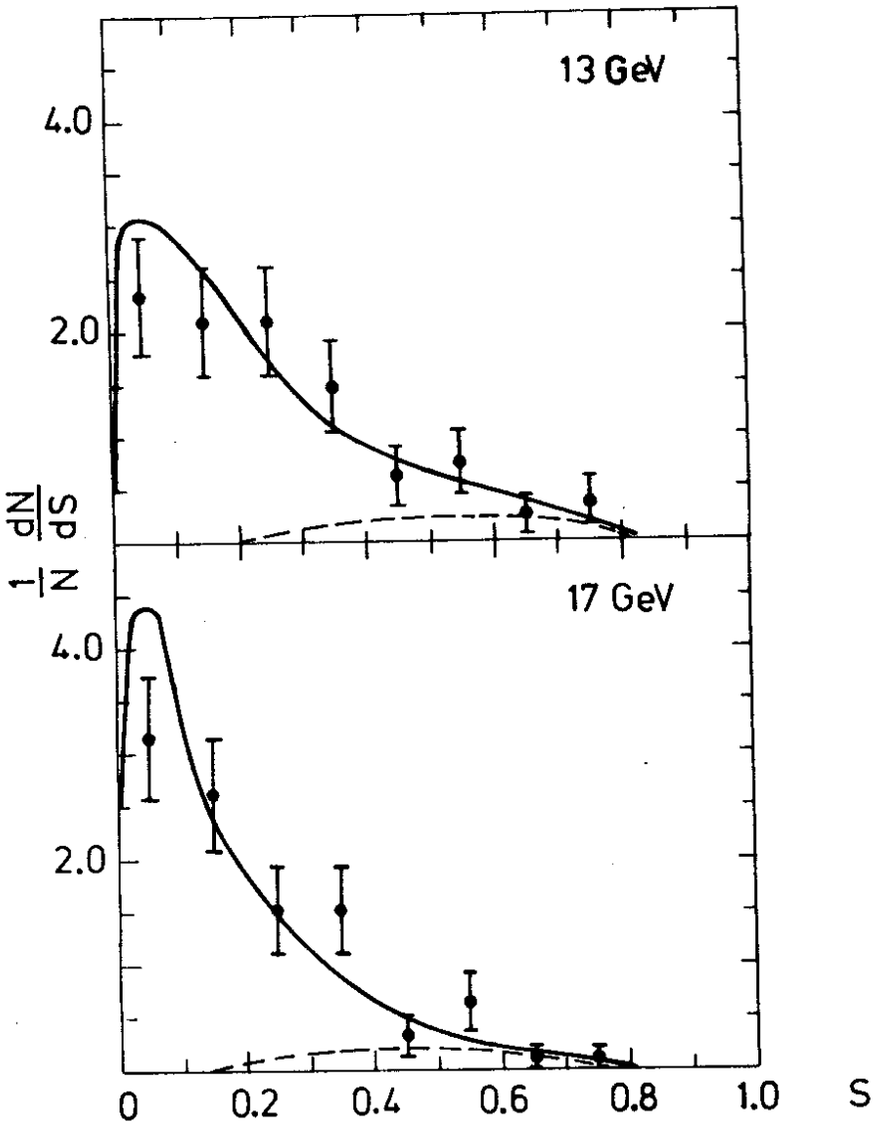

Fig. 63 PLUTO: observed sphericity distributions at 13 and 17 GeV. The expectation for b quark production is indicated by a dashed line[90]. The full line is the two-jet model including all corrections.

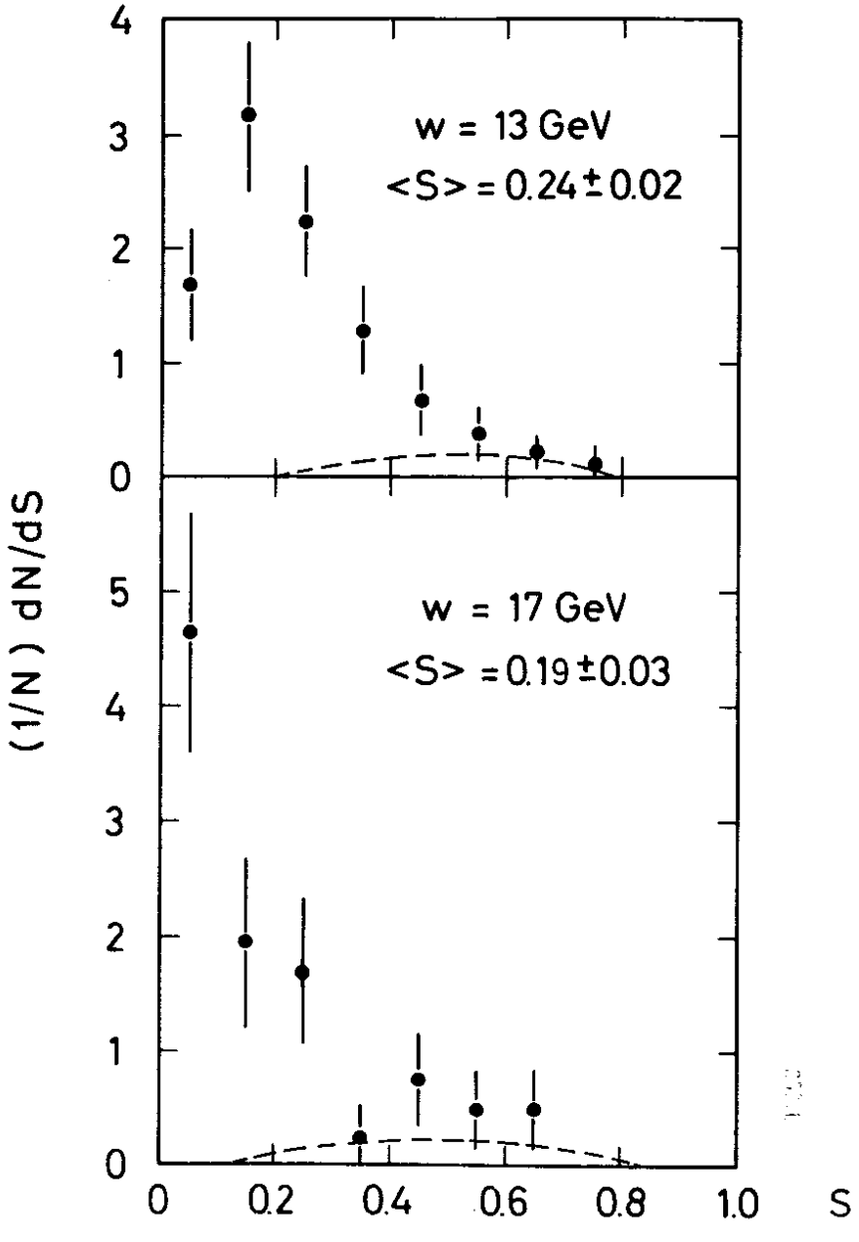

Fig. 64 TASSO: observed sphericity distributions at 13 and 17 GeV. The expectation for b quark production is indicated by a dashed line[90].

Fig. 61 which is taken from ref. 46 shows the expected behaviour of the different components which contribute to the event topology.

The PLUTO group has analysed the high energy data at 13 and 17 GeV in the same way described for the data below 10 GeV. Fig. 62 shows the mean observed sphericity as a function of c.m. energy now ranging from 3.6 to 17 GeV. The data of SLAC-LBL, TASSO and the NaJ-lead glass detector are given for comparison. The dashed curve shows the expectation of the Feynman-Field Monte Carlo (without radiative corrections). The dash-dotted line indicates the additional contribution from charm production. Note that part of the charm production is already contained in the Feynman-Field curve since it is normalized to the total cross section. The full line then shows the additional contribution expected from a new heavy quark of charge 1/3 [90]. A charged 2/3 new quark is indicated for comparison. It clearly shows that the data are consistent with $b\bar{b}$ (charge 1/3) production and that a charge of 2/3 can be excluded. Fig. 63 shows the differential sphericity distribution at 13 and 17 GeV.

A similar analysis was carried out in the TASSO group. The result of their observed sphericity distribution of charged particles is given in Fig. 64. We realize that the sphericity distributions of the TASSO group are narrower and that <S> is lower than in the PLUTO experiment. This is due to the better momentum resolution in the TASSO detector. The distributions exhibit a tail towards large values. For comparison the expectation for b quark production is indicated in all figures[90]. We see that there is room for this contribution in the data. Note that the mean sphericity of the bottom events is considerably higher than that of the old quarks. This difference is particularly pronounced at 17 GeV. Again a contribution of a new quark with charge 2/3 would be four times as high in rate as the indicated b quark contribution. This is certainly excluded form the data.

Inclusive distributions

Inclusive particle distributions obtained by the TASSO group are shown in fig. 65. Data at 13 and 17 GeV are compared with previous measurements of the DASP group at 5 GeV. We notice a remarkable scaling beyond x = 0.2 over the full energy swing from 5 to 17 GeV. Below x = 0.2 the distributions are filled up at high energies. Two interesting observations can be made in this region. Instead of approaching the high energy limit from below the 13 GeV data seem to be higher than the 17 GeV data. Neglecting the overall systematic unvertainties

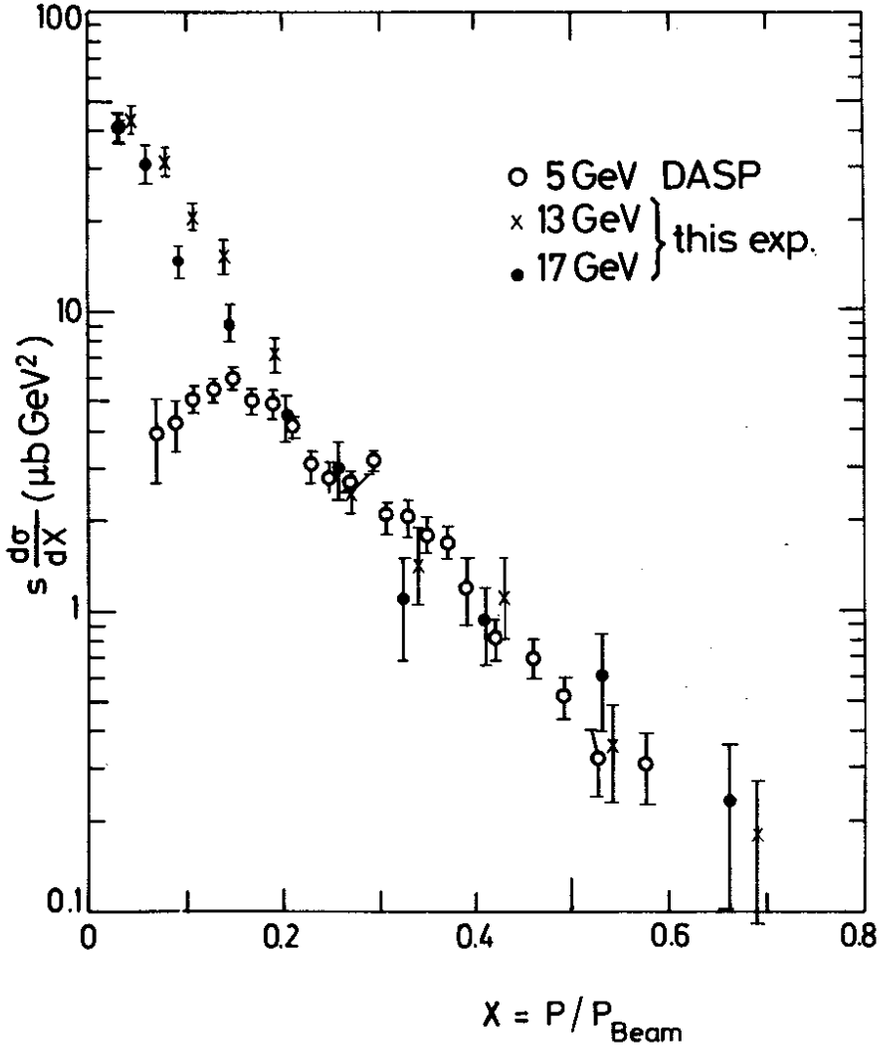

Fig. 65 TASSO: inclusive momentum distributions for charged particles.

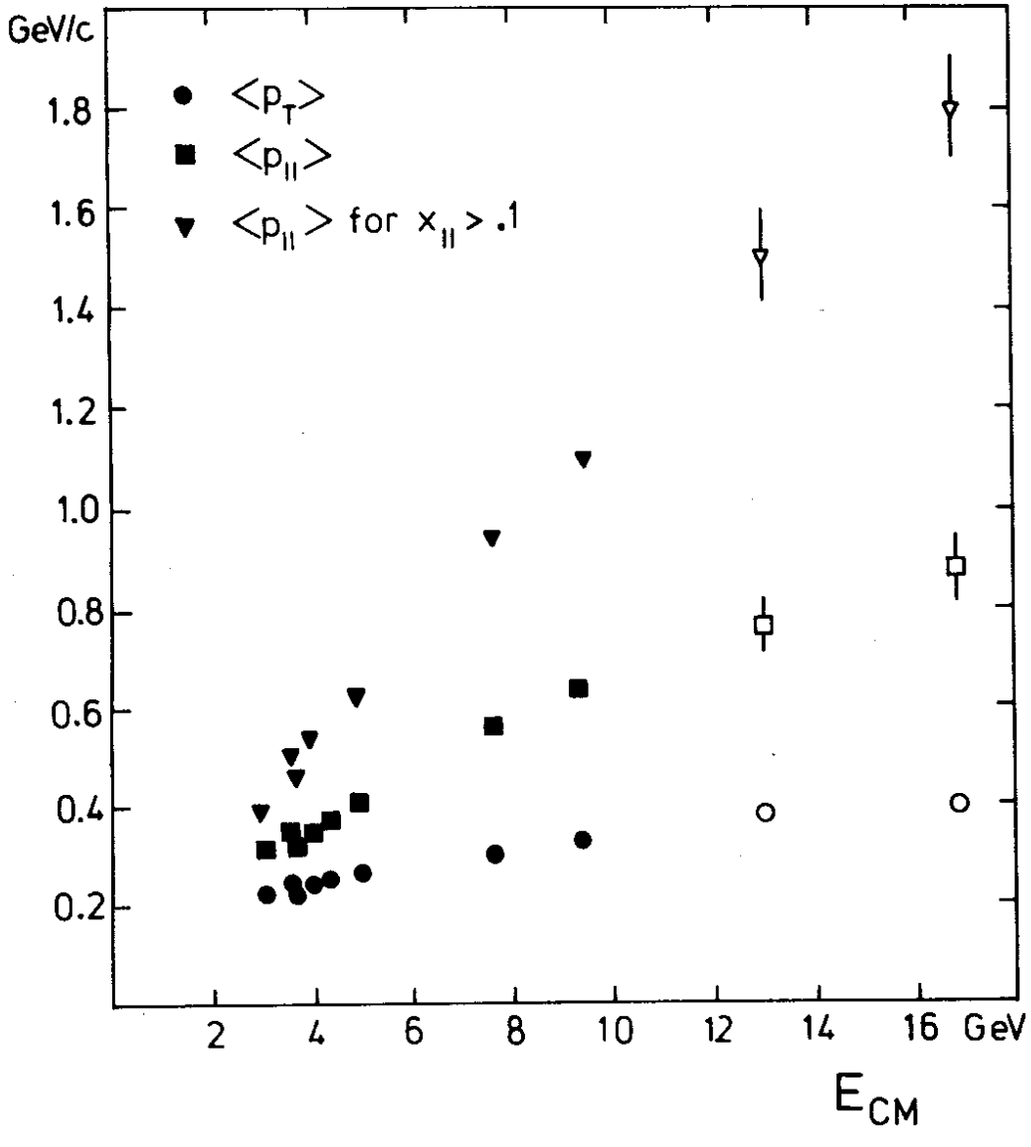

Fig. 66a) PLUTO: mean observed p_T and p_L as a function of energy. $\langle p_L \rangle$ is also shown for the scaling region $x_L > 0.1$.

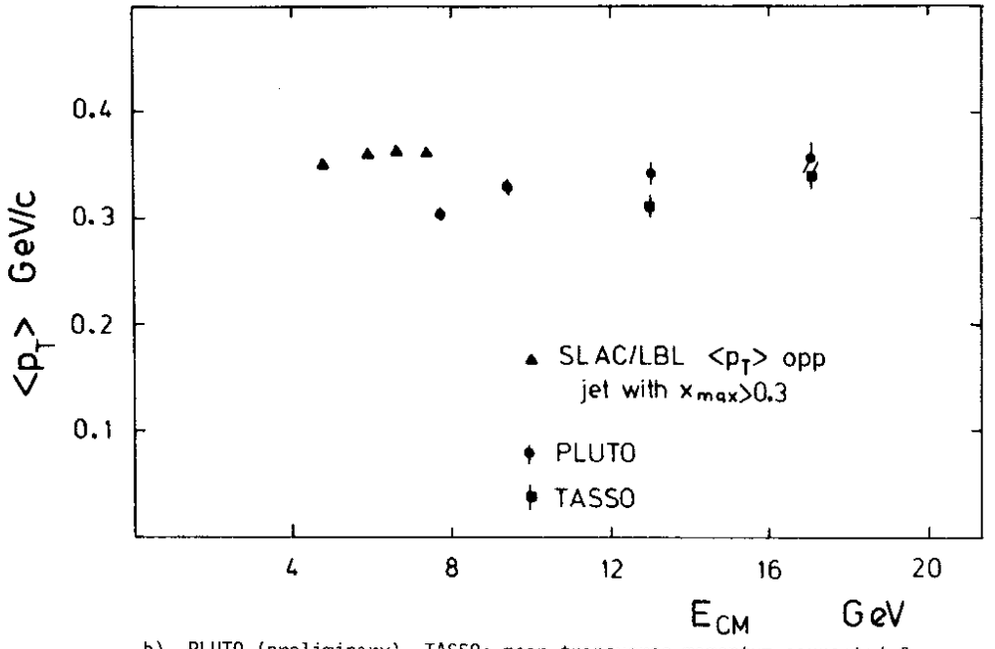

b) PLUTO (preliminary), TASSO: mean transverse momentum corrected for acceptance and resolution. SLAC-LBL values are shown for comparison.

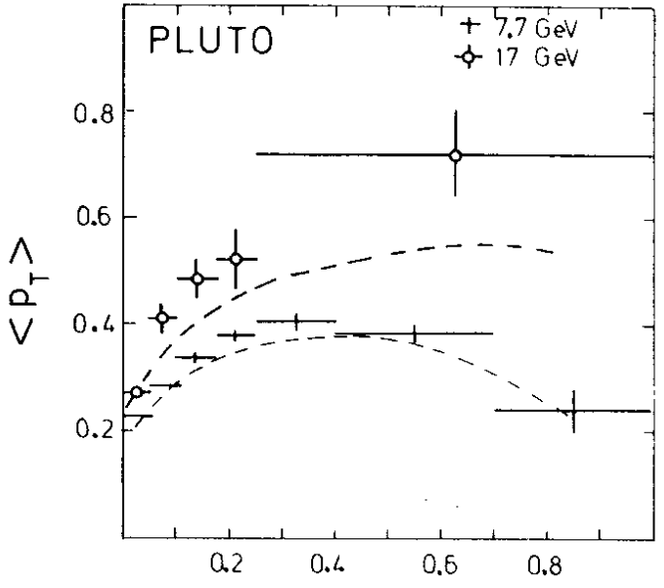

Fig. 67 PLUTO: "Seagull" effect at 7.7 and 17 GeV.
a) The mean observed p_T is shown as a function of $x_L = p_L/E_b$. The curves are two-jet model calculations.

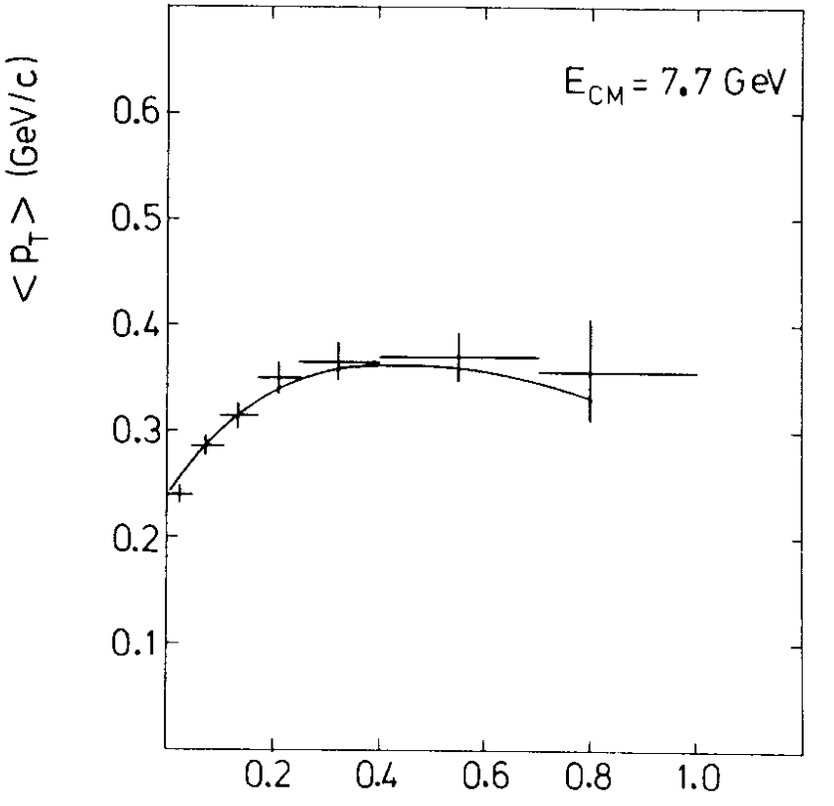

b) 7.7 GeV: $\langle p_T \rangle$ including all corrections. The two-jet model is shown for comparison.

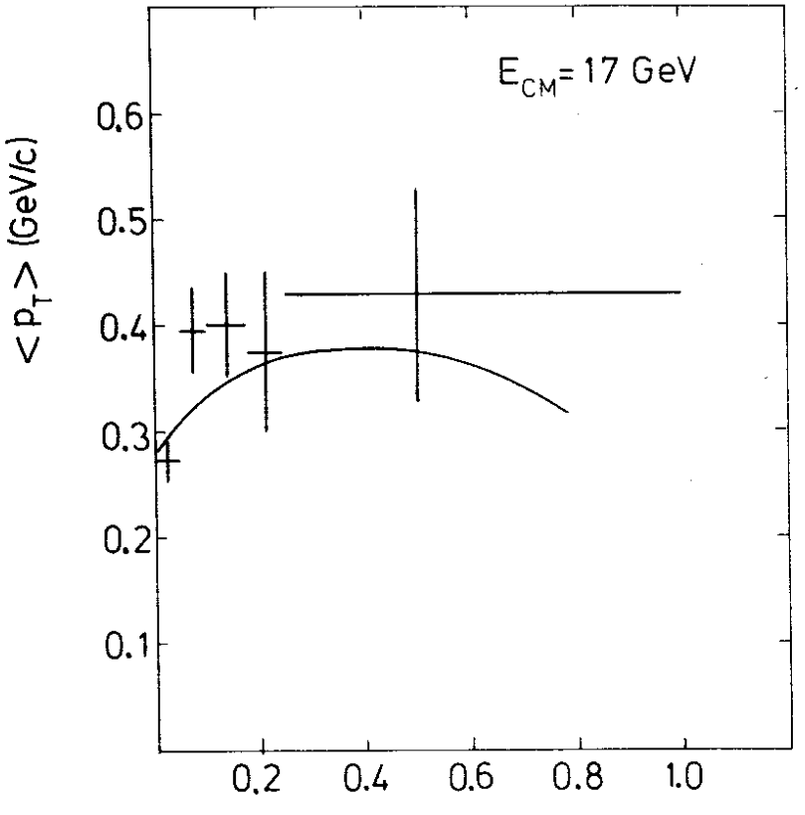

c) 17 GeV: $\langle p_T \rangle$ including all corrections. The two-jet model is shown for comparison.

this is a two standard deviation effect. Also the distribution does not simply follow an extrapolation of the high x data but seems to be steeper below x = 0.2. Further study of these effects which might be due to b production is certainly needed and of prime importance.

Transverse momentum

Whereas a fixed transverse momentum is the main ingredient of a simple quark parton model QCD predicts an increase of p_T with energy due to gluon bremsstrahlung. Fig. 66a shows the energy dependence of the longitudinal and transverse momentum with respect to the sphericity axis as observed in the PLUTO detector. The figure nicely demonstrates again how jets are developing with increasing energy through their limited p_T and rising p_L. In particular p_L is rising linearly in the scaling region x_L greater than 0.1. After a slight increase at low energies where the jets are not fully developed the mean p_T levels off at high energies. Comparing the values at 13 and 17 GeV as measured by the PLUTO and the TASSO groups (fig. 66b) one observes infact constance between the two energies within two standard deviations.(Fig. 66b shows corrected values.)

The value of mean p_T is, of course, governed by the plateau region. One might argue that this is the region of confinement effects and that, therefore, intermediate x_L might be a better place to look for QCD effects[94]. Indeed, if we compare the 'seagull' effect at 7.7 and 17 GeV (fig. 67a) we see a strong increase in mean p_T at intermediate x_L. However, the Feynman-Field Monte Carlo indicated in the figure shows a similar may be somewhat weaker increase. Since, however, this effect is strongly dependent on a proper handling of secondary decays any conclusion on the energy dependence of the 'seagull' effect is premature.

d) Two-photon physics

The importance of two-photon physics was realized by many people in several publications[95,96] in 1971. The process is illustrated schematically in fig. 68.

As the electrons approach each other they radiate photons which interact. The process can be visualized as the interaction of two photon beams which are produced by electron beams passing a radiator. The energy spectrum is given by:

$$N(k)\, dk = \frac{2\alpha}{\pi} \ln (E_b/m_e)\ \frac{dk}{k}$$

k = photon energy

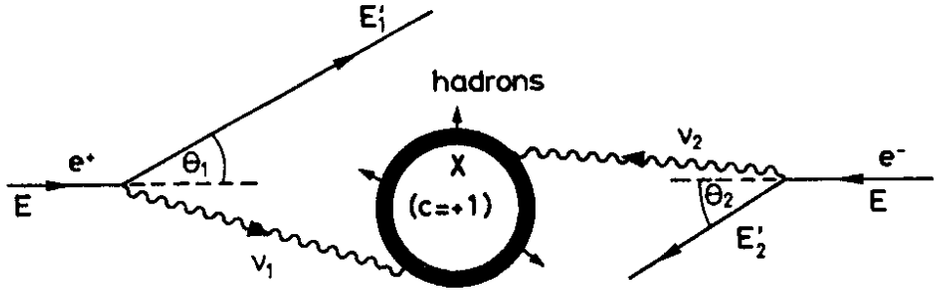

Fig. 68 The two-photon process.

Thus the photon rate is increasing logarithmically with beam energy. At E_b = 15 GeV the photon beam has reached an intensity of

$$N(k)\,dk \simeq 0.05\,\frac{dk}{k}$$

equivalent to a radiator of 5 % radiation length. Experimentally the occurance of a two-photon reaction in e^+e^- collisions can be detected by tagging devices (fig. 69).

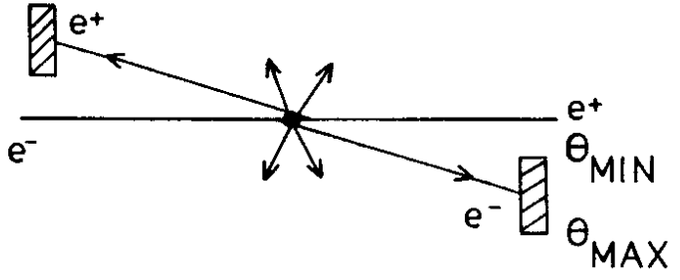

Fig. 69 Tagging in two-photon physics.

They usually measure energy and direction of the outgoing electrons (positrons). Thus if both particles are tagged the kinematics of the $\gamma\gamma$ reaction can be determined. Since the tagging devices cover only a limited solid angle the tagged photon beam intensity is reduced.

$$N(k)\,dk \simeq \frac{dk}{k}\cdot\frac{2\alpha}{\pi}\left(\ln\frac{E\sin\theta_{max}}{m_e} - \ln\frac{E\sin\theta_{min}}{m_e}\right)$$

For a typical tagging device ranging from 25 to 250 mrad this corresponds to a reduction of the tagged photon flux by about a factor of 5 with respect to the total flux.

In the naive picture of figure 68 the reaction will occur in two steps, the emission of the two nearly real photons and their collision with a cross section $\sigma_{\gamma\gamma}$ (equivalent photon approximation[97]). The order of magnitude of this cross section is given by the vector meson dominance model. In the simplest version of this description the gamma-proton and proton-proton cross section can be related to the gamma-gamma cross section.

$$\sigma_{\gamma\gamma} = \frac{\sigma^2(\gamma p)}{\sigma(pp)} \simeq 300\ \text{nb}$$

A more refined description[98] yields additional terms in the resonance region below about 3 GeV invariant mass of the two photons. The energy dependence of the two-photon cross section is shown in fig. 70 together with the annihilation cross section[99]. Already at moderate beam energies the two curves cross over and the two-photon cross section gains sizable values compared to the annihilation cross section.

At first sight one might realize little interest in $\gamma\gamma$ reactions except getting rid of them in the e^+e^- annihilation data. Infact nearly real photons are supposed to behave very much like hadrons. Their collisions are much better studied, for instance at the ISR. There are, however, two aspects which show the topical importance of two-photon reactions.

C=+1 resonances

C=+1 resonances like η and η_C can be produced directly in $\gamma\gamma$ reactions. In view of the latest conflicting results on the η_C the importance of this does not need further advertisement. Apart from spotting a particle like the η_C a measurement of the cross section would yield the two-photon width $\Gamma_{\gamma\gamma}$ which provides a very sensitive test of the constituent quark charge. As one can see from fig. 70 the estimated cross sections are not out of reach at 15 GeV.

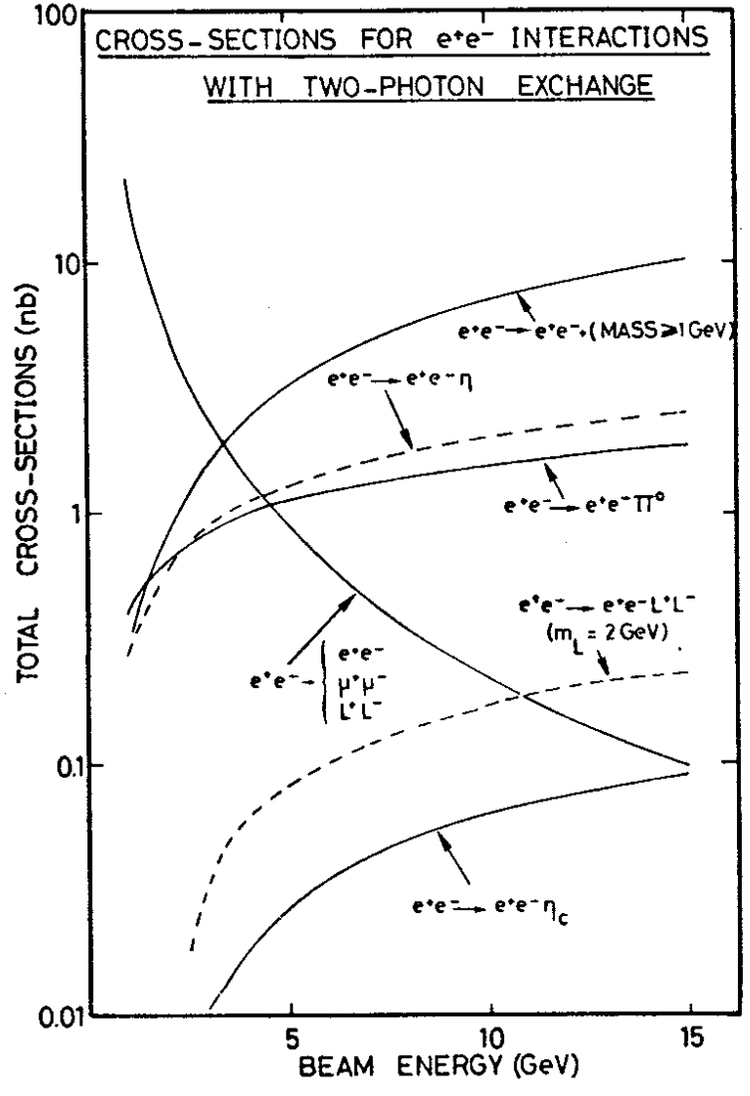

Fig. 70 The expectation for various two-photon cross sections compared to the annihilation cross section[99].

Jet production

The most outstanding aspect of two-photon processes is, however, the direct production of quark jets[100,101].

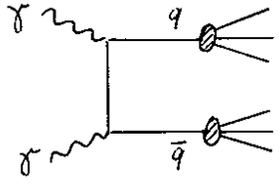

$\rightarrow e^+e^- \rightarrow e^+e^- + q\bar{q}$

$\rightarrow e^+e^- + 2$ jets

Similar to the annihilation processes this mechanism can be related to the QED process $e^+e^- \rightarrow e^+e^-\mu^+\mu^-$ defining a quantity

$$R^{2\gamma} = 3 \sum_q Qq^4.$$

Evidende of hadronic $\gamma\gamma$ events

In 1974 two candidates for hadronic $\gamma\gamma$ events were reported at Frascati[102]. Since then no further evidence was observed. To search for two-photon processes the PLUTO group[103] looked for coincidences between the inner detector and one or two of the forward spectrometers. In the data presented here only the SAT part of the forward spectrometer was used. A tagged electron was defined by an energy deposition of more than 3 GeV. To look for hadron production at least three tracks or two tracks plus additional energy were required in the central detector.

Single tag events

A vertex distribution of single tag events of the type

$$e^+ e^- \rightarrow e^{\pm} + \text{hadrons}$$

is shown in fig. 71. The distribution exhibits a clear excess of events near to the interaction point. The relatively large background can be attributed to beam gas scattering. After subtraction of this background (15 events) a signal of 38 ±11 events remains. Accidental coincidences between hadronic annihilation events and off-momentum beam particles hitting the SAT could fake the above signature. Since no such event was found in the hadronic annihilation events, this background is estimated to be less than 0.1 %. Therefore, a clear signal

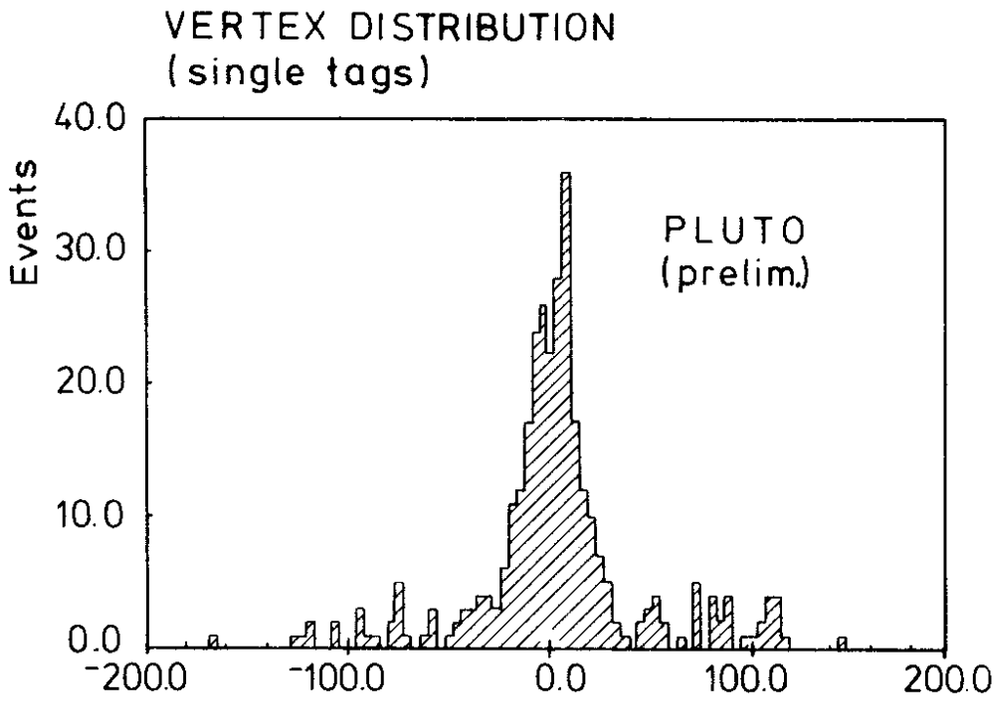

Fig. 71 PLUTO: (preliminary) vertex distribution of single tag two photon candidates.

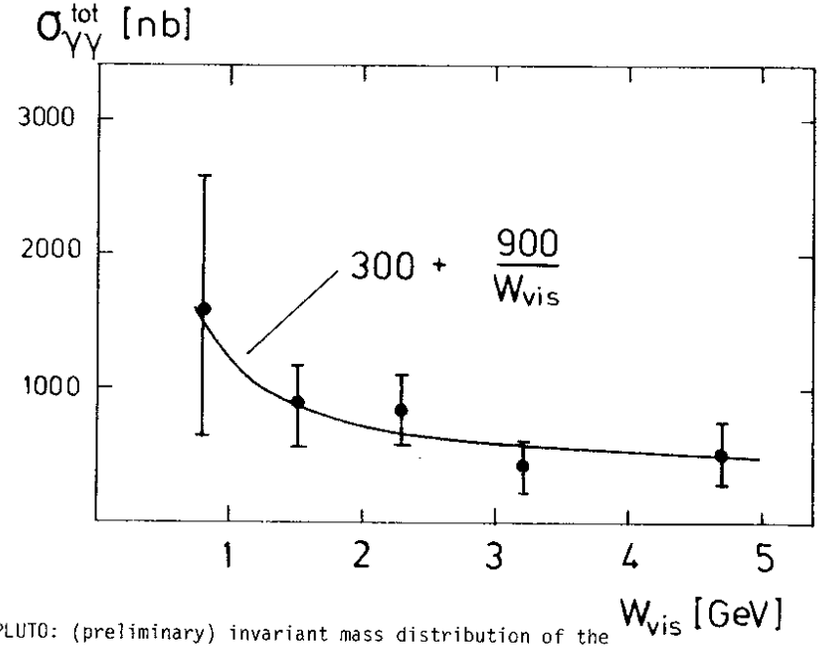

Fig. 72 PLUTO: (preliminary) invariant mass distribution of the hadronic system for single tag two photon events.

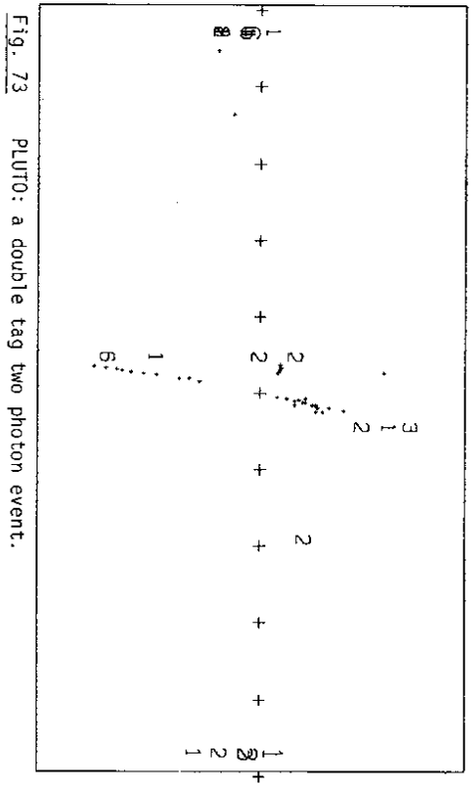

Fig. 73 PLUTO: a double tag two photon event.

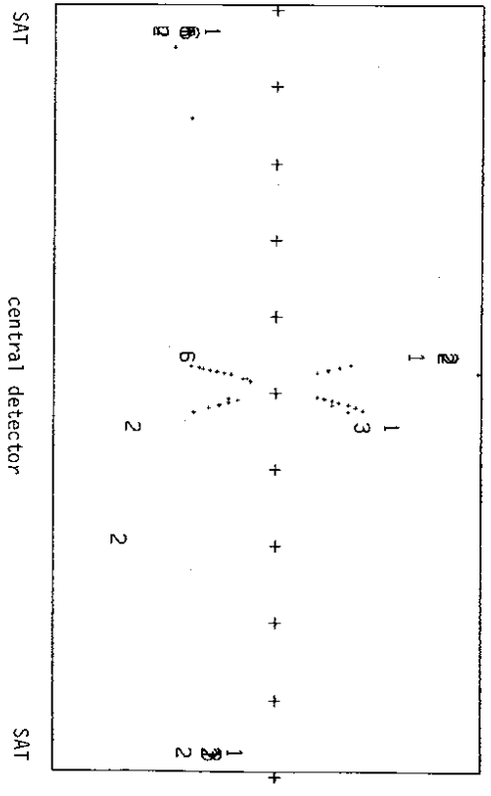

remains which can only be attributed to the two-photon production of hadronic final states. A preliminary evaluation of the cross section (fig. 72) yields an asymptotic value of about 300 nb above 3 GeV invariant mass of the two photons.

Double tags

The above evidence is corroborated by 12 events with the signature

$$e^+ e^- \rightarrow e^+ e^- + \text{hadrons}$$

in the PLUTO detector. The accidental background for this data sample is less than 1 %. Fig. 73 shows a clean example with 2 electrons in the forward spectrometer and 4 non showering tracks in the central detector.

In conclusion the PLUTO group has found the first clear evidence for the production of hadrons in two-photon processes:

$$e^+ e^- \rightarrow e^+ e^- + \text{hadrons}$$

This opens a new field of e^+e^- physics.

4. Physics plans at PETRA

In this last section I would like to describe some of the physics plans for the immediate future at PETRA.

Search for the top quark

The search for the proposed t quark is of literally topical interest for the near future of PETRA. Therefore, PETRA has been prepared for energies of the order of 30 GeV c.m. by introducing further cavities. There are a number of handels and strategies to look for the new top quark. I will follow the common prejudice that this new quark has a charge of 2/3. The expected step in R will then be of the order of 1.5 including gluon corrections. Our measurements at 13 and 17 GeV have shown that the detectors at PETRA would be sensitive to such a threshold on the statistical basis of a few hundred events, provided the background can be controlled.

The ultimate aim of finding the toponium resonances will then probably be attacked in two steps. First the position of the threshold will be estimated from a sequence of R measurements at large energies. Once the threshold is roughly localized one could apply theoretical estimates to predict the position of the toponium resonances. A fine scan in steps of the machine resolution will then

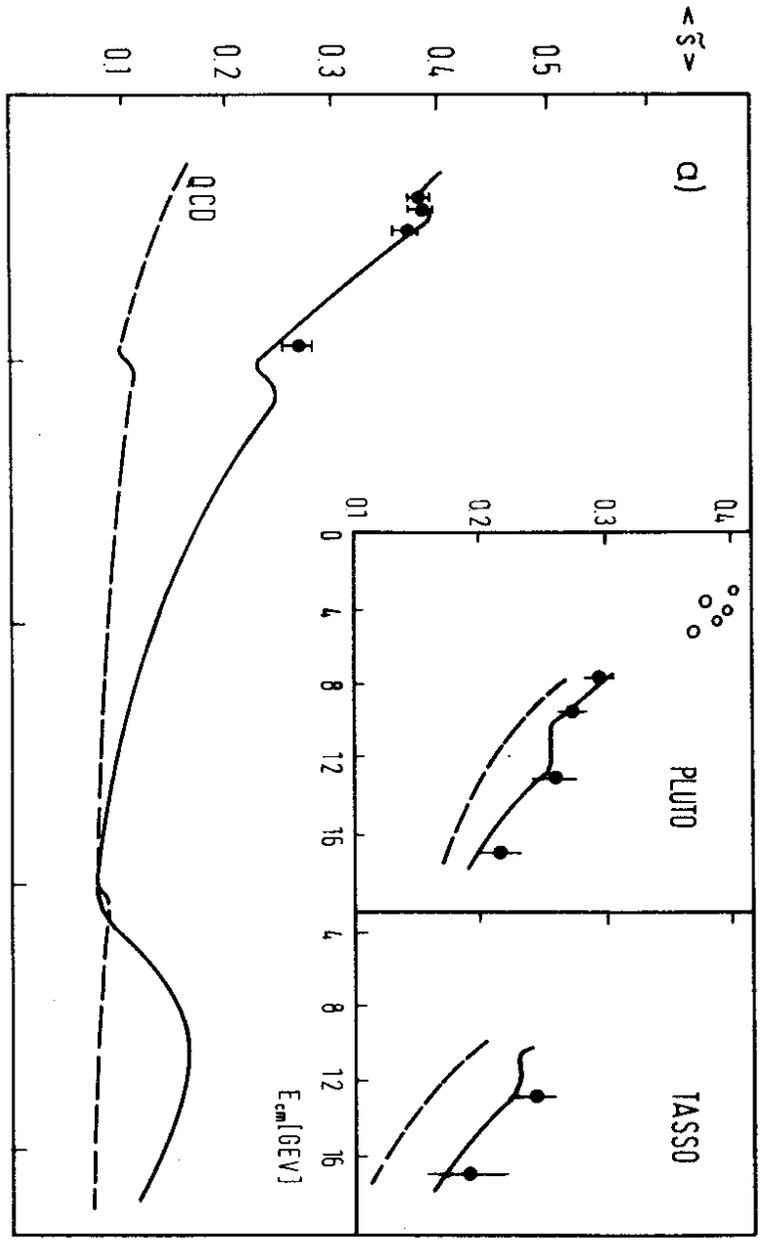

Fig. 74 Predicted change of sphericity and thrust above t threshold[90].
a) mean sphericity as a function of energy

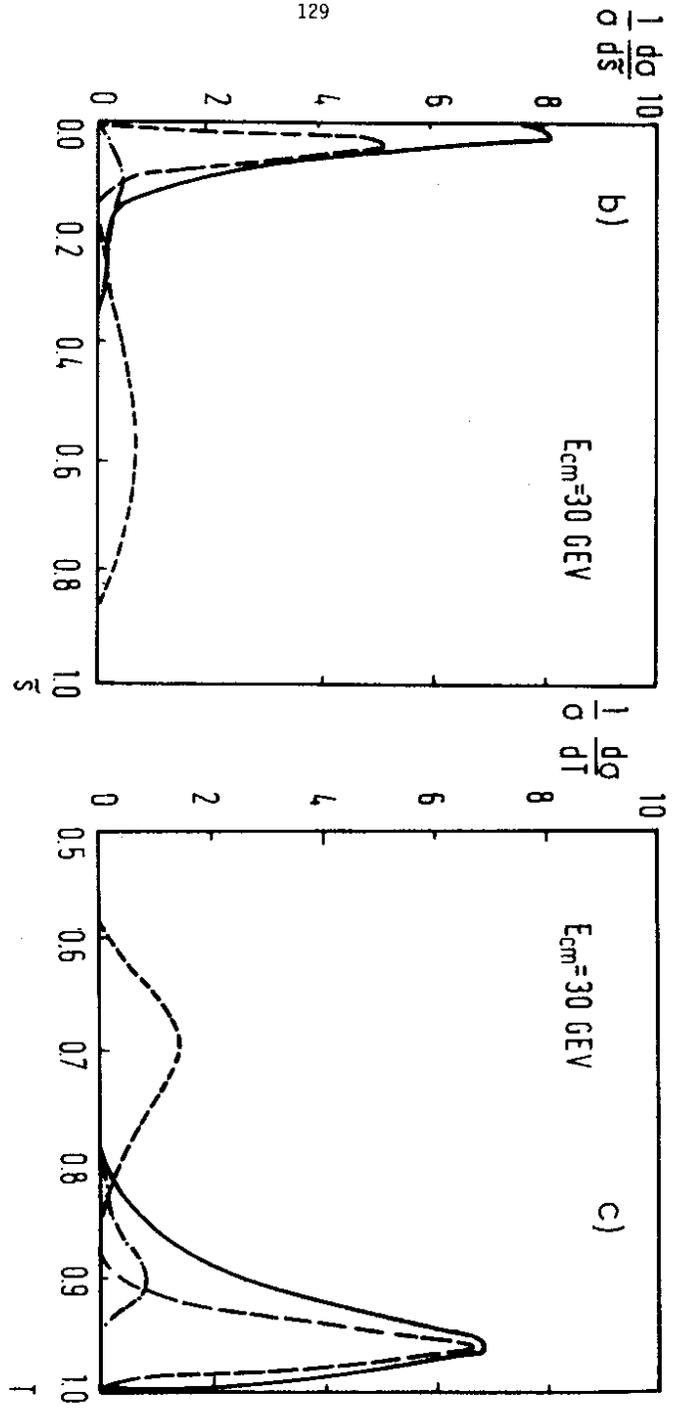

b) sphericity distribution at the t threshold

c) thrust distribution. The "old" contribution (——) including b (-·-) compared to the t part (---).

be applied to look for resonance structures in this region. To get an estimate of the relative height of the resonance (σ_p) compared to the continuum (σ_c) we can scale the relative cross sections from the Y region to the toponium region (assuming $M_{t\bar{t}}$ = 25 GeV):

$$\left(\frac{\sigma_p}{\sigma_c}\right)_{t\bar{t}} \simeq \left(\frac{\sigma_p}{\sigma_c}\right)_Y \cdot \frac{\Delta W(9.4)}{\Delta W(25)} \cdot \frac{\Gamma_{ee}(t\bar{t})}{\Gamma_{ee}(b\bar{b})} \simeq 1.3 \cdot \left(\frac{\sigma_p}{\sigma_c}\right)_Y$$

Since the energy resolution ΔW is about three times worse at the toponium and Γ_{ee} will scale like Q_q^2 the relative peak cross section at the toponium will be roughly as large as at the Y. Therefore, from a total cross section measurement the toponium could be found if it exists in the PETRA energy region.

Still there are at least 3 additional weapons which might turn out to be of great importance in the toponium search. The topology of the new events coming in above threshold will be drastically different from the dominant two-jet behaviour below threshold. Fig. 74 shows the expectation above top threshold[90]. If the differences are as large as expected one might even get a separation of top production by a simple cut in sphericity.

A further handle would then be to look for excessive lepton production[104]. If we follow the common believe that the top quark is cascading down the chain

$$t \rightarrow b \rightarrow c \rightarrow s$$

in successive weak decays we can estimate the total number of leptons per event. Assuming a branching ratio of 8 % into each type of lepton in each branch of the decay chain we arrive at an average of about 1 lepton (μ or e) for each $t\bar{t}$ event. In addition spectaculare events with up to 6 leptons may occur.

Search for heavy leptons

If further heavy sequential leptons exist their branching ratio into hadrons will be larger than for the τ. For masses between 10 and 15 GeV the leptonic branching ratio is expected to be of the order of 11 % (for e, μ and τ) whereas the remaining 67 % will be hadronic decays[105]. The prominent signature for these events will, therefore, be an isolated electron and a hadronic jet in oposite directions with large missing energy. Of course, also two-lepton events with large missing mass are expected, however, on a much lower statistical level.

Two-photon physics

Last not least the wide field of two-photon physics will be open in the high energy region, looking for even C resonances and jet production.

PETRA detectors

Let me close this lecture with a survey of the five detectors which are either installed or in preparation for the next running periods. A very short summary of the physics abilities of the five detectors is given in table 13. Since it is a hopeless attempt to describe five detectors in the framework of this lecture I just try to summarize the main physics goals of the different experiments. Most detectors (except MARK J) provide charged particle detection in large solenoidal magnetic volumes over 80 to 90 % of the solid angle. The typical momentum resolution at 5 GeV is of the order of 5 % for the drift chamber detectors whereas it is only 15 % for the proportional chamber detector PLUTO. Myon identification over a large solid angle is available in all experiments. The same is true for electron and photon detection. However, the method is quite different for the various detectors as indicated in table 13. In the last column I have listed a few items which are special to the different devices. Fig. 75 and 76 show the detectors JADE and CELLO which are now being prepared for installation this year.

Table 13 PETRA detectors

	Main Physics Goals	Charged Hadrons σ_p/p at 5 GeV	Electrons	Special Items
PLUTO	σ_{tot}	15 %	lead-scintillator	$\gamma\gamma$ tagging 25 ./. 250 mrad
MARK J	μ pairs	hadron calorimetry	lead-scintillator + tubes	rotatable
TASSO	jets + hadron identification	4-6 %	liquid argon	full Č-identification in 2 x 1.5 sr
JADE	jets + leptons	3-5 %	lead glass	"jet chamber", 50 dE/dx samples
CELLO	leptons	3-5 %	liquid argon	thin superconducting coil 0.5 X_0

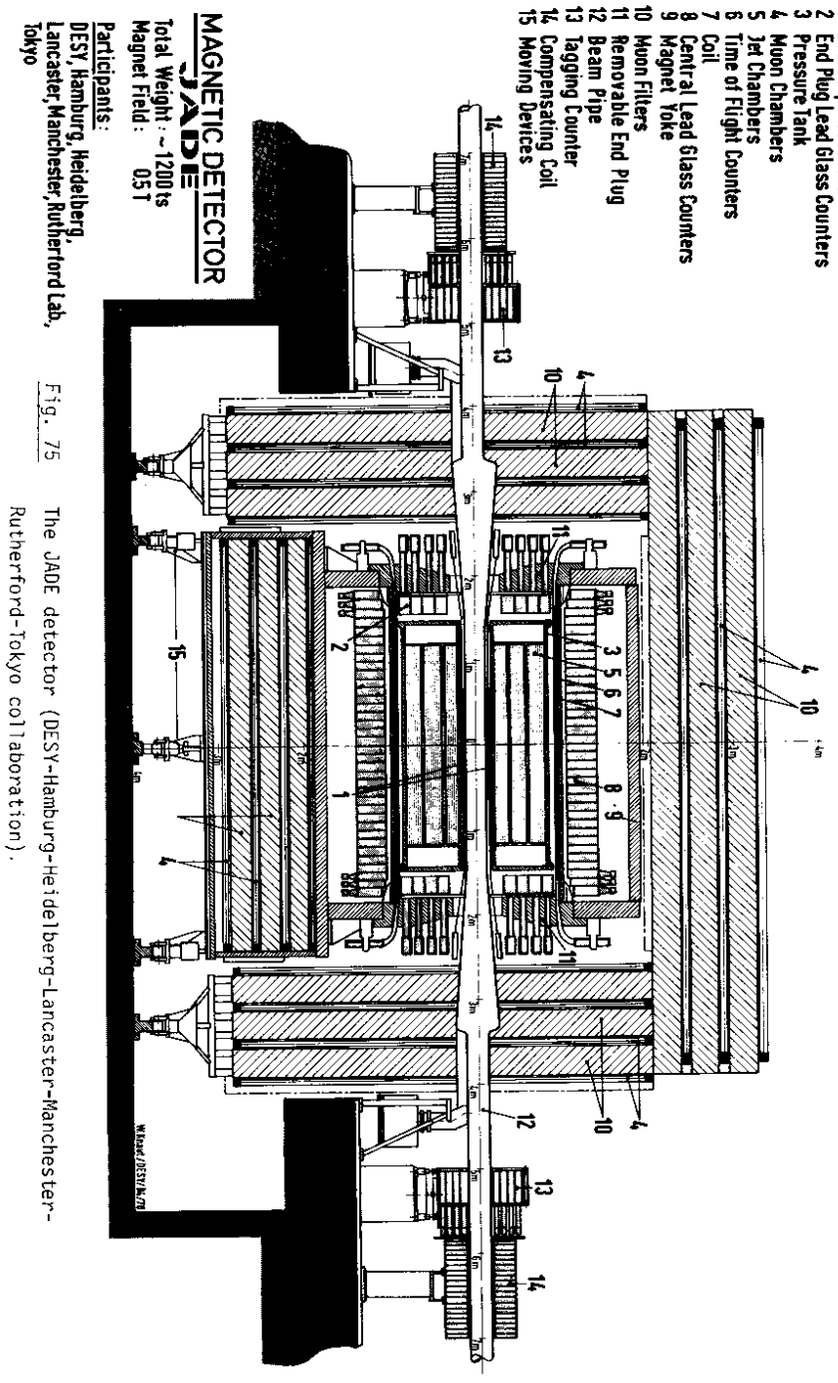

Fig. 75 The JADE detector (DESY-Hamburg-Heidelberg-Lancaster-Manchester-Rutherford-Tokyo collaboration).

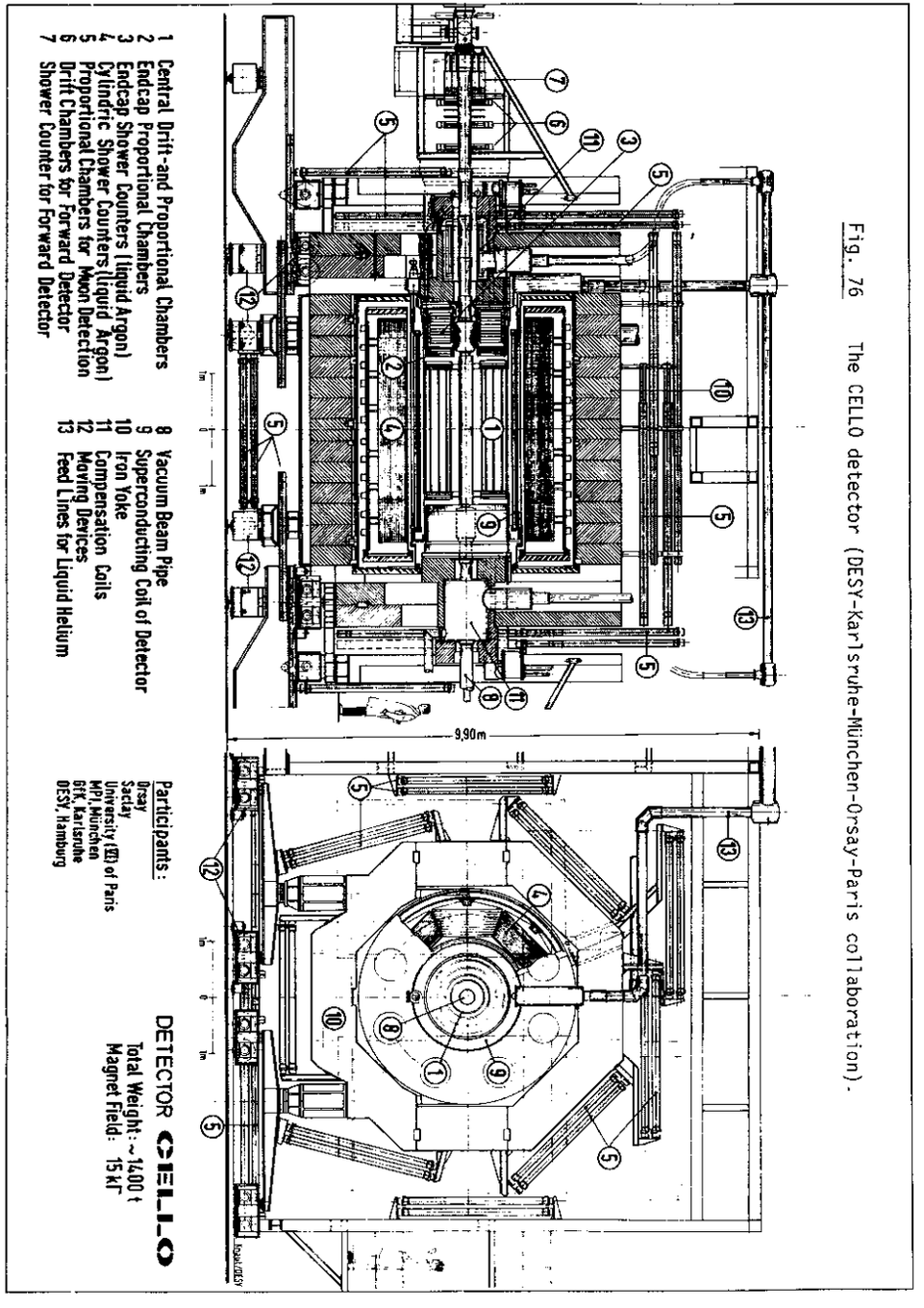

Fig. 76 The CELLO detector (DESY-Karlsruhe-München-Orsay-Paris collaboration).

5. Summary

First results at 13 and 17 GeV c.m. energy have been obtained at the new PETRA storage ring. The total cross section and the event topology are consistent with a fifth quark b and exclude that the $t\bar{t}$ threshold is below 17 GeV. Statistics is too scarce yet to draw any conclusion about QCD gluon bremsstrahlung effects. QED remains valid up to the highest energy. Hadronic events from two-photon reactions have been found. The race is on for top.

Acknowledgement

I am indebted to all my collegues at DESY who helped me in preparing these lectures, in particular the members of the PLUTO collaboration[106]. I want to thank B. Koppitz and H. Spitzer for a critical reading of the manuscript and R. Siemer for careful typing. I am grateful to Prof. H. Mitter for his invitation and the pleasant stay (and skiing) at Schladming.

REFERENCES

1) C. Bernardini, G.F. Corazza, G. Ghigo and B. Touschek, Nuovo Cim. 18 (1960) 1293

2) J. Le Francois, raporteurtalk, Cornell Conf. 1971
V. Sidorov,raporteur talk, Cornell Conf. 1971
Pioneering work: G.K. O'Neill, Bulletin A. Phys. Soc. Ser. 23 (1958) 158

3) B.H. Wiik and G. Wolf, DESY 78/23
P. Waloschek, Kerntechnik, Isotopentechnik und -chemie 12 (1970) 525

4) Doris proposal, Hamburg, DESY, Oct. 1967

5) PETRA proposal, Hamburg, DESY, Nov. 1974
Updated Feb. 1976

6) K.G. Steffen, High Energy Beam Optics, John Wiley, New York 1965

7) T. Appelquist and H.D. Politzer, Phys. Rev. D12 (1975) 1404
and Phys. Rev. Lett. 34 (1975) 43

8) L. Criegee et al., Proc. 1973 Int. Conf. on Instrum. for HEP, Frascati 1973
PLUTO Coll., J. Burmester et al., Phys. Lett. 64B (1976) 369

9) PLUTO Coll., J. Burmester et al., Phys. Lett. 66B (1977) 395
A. Bäcker, Thesis, Siegen (1977)
Internal report DESY F33-77/03 (unpublished)

10) G. Feldman, Proc. of the XIX Int. Conf. on HEP, Tokyo, 1978
and SLAC-PUB-2224 (1978)

11) J. Siegrist et al., Phys. Rev. Lett. 36 (1976) 700

12) DASP Coll., R. Brandelik et al., Phys. Lett. 70B (1977) 125
and Phys. Lett. 73B (1978) 109

13) J. Kirz, Contrib. to the XIX Int. Conf. on HEP, Tokyo, 1978

14) J.J. Aubert et al., Phys. Rev. Lett. 33 (1974) 1404
J.E. Augustin et al., Phys. Rev. Lett. 33 (1974) 1406

15) Recent reviews:
G. Goldhaver, EPS conf., Budapest, 1977
G. Feldman, Banff Summer Inst., Alberta (CA), 1977
H. Schopper, DESY-report 77/79 (1977)
B.H. Wiik and G. Wolf, DESY-report 78/23 (1978)

16) G. Flügge, loco cit. (ref. 10) and DESY 78/55 (1978)

17) M. Krammer and H. Krasemann, this school

18) DASP Coll., W. Braunschweig et al., Phys. Lett. 67B (1977) 243 and 249
W.D. Apel et al., Phys. Lett. 72B (1978) 500
The state X(2820) was questioned in recent experimental results obtained by the Cristal ball group (E. Bloom, XIV rencontre de Moriond, Les Ares, 1979)

19) W. Bartel et al., Phys. Lett. 79B (1978) 492
C.J. Biddik et al., Phys. Rev. Lett. 38 (1977) 1324
W. Tannenbaum et al., Phys. Rev. Lett. 35 (1975) 1323
PLUTO Coll., V. Blobel, XII Rencontre de Moriond, Flaine, 1977
S. Yamada, Hamburg Conf., 1977
Recent results from the MARK II group do not confirm the $\chi(3.45)$
(talk given at DESY by H. Taureg)

20) G. Goldhaber et al., Phys. Rev. Lett. 37 (1976) 255
I. Peruzzi et al., Phys. Rev. Lett. 37 (1976) 569

21) DASP Coll., R. Brandelik et al., Phys. Lett. 70B (1977) 132
and 80 B (1979) 412

22) M.L. Perl et al., Phys. Rev. Lett. 35 (1975) 1489
and 38 (1976) 117

23) S.W. Herb et al., Phys. Rev. Lett. 39 (1977) 252
W.R. Innes et al., Phys. Rev. Lett. 39 (1977) 1240

24) PLUTO Coll., J. Burmester et al., Phys. Lett. 68B (1977) 297 and 301

25) G.J. Feldman et al., Phys. Lett. 63B (1976) 466
M.L. Perl et al., Phys. Lett. 70B(1977) 487

26) M. Rößler, Thesis, Hamburg (1978),
Internal report DESY F14-78/01 (unpublished)

27) G. Flügge, Proc. of the Vth Int. Conf. on Experimental Meson Spectroscopy, Boston (1977)
M.L. Perl, Hamburg Conf. (1977)

28) DASP Coll., R. Brandelik et al., Phys. Lett. 73B (1978) 109

29) W. Bartel et al., Phys. Lett. 77B (1978) 331

30) W. Bacino et al., Phys. Rev. Lett. 41 (1978) 13

31) PLUTO Coll., G. Alexander et al., Phys. Lett. 73B (1978) 99
W. Wagner, Thesis, Aachen 1978 (unpublished)

32) Y.S. Tsai, Phys. Rev. D4 (1971) 2821
H.B. Thacker, J.J. Sakurai, Phys. Lett. 36B (1971) 103
J.D. Bjorken, C.H. Llewellyn-Smith, Phys. Rev. D7 (1973) 887

33) PLUTO Coll., G. Alexander et al., Phys. Lett. 78B (1978) 162

34) A.M. Cnops et al., Phys. Rev. Lett. 40 (1978) 144

35) J. Kirkby, Summer Institute, Stanford 1978 (SLAC-PUB-2231)
W. Bacino et al., Phys. Rev. Lett. 42 (1979) 6 and 42 (1979) 749

36) L. Lederman, XIX Int. Conf. on HEP, Tokyo, 1978

37) K. Ueno et al., Phys. Rev. Lett. 42 (1979) 486

38) PLUTO Coll., Ch. Berger et al., Phys. Lett. 76B (1978) 243

39) C.W. Darden et al., Phys. Lett. 76B (1978) 246

40) PLUTO Coll., Ch. Berger et al., DESY 79/19, submitted to Zeitschr. f. Physik C

41) J.K. Bienlein et al., Phys. Lett. 78B (1978) 360

42) G.W. Darden et al., contribution to the XIX Int. Conf. on HEP, Tokyo, 1978 and Internal report DESY F15-78/01 (1978)

43) J.L. Rosner, C. Quigg, H.B. Thacker, Phys. Lett. 74B (1978) 350

44) D.R. Yennie, Phys. Rev. Lett. 34 (1975) 219
F.E. Close, D.M. Scott, D. Sivers, Phys. Lett. 62B (1976) 213
T. Walsh, DESY report 76/13 (1976)
G.J. Gounaris, Phys. Lett. 72B (1977) 91
M. Greco, Phys. Lett. 77B (1978) 84

45) G. Sterman and S. Weinberg, Phys. Rev. Lett. 39 (1977) 1436

46) A. de Rujula, J. Ellis, E.G. Floratos and M.K. Gaillard, Nucl. Phys. B138 (1978) 387

47) J.D. Bjorken and S.J. Brodsky, Phys. Rev. D1 (1970) 1416

48) E. Fahri, Phys. Rev. Lett. 39 (1977) 1587. See also
S. Brandt, Ch. Peyrou, R. Sosnowski and A. Wroblewski, Phys. Lett. 12 (1964) 57
S. Brandt and H. Dahmen, Zeitschr. f. Phys. C1 (1979) 61

49) H. Georgi and M. Machacek, Phys. Rev. Lett. 39 (1977) 1237

50) G. Hanson et al., Phys. Rev. Lett. 35 (1975) 1609
G. Hanson, XIII Rencontre de Moriond, Les Ares (1978)
SLAC-PUB-2118 (1978)

51) PLUTO Coll., Ch. Berger et al., Phys. Lett. 78B (1978) 176

52) R.D. Field and R.P. Feynman, Phys. Rev. D15 (1977) 2590
and Nucl. Phys. B136 (1978) 1

53) V.P. Sukhatme, XIII Rencontre de Moriond, Les Ares, 1978

54) K. Koller, H. Krasemann, T.F. Walsh, Zeitschr. f. Phys. C1 (1979) 71

55) K. Koller, T.F. Walsh, Phys. Lett. B72 (1977) 227, B73 (1978) 504
and Nucl. Phys. B140 (1978) 449

56) T.A. De Grand et al., Phys. Rev. D16 (1977) 3251
S. Brodsky et al., Phys. Lett. B73 (1978) 203
H. Fritzsch, K.H. Streng, Phys. Lett. B74 (1978) 90

57) E.g.: K. Shizuya, S.H.H. Tye, preprint Fermilab-PUB-79/16-THY
with further references

58) PLUTO Coll., Ch. Berger et al., DESY report 78/71 (1978)
Phys. Lett. B82 (1979) 449

59) J. Bienlein et al., to be published

60) A. Ore, J.L. Powell, Phys. Rev. 75 (1949) 1696

61) Compare also: K. Hagiwara, Nucl. Phys. B137 (1978) 164

62) G. Alexander, XIX Int. Conf. on HEP, Tokyo, 1978

63) R.P. Feynman, Phys. Rev. Lett. 23 (1969) 1415

64) V. Blobel et al., Nucl. Phys. B69 (1974) 454

65) M. Breidenbach et al., Phys. Lett. 39B (1972) 654
M. Breidenbach, G. Flügge, K.R. Schubert, E.G.H. Williams, contribution to XVI Int. Conf. on HEP, Batavia, 1972
J.C. Sens, Proc. 4th Int. Conf. on High Energy Coll., Oxfort, 1972
G. Giacomelli, NAL-PUB-73/74-EXP (1973)

66) I.I. Bigi, S. Nussinov, Phys. Lett. 82B (1979) 281

67) PLUTO Coll., J. Burmester et al., Phys. Lett. 67B (1977) 367
DASP Coll., R. Brandelik et al., Phys. Lett. 67B (1977) 363
V. Lüth et al., Phys. Lett. 70B (1977) 132

68) H. Fritzsch, K.H. Streng, Phys. Lett. 77B (1978) 299

69) K. Wacker, talk at the DPG-Frühjahrstagung, Bonn, 1979

70) H. Schopper, Hamburg Conf., 1977
G. Weber, Symp. on HEP and the Role of Quarks, Stockholm, 1978

71) PETRA proposal, Hamburg, 76/19 (1976)

72) PETRA proposal, Hamburg, 76/15 (1976)

73) PETRA proposal, Hamburg, 76/13 (1976)

74) PETRA proposal, Hamburg, 76/16 (1976)

75) PETRA proposal, Hamburg, 76/14 (1976)

76) G.A. Voss, progress report at DESY, Febr. 1979

77) M. Kobayashi, K. Maskawa, Prog. Theor. Phys. 49 (1973) 652

78) T. Kinoshita et al., Phys. Rev. D2 (1970) 910

79) Recent experimental limit: T. Himel et al., Phys. Rev. Lett. 41 (1978) 449
Recent review: J.J. Sakurai, III Int. Symp. on HEP with Pol. Beams and Targets, Argonne, 1978

80) E. Iarocci, P. Waloschek, DESY report 72/13
H. Mehrgardt et al., Int. Conf. on Instr. in HEP, Frascati, 1973

81) PLUTO Coll., Ch. Berger et al., Phys. Lett. 81B (1978) 410

82) H. Salecker, Z. Physik 160 (1960) 385

83) D. Barber et al., Phys. Rev. Lett. 42 (1979) 1110

84) PLUTO Coll., H. Spitzer, talk given at DESY, April 1979

85) TASSO Coll., H. Martyn, talk given at DESY, April 1979

86) J.E. Augustin et al., Phys. Rev. Lett. 34 (1975) 233
L.H. O'Neill et al., Phys. Rev. Lett. 37 (1976) 395
B.L. Beron et al., Phys. Rev. Lett. 33 (1974) 663

87) F.A. Berends et al., Nucl. Phys. B57 (1973) 381, B68 (1974) 541, B101 (1975) 234 and Phys. Lett. 63B (1976) 433

88) D. Barber et al., Phys. Rev. Lett. 42 (1979) 1113

89) TASSO Coll., R. Brandelik et al., DESY report 79/14 (1979) submitted to Phys. Lett.

90) A. Ali, J.G. Körner, G. Kramer, J. Willrodt, Z. Physik C1 (1979) 203 and DESY report 79/16 (1979), to be published

91) J. Ellis, M.K. Gaillard, G.G. Ross, Nucl. Phys. B111 (1976) 253

92) C.L. Basham et al., Phys. Rev. D17 (1978) 2298
F. Steiner, DESY 78/59 (1978)

93) I.I.Y. Bigi, R.F. Walsh, Phys. Lett. 82B (1979) 267
I.I.Y. Bigi, preprint Th 2626 CERN (1979)

94) G. Kramer, G. Schierholz, Phys. Lett. 82B (1979) 108

95) S.J. Brodsky, T.Kinoshita, H. Terazawa, Phys. Rev. Lett. 25 (1970) 972 and Phys. Rev. D4 (1971) 1532
A. Jaccarini, N. Artega-Romero, J. Parisi, P. Kessler, Lett. Nuovo Cim. 4 (1970) 933

96) H. Terazawa, Rev. Mod. Phys. 45 (1973) 615

97) C. Weizsäcker, E.J. Williams, Z. Physik 88 (1934) 612

98) M. Greco, Y. Srivastava, Nuovo Cim. 43A (1978) 88

99) G.J. Bobbink et al., PETRA proposal 76/18, Hamburg (1976)

100) S.J. Brodsky, T.A. De Grand, J.F. Gunion, J.H. Weis, Phys. Rev. Lett. 41 (1978) 672

101) Compare also: K. Kajantie, this school

102) G. Barbiellini et al., Phys. Rev. Lett. 32 (1974) 385
L. Paoluzzi et al., Lett. Nuovo Cim. 10 (1974) 435

103) PLUTO Coll., W. Wagner, XIV Rencontre de Moriond, Les Ares, 1979

104) J. Ellis, M.K. Gaillard, D.V. Nanopoulos, S. Rudaz, Nucl. Phys. B131 (1977) 285
A. Ali, Z. Physik C1 (1979) 25
V. Barger, T. Gottschalk, R.J.N. Phillips, Wisconsin preprint COO-881-82 (1979)
F. Bletzacker, H.T. Nieh, preprint ITP-SB-79-10, Stony Brook, 1979

105) Y.S. Tsai, SLAC-PUB 2105 (1978)

106) PLUTO Collaboration:
Ch. Berger, H. Genzel, R. Grigull, W. Lackas, F. Raupach, W. Wagner
I. Physikalisches Institut der RWTH Aachen, Germany
A. Klovning, E. Lillestöl, E. Lillethun, J.A. Skard
University of Bergen, Norway
H. Ackermann, G. Alexander, F. Barreiro, J. Bürger, L. Criegee, H.C. Dehne, R. Devenisch, G. Flügge, G. Franke, W. Gabriel, Ch. Gerke, G. Horlitz, G. Knies, E. Lehmann, H.D. Mertiens, B. Neumann, K.H. Pape, H.D. Reich, B. Stella, U. Timm, P. Waloschek, G.G. Winter, S. Wolff, W. Zimmermann
Deutsches Elektronen-Synchrotron DESY, Hamburg , Germany
O. Achterberg, V. Blobel, L. Boesten, H. Kapitza, B. Koppitz, W. Lührsen, R. Maschuw, R. van Staa, H. Spitzer
II. Institut für Experimentalphysik der Universität Hamburg, Germany
C.Y. Chang, R.G. Glasser, R.G. Kellog, K.H. Lau, B. Sechi-Zorn, A Skuja, G. Welch, G.T. Zorn
University of Maryland, USA
A. Bäcker, S. Brandt, K. Derikum, C. Grupen, H.J. Meyer, M. Rost, G. Zech,
Gesamthochschule Siegen, Germany
T. Azemoon, H.J. Daum, H. Meyer, O. Meyer, M. Rössler, D. Schmidt, K. Wacker
Gesamthochschule Wuppertal, Germany